SPRING/SUMMER 2011
VOLUME 3, NUMBER 1

Print ISSN: 2152-4157
Online ISSN: 2152-4165

WWW.IJERI.ORG

International Journal of Engineering Research & Innovation

Editor-in-Chief: Mark Rajai, Ph.D.
California State University Northridge

Published by the
International Association of Journals & Conferences

Time to change the way academics work? Try acamedics!

If you are not using the Internet, please skip this ad and enjoy the rest of the journal. The average burden of reading this ad is two minutes, which may add two months of productivity to your academic life. Seriously!

Whether you organize a conference, publish a journal, or serve on a committee to collect and review applications, you can use the Internet to make your life easier. We are not talking about emails. We are talking about state-of-the-art online systems to collect submissions, assign them to reviewers, and finally make a decision about each submission. We are talking about value-added services, such as payment and registration systems to collect registration fees online. We are talking about digital document services, such as proceedings CD/DVD development and duplication, or creating professional looking digital documents.

Finally, we are talking about AFFORDABLE PRICE, QUALITY, and CUSTOMIZATION. And we are talking about each of them at the same time.

By the way, you don't have to be a computer geek to use our systems. We have a couple them, and they will do all the technical mumbo jumbo for you. We also have a few select people from academics like you, and they know what you do. You just relax and enjoy our systems.

If you are still reading this ad, chances are you are interested in our systems or services. So, visit us at *www.acamedics.com*. While you are there, check the names of our clients as well. Most of them are quite familiar, and the list is quite long to put here.

ACAMEDICS
Enjoy Technology!

Acamedics.com • 44 Strawberry Hill Ave Suite 7B, Stamford, CT 06932 • Phone: 203.554.4748 • sales@acamedics.com •

INTERNATIONAL JOURNAL OF ENGINEERING RESEARCH AND INNOVATION

INTERNATIONAL JOURNAL OF ENGINEERING RESEARCH AND INNOVATION (IJERI) is an independent and nonprofit publication which aims to provide the engineering community with a resource and forum for scholarly expression and reflection.

IJERI is published twice annually (Fall and Spring issues) and includes peer-reviewed research articles, editorials, and commentary that contribute to our understanding of the issues, problems, research associated with the engineering and related fields. The journal encourages the submission of manuscripts from private, public, and academic sectors. The views expressed are those of the authors, and do not necessarily reflect the opinions of the IJERI or its editors.

EDITORIAL OFFICE:

Mark Rajai, Ph.D.
Editor-In-Chief
Office: (818) 677-5003
Email: mrajai@csun.edu
College of Engineering and Computer Science
California State University
Northridge, CA 91330-8332

THE INTERNATIONAL JOURNAL OF ENGINEERING RESEARCH AND INNOVATION EDITORS

TABLE OF CONTENTS

Editor's Note: Reflections on IAJC and the 2011 Joint International Conference with ASEE

Philip Weinsier, IJERI Manuscript Editor

As we in higher education and industry reflect back on the first decade in this new millennium, we realize that the sharing of ideas and resources is the best way for us to create a better future for the next generation of students, faculty, and researchers. In the competitive and tight global markets of the 21st century, leading companies across industry have embarked on massive reorganizations, mergers, partnerships, and all sorts of collaborative projects with their like-minded peers and rivals in order to not only survive but grow and thrive. But, as industry changes with time, so must academia. Conversely, as academic R&D efforts provide advancements in technology, so must industry provide a quick turnaround from concept to market. However, many academic organizations, journals, and conferences have been slow to adapt and provide the necessary platforms for the dissemination of knowledge.

Beginning in 2006, the editorial board of the International Association of Journals and Conferences (IAJC) embarked on groundbreaking and unprecedented efforts to establish strategic partnerships with other major rival journals and organizations to share resources and offer authors a unique opportunity to come to one conference and publish their papers in a broad selection of journals representing interests as diverse as those of the researchers and educators in fields related to engineering, engineering technology, industrial technology, mathematics, science and teaching. These efforts resulted in an innovative model of joint international conferences that includes a variety of organizations and journals.

IAJC joint and independent international conferences have been a great success with the main conferences being held in the United States and regional, simultaneous conferences, in other parts of the world. In additional to bringing people together at its conference venues, IAJC attracts myriad journals that wish to publish the best of what its attendees have to offer, thereby creating excitement in academic communities around the world. IAJC is a first-of-its-kind, pioneering organization. It is a prestigious global, multi-layered umbrella consortium of academic journals, conferences, organizations and individuals committed to advancing excellence in all aspects of technology-related education.

Conference Statistics: A total of 285 abstracts from more than 100 educational institutions and companies were submitted from around the world. In the multi-level review process, papers are subjected to blind reviews by three or more highly qualified reviewers. For this conference, a total of 80 papers were accepted. Most of these were presented and are published in the conference proceedings. This reflects an acceptance rate of less than 30%, which is one of the lowest acceptance rates of any international conference.

This conference was sponsored by the International Association of Journals and Conferences (IAJC), which includes 13 member journals and a number of universities and organizations. Other sponsors were the American Society for Engineering Education (ASEE) and the Institute of Electrical and Electronics Engineers (IEEE). Selected papers from this conference will be published in one of the 13 IAJC member journals. Organizing such broad conferences is a monumental task and could not be accomplished without the help and support of the conference committee, the division/session chairs and the reviewers. Thus, we offer our sincerest thanks to all for their hard work and dedication in the development of the outstanding 2011 conference program. We personally hope you will seek them out to thank them for their fine work.

IJME is steered by IAJC's distinguished Board of Directors and is supported by an international review board consisting of prominent individuals representing many well-known universities, colleges, and corporations in the United States and abroad. To maintain this high-quality journal, manuscripts that appear in the *Articles* section have been subjected to a rigorous review process. This includes blind reviews by three or more members of the international editorial review board—with expertise in a directly related field—followed by a detailed review by the journal editors.

Editorial Review Board Members

Listed here are the members of the International Review Board, who devoted countless hours to the review of the many manuscripts that were submitted for publication. Manuscript reviews require insight into the content, technical expertise related to the subject matter, and a professional background in statistical tools and measures. Furthermore, revised manuscripts typically are returned to the same reviewers for a second review, as they already have an intimate knowledge of the work. So I would like to take this opportunity to thank all of the members of the Board.

As we continually strive to improve upon our conferences, we are seeking dedicated individuals to join us on the planning committee for the next conference—scheduled for fall, 2012. Please watch for updates on our web site (**www.IAJC.org**) and contact us anytime with comments, concerns or suggestions. On behalf of the 2011 IAJC conference committee and IAJC Board of Directors, we thank all of you who participated in this great conference and hope you will consider submitting papers in one or more areas of engineering and related technologies for future IAJC conferences.

If you are interested in becoming a member of the IAJC International Review Board, send me (Philip Weinsier, IAJC/IRB Chair, philipw@bgsu.edu) an email to that effect. IRB members review manuscripts in their areas of expertise for all three of our IAJC journals—IJME (the International Journal of Modern Engineering), IJERI (the International Journal of Engineering Research and Innovation), TIIJ (the Technology Interface International Journal)—and papers submitted to the IAJC conferences.

Mohammad Badar
Mehmet Bahadir
Rendong Bai
Terrance Barkan
Kevin Berisso
Kanninika Bhatnagar
Elinor Blackwell
Boris Blyukher
Walter Buchanan
Jessica Buck
John Burningham
Shaobiao Cai
Vigyan Chandra
Isaac Chang
Hans Chapman
Rigoberto Chinchilla
Raj Chowdhury
Michael Coffman
Kanchan Das
Paul Deering
Brad Deken
Raj Desai
Dave Dillon
David Domermuth
Marilyn Dyrud
Mehran Elahi
Ahmed Elsawy
Bob English
Rasoul Esfahani
Fereshteh Fatehi
Dominic Fazarro
Verna Fitzsimmons
Richard Freeman
Hamed Hakimzadeh
Mohsen Hamidi
Bernd Haupt
Rita Hawkins
David He
Youcef Himri
Xiaobing Hou
Shelton Houston
Luke Huang
Charles Hunt
Dave Hunter
Pete Hylton
Ghassan Ibrahim
John Irwin
Fawaz Jabri
Anwar Jawad
Sudershan Jetley
Keith Johnson
Julius Jow
Rex Kanu
Khurram Kazi
Satish Ketkar
Daphene Cyr Koch
John Kugler
Ognjen Kuljaca
Chakresh Kumar
Zaki Kuruppalil
Ronald Land
Jane LeClair
Jay Lee
Margaret Lee
Shiyoung Lee
Soo-Yen Lee
Chao Li
Stanley Lightner
Jimmy Linn
Dale Litwhiler
Daniel Lybrook
Mani Manivannan
G.H. Massiha
Jim Mayrose
Thomas McDonald
David Melton
Richard Meznarich
NagaMani Molakatala
Ali Mottahedi
Sam Mryyan
Wilson Naik
Arun Nambiar
Ramesh Narang
Argie Nichols
Hamed Niroumand
Troy Ollison
Reynaldo M Pablo Jr.
Basile Panoutsopoulous
Jose Pena
Karl Perusich
Thongchai Phairoh
Patty Polastri
Mike Powers
Huyu Qu
John Rajadas
Desire Rasolomampionona
Mohammad Razani
Mulchand Rathod
Sangram Redkar
Michael Reynolds
Marla Rogers
Mehdi Safari
Anca Sala
Darrel Sandall
Balaji Sethuramasamyraja
Mehdi Shabaninejad
Hiral Shah
Ajay K. Sharma
J.Y. Shen
Ehsan Sheybani
Musibau Shofoluwe
Carl Spezia
Randy Stein
Adam Stienecker
Pingping Sun
Jalal Taheri
Roohallah Taherkhani
Li Tan
Ravindra Thamma
Li-Shiang Tsay
Jeffrey Ulmer
Mihaela Vorvoreanu
Philip Waldrop
Abram Walton
Haoyu Wang
Jyhwen Wang
Liangmo Wang
Tom Warms
Baijian (Justin) Yang
Faruk Yildiz
Emin Yilmaz
Yuqiu You
Pao-Chiang Yuan
Biao Zhang
Chongming Zhang
Jinwen Zhu

USING SIX SIGMA FOR CONTINUOUS IMPROVEMENT IN ENGINEERING TECHNOLOGY

Sarai Hedges, University of Cincinnati; Virginia Westheider, University of Cincinnati

Abstract

A grassroots team at the College of Applied Science, University of Cincinnati, formed to use Six-Sigma methodology, an industry-familiar process, to develop an improved assessment plan that is responsive to the Technology Accreditation Commission division of the Accreditation Board for Engineering and Technology (ABET/TAC) accreditation requirements. Using Six Sigma in the evaluation process fits nicely with the engineering technology programs and was readily accepted by faculty.

The scope of the project focused on improving the assessment of ABET/TAC Criteria 3h (lifelong learning) and continuous improvement in accordance with the documented process. In Six Sigma process improvement, a process that works at a "Six Sigma Level" only has approximately 3.4 defects per million opportunities. This paper describes the project selection, definition of the process, calculation of the sigma level, implementation of the DMAIC method, and the level of success of the team in improving the process of assessing graduates' abilities to recognize the need for and to engage in lifelong learning.

Introduction

Six Sigma, started in 1986 by Motorola, has been defined in numerous ways. It has been called a philosophy, a methodology, and a set of tools [1]. One of the more concise definitions is "a disciplined, data-driven approach and methodology for eliminating defects … in any process -- from manufacturing to transactional and from product to service"[2]. Six Sigma is now endemic to industry—automotive, chemical, financial, manufacturing and retail, to name a few—from American Express to GE, Advanced Micro Devices to Xerox, and is credited with saving millions of dollars while improving product or service quality and customer satisfaction.

In June of 2008, the authors met with Dean Allen Arthur to discuss using the Six Sigma methodology for process improvement within the college. ABET/TAC accreditation was selected as an appropriate area for such an endeavor. The authors met regularly throughout the year on the project with Dean Arthur providing management support. This paper is a summary of the team's progress to-date and is organized according to the phases of the six-sigma process improvement model (DMAIC):

Figure 1. DMAIC Phases

Define Phase

The first phase of Six Sigma projects is the "Define" phase in which the team "defines the Customer, their Critical to Quality (CTQ) issues, and the Core Business Process involved" [3]. Many common Six Sigma and Project Management tools are appropriate to use in this phase, but the authors chose a Pareto Chart, Thought Process Map, SIPOC diagram, CTQC tree, and a Project Charter.

Figure 2 is the Pareto Chart that shows that for Criterion 3 (C3), related to assessment and continuous improvement, the vast majority of programs received "Weakness" ratings in the ABET/TAC evaluators' comments immediately after their 2006 visit. Criterion 1 (C1), program educational objectives, Criterion 2 (C2), program outcomes, and Criterion 7 (C7), institutional and external support, also received weakness ratings but none was consistently rated so poorly as Criterion 3 across programs.

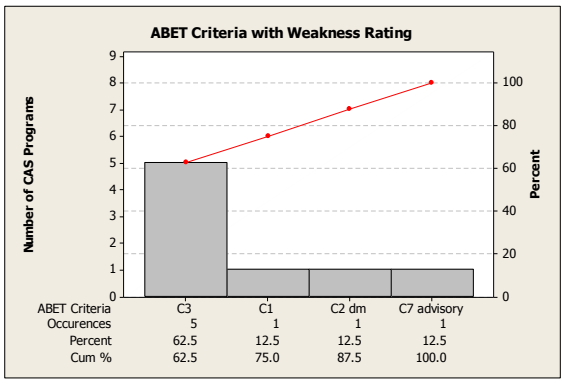

Figure 2. Pareto Chart

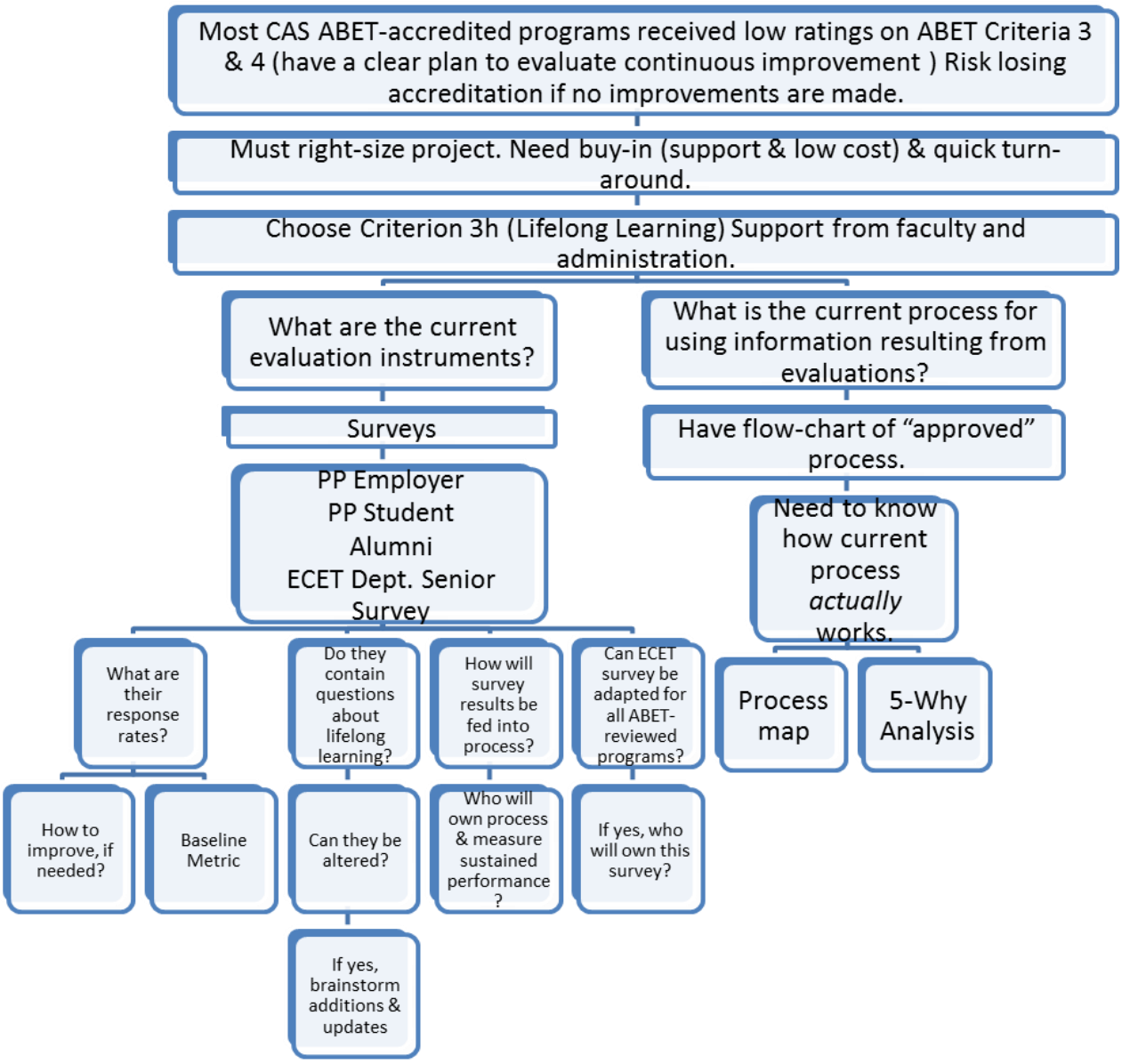

Figure 3. Thought Process Map

The Thought Process Map (Figure 3) illustrates the benefits of focusing on Criterion 3h and further illustrates several surveys administered by different bodies within the university that were vehicles that somewhat assessed lifelong learning and need further exploration for possible improvement. Table 1, the Supplier Input Process Output (SIPOC) diagram, more fully describes the process as it pertains to the survey instruments at the beginning of the project. Further investigation of the 4 surveys in the SIPOC diagram found that in 2006 the Alumni Survey was administered by the CAS Career Placement Office and had an abysmal 5.7% response rate. The 2007-08 Employer Survey, administered by the University of Cincinnati Professional Practices Office, had a 69.7% response rate for all CAS students. The Student Professional Practice (PP) Survey, administered by the same office, does not have questions pertaining to lifelong learning and is very difficult to alter. The College Student Services Office administered a Senior Survey until the spring quarter of 2008 when it was discontinued due to a change in university policy and refusal by a university office to continue its administration. The CAS ECET program developed a Senior Survey for its students, which garnered a 75% response rate upon its first implementation in November of 2008, and was willing to share the survey instrument for other programs to use.

Table 1. SIPOC Diagram

Original Process:			
Supplier	**Input**	**Process**	**Output**
Career Placement Office	Alumni Survey	Assessing Graduates' Abilities to Recognize the Need for and to Engage in Lifelong Learning	Graduates' responses
CAS Office of Professional Practice	Employer PP Survey Student PP Survey		Employers' responses Students' responses
Student Services (until 08S)	Senior Student Survey		Seniors' responses
ECET department (08S – 09S)	Senior Student Survey		Seniors' responses

Using the Critical To Quality Characteristic (CTQC) Tree Diagram (Figure 4), the team identified specific measureable aspects of the process (metrics) that could be used to measure process improvement:

- alumni survey response rate,
- the number of questions on each survey measuring lifelong learning,
- the creation of *one* senior survey, and
- an approved process flow chart.

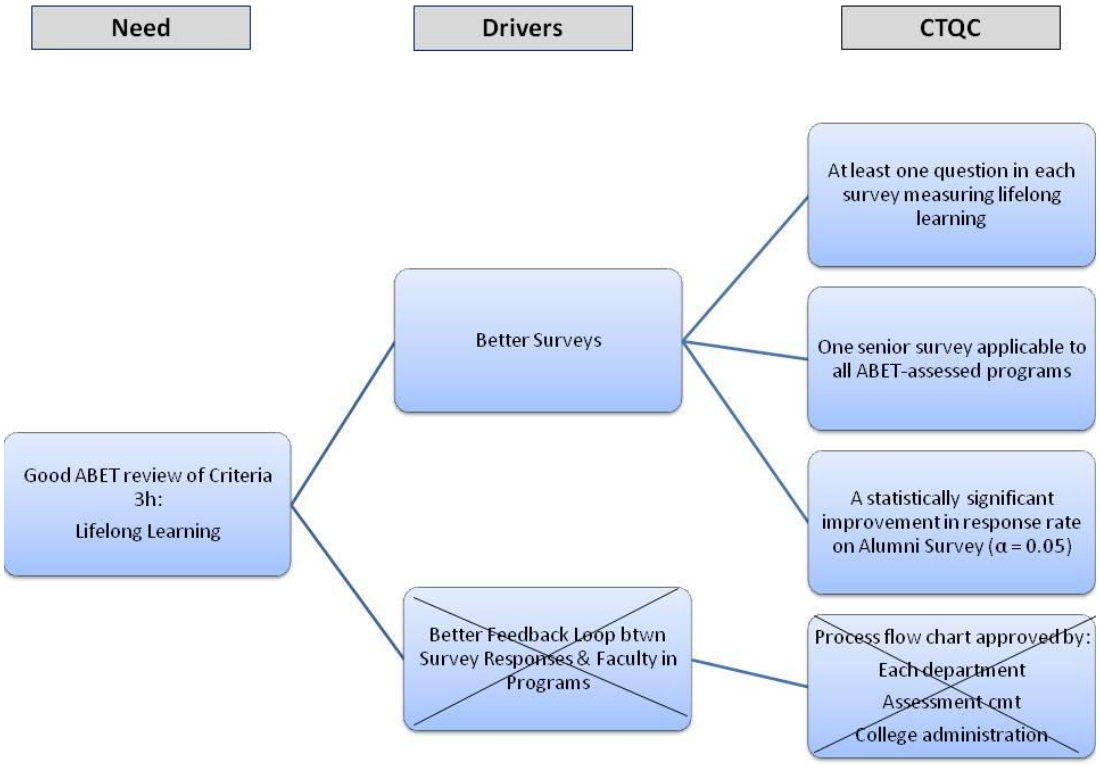

Figure 4. Critical to Quality Characteristics (CTQC) Tree

The decision to measure only an improvement in the response rate for the Alumni Survey will be discussed in the "Analyze" section of this report. The other two CTQC's following the "Better Surveys," were chosen with the consultation of the College Assessment Committee, that has members from the suppliers of the survey instruments, those familiar with the ABET/TAC requirements, and those in contact with students past and present. The last CTQC involving the process flow chart was removed from the project after the announcement of a Collegiate Restructuring Initiative in which the College of Applied Science was to be merged with another college. As the structure of the college

was destined to change, so would the feedback loop for this process in a manner that cannot be anticipated with any certainty. As a result, the authors were given permission to scale back on this aspect of the project. This led the team to create the following Business Case and Problem Statement for the project (taken from the Project Charter):

BUSINESS CASE: The majority of degree-granting programs in the College of Applied Science are accredited by ABET/TAC. ABET is "the recognized accreditor for college and university programs in applied science, computing, engineering, and technology, [which] is a federation of 29 professional and technical societies representing these fields" [4]. Failure to meet ABET accreditation requirements may lead to loss of accreditation, having significant and adverse affects on these programs as for "employers, graduate schools, and licensure, certification, and registration boards, graduation from an accredited program signifies adequate preparation for entry into the profession. In fact, many of these groups require graduation from an accredited program as a minimum qualification" [5]. Hence, it is an understatement to say that maintaining ABET/TAC accreditation and achieving positive reviews from ABET/TAC evaluators are important to the college.

The 2006 findings of the ABET/TAC review of the appropriate College of Applied Science programs varied among the programs. Although no program had any ABET/TAC Criteria ratings in the lowest category, "deficiency", the majority of the programs had ratings in the next lowest category, "weakness", for the same criterion, ABET/TAC Criterion 3: Assessment and Evaluation, which states that "[e]ach program must utilize assessment measures in a process that provides documented results to demonstrate that the program objectives are being met…" This is related to Criterion 4 "Continuous Improvement:… us[ing] a documented process incorporating relevant data to regularly assess its program educational objectives and program outcomes, and to evaluate the extent to which they are being met. The results of these evaluations of program educational objectives and program outcomes must be used to effect continuous improvement of the program through a documented plan" [6]. None of the reviewed programs had either of these criteria listed as a program strength. Lack of a documented program assessment process that is part of a feedback loop for continuous program improvement is a systematic problem throughout the college's programs and ranks high among the programs' faculty and college administration as a problem to solve.

PROBLEM STATEMENT: The ABET/TAC evaluator findings indicated that the majority of degree programs seeking renewal of their accreditation did not have a clearly defined plan for evaluating continuous improvement of program objectives and outcomes (ABET/TAC Criteria 3 & 4). The team seeks to remedy these issues by clearly defining an appropriate feedback loop for improving the process of assessing Criterion 3h: demonstration that graduates have a recognition for the need for, and an ability to engage in lifelong learning. This specific ABET/TAC criterion was chosen because it was identified by the programs' faculty and college administration as difficult to evaluate and because there exist survey instruments in various areas of the college that can be adapted to evaluate this criterion across all of the programs. As this is a grass-roots effort in implementing the Six Sigma methodology at the College of Applied Science, the team also believes that working on this ABET/TAC criterion makes for a right-sized project in terms of faculty and administrative support, probability of success, low implementation costs, and timeliness of completion. The team hopes the successful completion of this project will lead to more support for bigger projects in the future.

There are currently four (4) surveys at CAS that contain questions that assess lifelong learning at least to some extent. They are used in various ways and administered by various bodies. In 2006, the Alumni Survey, which includes some questions related to lifelong learning and is administered by the CAS Career Placement Office, had an abysmal 5.7% response rate. The CAS ECET program developed a Senior Survey for its students, which garnered a 75% response rate upon its first implementation in November of 2008 but the survey needs to be adapted for other programs' use. The University of Cincinnati Professional Practices Office Employer and Student Surveys, which evaluates students on co-op, also have the possibility of being used. The 2007-08 Employer Survey had a 69.7% response rate for all CAS students.

The project team was expected to adapt the most appropriate surveys to evaluate ABET/TAC Criterion 3h. The team was also expected to implement techniques that would increase the response rates for those surveys with low responses and further to improve the feedback loop between the programs being assessed, the entities which administer the surveys and collect the data and the decision points in the process where changes based on the data are recommended and implemented so that program assessment is effectively incorporated in a manner of documented continuous improvement leading to successful ABET/TAC reviews.

Measurement Phase

After defining the project, the authors measured the current process. Tools used were DPMO and Sigma Level calculations and a histogram. The authors could not perform a Measurement System Analysis. A near-perfect process works at a "Six Sigma Level," which corresponds to 3.4

defects per million opportunities. Tables 2 and 3 show the team's definitions of Defects, Units, and Opportunities and the calculations for the DPMO and Sigma Level.

Although originally used for continuous ratio data, in concordance with statistical theory, this technique is commonly used for discrete, or attribute data. In this project, the authors focused on the proportion of "bad" (deficiency or weakness) ABET/TAC evaluator ratings for ABET/TAC criterion 3h, binomial data. To calculate the sigma level for such data, the fraction of "bad" ratings was treated as the alpha of the normal distribution and then a conversion table was used to determine the sigma level. The 1.5 Sigma Shift was a convention that assumed that the process would shift over time.

The initial process of assessing lifelong learning showed plenty of room for improvement at a baseline Sigma Level of 1.2.

Table 2. DPMO Definitions

DEFINITIONS	Assessing ABET/TAC Criterion 3
Defect	rating of Weakness or Deficiency
Unit	CAS program reviewed by ABET/TAC
Opportunity	1 per program

Table 3. DPMO and Sigma Level Calculations

CALCULATIONS	Assessing ABET/TAC Criterion 3
Defects	5
Opportunities	8
DPMO	(5/8)*1,000,000 = 625,000
Sigma Level (assumed 1.5 Sigma Shift)	1.2

The DPMO and Sigma Level in a process are affected by how defects are defined and who or what measures the defects. To have reliable measurements, the measuring devices must have repeatability and reproducibility (R&R). In Six Sigma projects, a Measurement System Analysis (MSA) was conducted to determine the measurement R&R of a process. For this particular process, outside evaluators from other institutions were used to rate the ABET/TAC criteria for the programs. Neither this team nor the university had access to ABET/TAC evaluators to conduct an MSA. Thus, the authors had to proceed under the assumption that, for a given accreditation visit, individual evaluators would repeatedly rate a program about the same and a program would be rated similarly by different evaluators. As a sidebar, the undertaking of an MSA of evaluators by the ABET/TAC accrediting body would be an excellent opportunity for it to elevate its credibility.

Coding the evaluator ratings as shown in Table 4 allows further analyses. Although the rating "Observation", on the face of it, does not connote a level between "Concern" and "Strength", the team's reading of the "Observation" rating comments made by ABET/TAC evaluators and its listing under "Corrections and Improvements" in the ABET/TAC report gave evidence to such a use for this project.

Table 4. Evaluator Rating Codes

Evaluator Rating	Code
Deficiency	1
Weakness	2
Concern	3
Observation	4
Strength	5

The histogram in Figure 5 illustrates all evaluator ratings over all ABET/TAC-accredited programs received during the 2006 visit. In other words, the graph lumps all ratings together. It shows that, thankfully, there were no "Deficiency" ratings and rating "3", or "Concern", was the most common rating given, with 12 occurrences. Looking back at the data, the team found that seven (7) of the occurrences were related to Criterion 8. Although a "Concern" rating is not as urgent to improve as a "Weakness" rating, it is worth noting and perhaps should be investigated in another project.

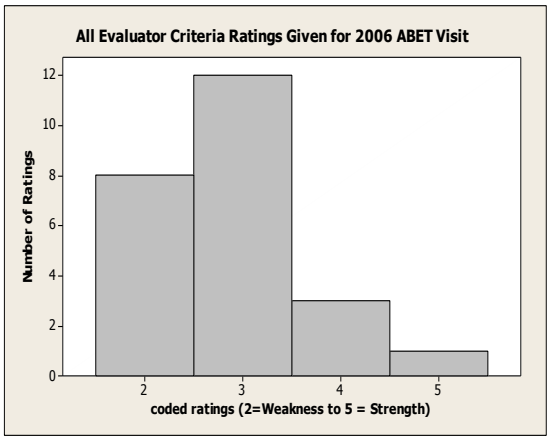

Figure 5. Histogram of Evaluator Coded Ratings

Analysis Phase

This phase includes analyzing the data collected and determining the "root causes of defects and opportunities for improvement" [3]. Tools used were a Cause & Effect Diagram, Brainstorming, a 5-Why Analysis, and a variation on

the traditional Failure Mode and Effects Analysis (FMEA), which is called a "Significant Factor Selection Matrix".

The Cause & Effect Diagram (also called a Fishbone Diagram) in Figure 6 shows a multitude of factors that affect the process. The team used written Criteria 3 and 4 comments from evaluators and brainstormed to come up with factors (also known as "root causes" or "X's").

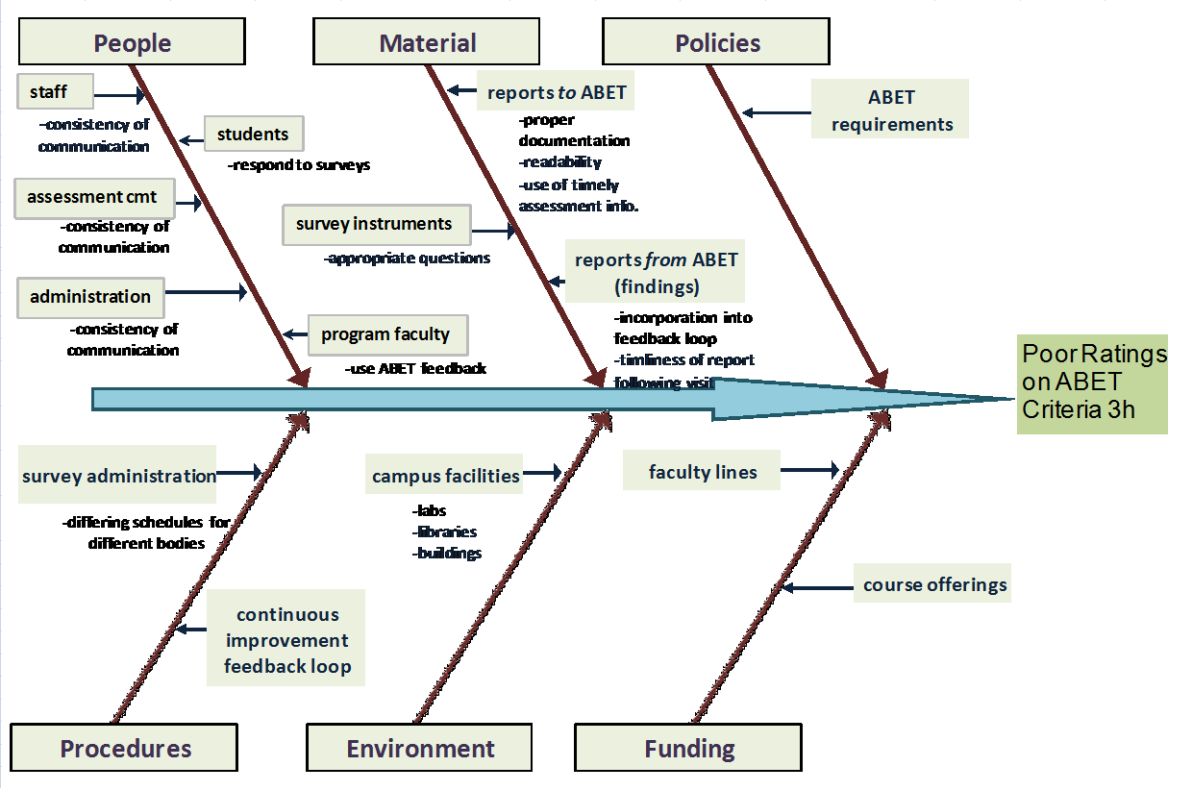

Figure 6. Fishbone Diagram

Procedures involved in the feedback loop, students, and the survey instruments were selected as factors to pursue to improve the process using Table 5, the Significant Factor Selection Matrix. As factors related to the feedback loop could not be pursued due to the Collegiate Restructuring Initiative, the team focused its efforts on the survey instruments.

The team attended the monthly College Assessment Committee meetings from November 2008 – April 2008 and was able to work with them to review and update the Professional Practices Employer Survey and the Alumni Survey to include questions relevant to assessing ABET/TAC Criteria 3h. During this review, the Committee additionally updated the Alumni Survey for readability and brevity.

At the beginning of this project, the ECET department was conducting its own Senior Survey. A 5-Why Analysis (Table 6) shows the thought process in analyzing this problem. The outcome was that the College Assessment Committee altered the ECET Senior Survey and adopted it for all ABET/TAC-assessed programs in the college.

Preliminary investigation of the process showed that the Alumni Survey had only a 5.7% response rate. Both a paper copy and online option were available for alumni to take the survey. During the February College Assessment Committee meeting, attendees brainstormed ideas to improve the response rate. Incentive ideas such as book bags and key chains were mentioned. The team further studied ways to improve the response rate of the Alumni Survey by performing a literature review of survey response and by benchmarking with Alumni Surveys at other institutions of higher learning.[7-15] Originally, the Alumni Survey was administered by the College Career Development Office by paper and then in 2006 by paper or with an option to complete the survey of the college's web site. The team decided that it would call a new Alumni Survey administration method a success if the response rate had a statistically significant increase from the previous year at a 0.05 level of significance.

Table 5. Significant Factor Selection Matrix

Significant Factor Selection Matrix					
Improving Assessment of Lifelong Learning for ABET Accreditation					
	Selection Criteria				
Possible Causes (X's) for Poor Ratings on ABET Criterion 3h Applicability Rating (1 = low to 5 = high)	Covers all Programs	Low Cost To Fix	Ease of Implementation	Ability to Influence	**TOTAL SCORE (add ratings):**
Consistency of Communication from Staff	5	4	5	5	19
Consistency of Communication from Assessment Cmt	5	5	5	4	19
Consistency of Communication from Administration	5	5	5	4	19
Use of ABET feedback by faculty	5	5	4	5	19
Students Don't Respond to Surveys	5	4	5	5	19
Poor Documentation to ABET	3	3	3	3	12
Report Not Readable	3	5	5	3	16
Report Doesn't Use Timely Assessment Info	4	5	3	2	14
Survey Instruments Contain Appropriate 3h Questions	5	5	5	5	20
ABET Findings Not Incorporated Well Into Feedback Loop	5	5	4	5	19
ABET Findings Not Provided in Timely Manner Following Visit	5	5	1	1	12
ABET Requirements Unclear	1	5	1	1	8
Reporting Schedule Vary Widely for Surveys	5	5	1	1	12
Poor/Nonexistent Continuous Improvement Feedback Loop	5	5	4	5	19
Few/Poor Quality Lab Facilities	1	1	1	1	4
Few/Poor Quality Libraries	1	1	1	1	4
Few/Poor Quality Buildings	3	1	1	1	6
Not Enough Faculty Lines	2	1	1	1	5
Not Enough/Not Appropriate Course Offerings	1	1	1	1	4

Table 6. 5-Why Analysis

5-Why Analysis For Senior Survey	
Why does ECET do their own Senior Survey?	**1**
There is no other Senior Survey available.	
Why?	**2**
College office stopped administering Senior Survey.	
Why?	**3**
University Admissions took over senior graduation documents and refused to continue administering the College Senior Survey.	
Why?	**4**
They say it is out of their purview.	
Why?	**5**
They want another office to take over that task. Can we get another college office to do it?	
Yes--the College Director of Assessment will take it over and facilitate through Assess. Cmt. to adapt ECET Senior Survey to all ABET/TAC programs.	**How**

Improvement Phase

In this phase, the team implemented solutions aimed at correcting the problems that were defined, measured, and analyzed in the previous phases. Tools used were a Correction Action Matrix and a statistical hypothesis test to verify and measure improvement.

The team implemented an action plan to improve the surveys that included creating one Senior Survey for all ABET/TAC-accredited programs within CAS, adding/updating lifelong learning questions in the Alumni Survey and Employer PP Survey and the Senior Survey, changing the administering body for the Alumni Survey to the Director of Assessment, and updating the administration methodology for the Alumni Survey. The action plan relates to those factors rated most highly in the Significant Factor Selection Matrix (Table 5), with the exception of improving the feedback loop. Further details of the action plan for improvement are in the Correction Action Matrix (Table 7).

Table 7. Corrective Action Matrix

Corrective Action Matrix					
Action	**Champion**	**Implementation Target Date**	**Effective? (yes, no)**	**Measure of Effectiveness**	**Current Status**
Create one Senior Survey	assess cmt	Jun-09	yes	document	complete
Change Administering Body for Senior Survey to Prof. Practice Office	Westheider	Jun-09	yes	document	complete
Add/Update Lifelong Learning Questions in Alumni Survey	assess cmt	Feb-09	yes	document	complete
Add/Update Lifelong Learning Questions in Employer PP Survey	assess cmt	Feb-09	yes	document	complete
Add/Update Lifelong Learning Questions in Senior Survey	assess cmt	Feb-09	yes	document	complete
Change Administering Body for Alumni Survey to Assessment Office	Westheider	May-09	yes	statistical test	complete
Update Administration Methods: paper/web and two reminders	Westheider	May-09	yes	email verification	complete

Using the changes just described, the improved surveys were piloted in the spring quarter of 2008. With the new College Assessment Committee-created College Senior Survey and its new method of administration by the university's Professional Practice Office, the response rate was 56.2%. Comparisons with previous College Senior Surveys cannot be made as those response rates are unavailable, but the rate is within those seen in other types of surveys studied during the Analysis Phase of the project. A new method to improve response rates in the Alumni Survey was implemented, which was created in response to the literature review done in the Analyze Phase. The team did not think that it could acquire funds for incentives and primarily used an experiment and cost-benefit analysis [7] to improve response rate with little cost. The Alumni Survey administration was moved from the College Career Development Office to the Director of Assessment's Office. In addition to an original mailing of the survey in June, students were also able to complete the survey using Survey Monkey on the college's web site in the Alumni area. In changing the administration method of the survey, follow-up postcard reminders were sent. As the team learned [7], the most important impact reminders have on response rate is not in their presentation but in their repetitiveness. The reminders were simple and inexpensive postcards. They were sent two weeks and five weeks after the original mailings. This new survey and method of administration proved highly successful with the rate of alumni responding, nearly doubling from 5.7% in 2006 to 11.4%. This represents a highly statistically significant increase (p-value = 0.000). The team met its goal here.

The Employer Professional Practice survey results showed a response rate of 65.1% for 2008-09. This is lower than the previous year but the decrease is not statistically significant at $\alpha = 0.05$.

Control Phase

The Control Phase of a Six Sigma project makes sure that process improvements are maintained into the future. The team has the following plans for future improvement: follow-up with improving the feedback loop when the new college structure is determined; investigate the possibility of incentives for survey completion to further improve survey response rates; further investigate, if there is managerial (decanal) support; and work to improve the assessment of Criterion 8, which received many "Concern" ratings at the last ABET/TAC visit; and, finally, determine a new DPMO and Sigma Level annually and after the next ABET/TAC visit in 2013. The team further plans to communicate the success of this project to build momentum for continuous improvement projects in areas such as classroom assessment and retention.

Conclusion

As this project has shown, the Six-Sigma methodology is an appropriate and effective tool for making improvements in educational assessment. Although a definitive conclusion as to the overall level of success of this project cannot be determined until the next ABET/TAC review, milestones along the way have had measurable success. The response rate of the Alumni Survey significantly improved (statistically and otherwise) and changes to survey instruments were achieved through consensus. The effects of the changes in administration of survey instruments other than the Alumni Survey remain to be seen. They will continue to be monitored. The need for an improved feedback loop will be addressed after the collegiate restructuring. Finally, the ABET/TAC evaluators' review of the college's assessment of students' lifelong learning after the next visit will determine if this process, currently running at a low 1.2 sigma level, improved overall.

References

[1] http://www.asq.org/learn-about-quality/six-sigma/overview/overview.html

[2] http://www.isixsigma.com/sixsigma/six_sigma.asp (viewed Dec. 10, 2007)

[3] http://www.isixsigma.com/dictionary/DMAIC-57.htm (viewed Sept. 28, 2009)

[4] http://www.abet.org (viewed Feb. 26, 2009)

[5] http://www.abet.org/why_choose.shtml (viewed Feb. 26, 2009)

[6] 2008-2009 Criteria for Accrediting Engineering Technology Programs

[7] IMPROVING ALUMNI SURVEY RESPONSE RATES: An Experiment and Cost-Benefit Analysis http://www.springerlink.com/content/u51528n44l822343/fulltext.pdf

[8] Strategies for Generalizing Findings in Survey Research, http://www.joe.org/joe/2008april/tt1.php

[9] How to Use the Data: Quality Measures - Response Rates http://www.census.gov/acs/www/UseData/sse/res/res_def.htm

[10] Measuring Customer Satisfaction 2nd Edition, Bob E. Hayes © 1998 published by ASQ Quality Press

[11] "Impact of Monetary Incentives and Mailing Procedures An Experiment in a Federally Sponsored Telephone Survey" by Brick, Collins Hagedorn, Montaquila, Brock Roth, Chapman—Methodology Report March 2006 published by the U.S. Department of Education Institute of Education Sciences NCES 2006-066

[12] "Incentives in a Business Survey: A Study in Improving Response Rates" by Kaplan and White from the Joint Statistical Meetings – Section on Survey Research Methods—2002

[13] North Carolina State University 2006 Baccalaureate Alumni Survey: Introduction, Methods, and Alumni Demographic Profile http://www2.acs.ncsu.edu/UPA/survey/reports/alum06/alum06intro.htm

[14] University of Colorado at Boulder Alumni Survey, Summer 2007 http://www.colorado.edu/pba/surveys/alumni/07/index.htm

[15] RIT dept of econ Alumni Survey http://www.rit.edu/cla/economics/alumnisurvey.html

Biographies

SARAI HEDGES is an Associate Professor at the University of Cincinnati. She earned her B.A. (Mathematics and Music, 1991) from SUNY Potsdam College and M.S. (Applied Statistics, 1993) from Bowling Green State University. She is a Certified Six Sigma Green Belt (CSSGB) and teaches courses in statistics and project management.

VIRGINIA WESTHEIDER is an Academic Director at the University of Cincinnati. She earned her B. A. (English Literature, 1983) from Rutgers, The State University of New Jersey and M.A. (Counseling Psychology, 1986) from the University of Cincinnati. She is a member of the founding class of the Institute for the Development of Excellence in

Assessment and Leadership (IDEAL) designated as a National Academy of Engineering's Center for the Advancement of Scholarship in Engineering Education (CASEE). She presents annually at the national ABET Symposium. Currently, she is Director of Assessment and Accreditation for the College of Engineering and Applied Science, University of Cincinnati.

VEHICLE PROFILE DESIGN VERSUS SOLAR ENERGY COLLECTION: STYLING CONSIDERATIONS FOR SOLAR-POWERED PERSONAL COMMUTER VEHICLES

Yi-hsiang Chang, California Polytechnic State University

Abstract

While current photovoltaic (PV) efficiencies limit the feasibility of a solar-powered personal commuter vehicle similar in size and shape to current gasoline powered automobiles, research into developing a hybrid design has been growing. The present focus of PV technologies in the automobile industry is directed towards creating a hybrid using a small gasoline motor in conjunction with PV cells. Sole use of solar energy for powering automobiles can be seen in several solar-car racing events, but the dominating designs tend to focus on maximum energy harvest/utilization efficiencies and streamlined designs, which results in a flat vehicle profile. This study looked at altering the profile to emulate the curved design of today's civilian automobiles. Using two different profiles, this study simulated a car being parked in a random orientation during a given period of time. The results were examined to determine the effect that altering the profile will have on overall solar energy collection under different weather conditions.

Introduction

Photovoltaic (PV) technology has been around for over a 150 years, but it was not until the successful demonstration of a silicon P-N junction solar cell in 1954 that its widespread usage was realized [1]. With the increasing need of alternative energy, and the continuous improvement of PV performance, it is likely that solar power will become cheaper and more prevalent. From its use in consumer devices, home and grid power generation, lighting, to stand-alone communication, warning, and monitoring systems, the pervasive use of PV is imminent [2].

While using solar energy in transportation is becoming more of a reality, little evidence exists that major automobile manufacturers are showing interest in full-scale production of solar-driven vehicles. As a result, the development of solar cars is mainly led by participants in events such as the American Solar Challenge and other solar races worldwide [3]. In this type of competition, many of the vehicles with similar designs were able to successfully finish the race. The vehicle design is bound by a certain set of rules, which limit items such as motor size, area of solar panels, amount of batteries, and type of battery. With a goal of traveling up to 1,500 miles across the country solely on solar power, the design is mainly governed by variables such as weight, energy-harvest capability, and wind resistance. The PV cells are usually oriented almost parallel to the earth. This is primarily done to enlarge energy harvest and reduce wind drag.

Bound by such limitations and being focused on maximum efficiencies results in solar vehicles with flat profiles that travel close to the ground and allow just enough space for one human driver, as shown in Figure 1. Designing the car in this manner allows for the PV cells to achieve a direct beam radiation at almost 0^o angle of incidence (AOI) during peak sunlight hours, resulting in less radiation loss from scatter [4]. In other words, the vehicle is able to collect a substantial amount of energy at peak irradiance hours, or when AOI is very small. In such a design, nevertheless, energy harvest in the morning and afternoon hours is not maximized due to large AOIs.

Figure 1. The solar car by University of Michigan, which took the first place in 2010 American Solar Challenge [5]

Minimizing AOI is crucial to achieving maximum power output, but in doing so the race vehicles sacrifice space and comfort because of their flat and compact design. Considering the practicality of a solar-powered personal commuter vehicle, the vehicle design would have to sacrifice some of the optimal AOI to create more cargo space. Furthermore, such a vehicle would need to have adequate head space for the driver to sit in an upright position, use a steering wheel, and even have space for safety features. While such a personal commuter vehicle would not have to adhere to the same set of rules established for various solar car races, the technologies used in these races provide a good baseline, and certain design considerations used in constructing these racers apply. Thus, the goal of this study was to investigate the influence of vehicle profile on its solar-energy harvest

capability in order to determine the feasibility of a solar-powered personal commuter vehicle.

Related Research

The energy-harvest capability of solar panels can be affected by factors such as cell operation temperature [2], dust accumulation [6], and environmental aspects of vehicle deployment regions including altitude, weather patterns and shadowing of landscapes [7]. Cloud cover during the harvest of solar energy also has an impact on the amount of spectral irradiance reaching the PV cell. Spectral irradiance, comprised of both direct and diffuse components, is measured in watts per square meter (Watt/m^2). In addition to absorbing visible (380-780nms) and near-infrared (780-4000nms) solar radiation, local cloud cover might reflect up to 70% of the direct radiation [8]. With varying weather patterns throughout the world, environmental attributes of each location must be carefully taken into account in order to maximize the module output, and keep associated hardware and operation costs to a minimum.

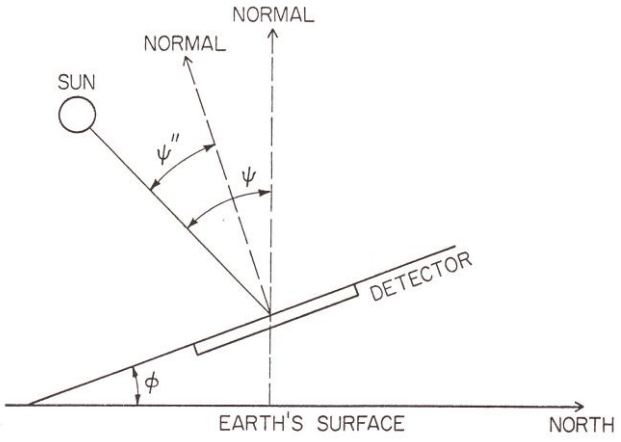

Figure 2. A diagram of the angle of incidence: The angle of incidence is represented by ψ'' and is referenced with the normal of the detector (solar panel). The actual tilted angle of the detector is denoted by ϕ [7]

Angle of incidence (AOI) of the PV panels, as illustrated in Figure 2, also influences the solar-energy harvest ability. An AOI above 45^o greatly reduces the absorption of the sun's direct radiation and must be considered when attempting to minimize reflectance on the cell itself [9], and thus is often considered undesirable for use on a solar-powered vehicle. In addition, the yearly orientation of the PV cell in relation to the sun is another crucial parameter to optimize power generation. The glass used on solar panels also causes reflectance, which is associated with an optical loss. When using a glass-covered module, the reflectance increases dramatically above an AOI of 60^o [10]. Such loss in diffuse spectral irradiance is important to note, and makes analysis of this factor crucial when setting up a fixed module. The study performed by King et al. [9] points out that while annual loss caused by a low AOI is small, it can have a significant monthly effect.

A study by Ahmad, Hussein, and El-Ghetany [11] used a computer model to predict optimal tilt angles for yearly power generation in Cairo, Egypt. The study concluded with the optimal tilt angle (20^o to 30^o) about solar power generation specifically in Cairo, and confirmed the importance of AOI and the tilt angle on the overall performance of the PV array. Using a mathematical model, Tang and Wu [12] created a table and map for optimal tilt angles in China. Considering that China's territory covers many climates and latitudes, such a model proved beneficial to this emerging country. Tang and Wu's study pointed out that different months of the year have different optimal tilt angles based on the change in the sun's angle to the fixed PV module and their mathematical model successfully predicted actual diffuse radiation values in 182 different locations throughout China where pollution levels were low [12]. This study can serve as a guide for PV module installation in China, and once again confirms the effects of both diffuse solar irradiation and AOI on a solar module's efficiency in any location.

Martin and Ruiz [6] discovered that angular losses due to AOI are generally not taken into account when estimating the energy production of PV systems. The resulting effects are inaccurate corrections to current systems, and the potential neglect of increased productivity of the cell. Their model, developed to analyze optical losses for silicon PV modules, uses reflectance and AOI as major contributors to overall decreased cell performance. Upon completing their study, Martin and Ruiz confirmed the effectiveness of their model, and noted that the type of solar technology used has no significant impact on the angular loss, but AOI and reflectance are significant contributors.

Recent research has looked into developing a hybrid solar car that reduces the consumption of gasoline. A study conducted by Arsie et al. [13] developed a model for optimizing a solar hybrid design. Using a calculator developed by the US National Renewable Energy Lab to determine optimal tilt angle in both the horizontal and vertical directions, they reported that panels aligned 90^o to the road (vertical direction) on an automobile would generate about only one third of their capable power, and about 45% to 65% of those placed horizontally. They also noted that the feasibility of these panel orientations is questionable. Such studies are beneficial as they look at aspects such as weight, aerodynamics, optimal solar tilt angle, power generation and energy storage. Investigating the design of solar hybrids is important as it allows many problems to be uncovered prior to

attempting the build and full-scale production of a commuter vehicle powered solely by a PV system. By adopting technologies such as multi-junction panels with efficiencies of nearly 35% could eventually result in an all-solar powered car [14].

Solar-powered Personal Commuter Vehicle

Positioning a solar array to minimize AOI and reduce reflectance results in better utilization of the available solar irradiance. A majority of PV technology is used for generating electricity for buildings and houses. These applications tend to rely on either fixed or tracking systems; the former is generally set between 20^o and 30^o of AOI (depending on latitude), while the later follows the sun and uses the most efficient AOI to maximize the conversion of direct spectral irradiance. Such knowledge can be applied to other technical areas such as automobiles by choosing angles that will reflect the best efficiencies for specific geographic locations.

Little research has trained on creating a solar-powered personal commuter vehicle, however. Every day, people commute to work; once they arrive, they proceed with their car parked outside. Given a parking area exposed to the sun, the commuter vehicle's PV cells could charge a set of batteries over the course of the day while sitting outside, and may collect enough electricity for its owner to commute to and from work. Once home, the automobile would then be hooked into either a standard 110V or 240V outlet to trickle charge during the night. This would ensure the user with enough electrical power in the batteries to commute back to work, thus restarting the cycle. With the shape of the car being curved instead of flat, as discussed previously, it would provide the driver more comfort and cargo space. With a proper design, such a vehicle may be able to offer a practical application for commutes up to a 30-mile round trip.

In addition to weather pattern and AOI, another factor that would affect a vehicle's solar harvest capability is parking orientation. Once arriving at work, the driver will face a multitude of parking options, and must make a choice as to the most efficient parking orientation (which way the front, rear, or side of the car will face). The user could be parking in a North/South orientation, an East/West orientation, or anything in between. Each of these orientations will offer users differing amounts of solar radiation over the course of their 8-hour workday, with the East/West and North/South orientations representing the potential extremes. The commuter, however, may have few parking options from time to time due to parking-lot configuration or space availability. This could result in a parking orientation that is less than optimal for overall solar-power generation.

To better understand the proposed vehicle profile and its performance of solar-energy harvest under various parking orientations and weather conditions, this study investigated the total amount of electricity collected by two different vehicle profiles, namely flat and curved profiles. Based on the previous discussion, the dependent and independent variables used in the study were identified. Independent variables included vehicle profile (flat or curved), parking orientation (North/South or East/West), peak solar irradiance, and daily high temperature; data for the latter two independent variables was retrieved from online public records. The dependent variable was actual energy collected in watt-hours. Each profile's daily output in wattage was compared on a daily basis, and the total energy collected was the area under the power or wattage curve. The hypotheses of this research are listed as below:

- **H_1**: During an 8-hour interval, there is a significant difference in the amount of total daily power produced by the curved and flat profiles.
- **H_2**: During an 8-hour interval, there is a significant difference in the amount of total daily power produced between curved profiles parked in East/West and in North/South orientations.
- **H_3**: During an 8-hour interval, there is a significant difference in the amount of total daily power produced between flat profiles parked in East/West and in North/South orientations.
- **H_4**: During an 8-hour interval, there is a significant difference in the amount of total daily power produced by the solar profiles between different weather patterns.

Experimental Design

This study looked at a scaled-down version of this possible solar commuter vehicle's profile. While not using as many angles as the envisioned vehicle, it examined the difference between a flat and curved profile of equal surface area. Each profile consisted of five equal-sized solar panels. Shown in Figure 3, the flat profile was built to position the PV panel in parallel with the earth's surface. The curved profile was made up of 5 sections. Four of the sections were tilted 15^o, 30^o, -30^o and -15^o, with respect to ground, while the fifth section was at a zero-degree orientation, much like the flat profile. The combination of panel tilt angle and corresponding area coverage percentage (in this case 20% for each tilt angle) could be used to describe the potential profile of a solar commuter vehicle. To simplify this study, the focus was on those profiles that were symmetrically flat or curved.

Figure 3. Flat (top) and curved profiles with five solar panels wired in series

In addition to examining the energy collection pattern of different profiles, this experiment also investigated whether parking orientation or weather patterns would change the amount of electricity harvested by specific vehicle profiles. The specific curved profile chosen could provide a good baseline for future investigations for several reasons: It could still effectively handle changes in irradiance through the day (and utilizing peak irradiance at midday); it resembled a realistic design for a personal commuter vehicle; and it was significantly different from the control (the flat profile). Based on the findings from this profile, future designers can decide whether to increase or decrease the tilt angles, change the percent coverage of certain angles, or revert back to a flat design.

Table 1. 2-way factorial design showing four treatments

Profile	**Parking Orientation**	
	East-West	North-South
Curved	Power/Day	Power/Day
Flat	Power/Day	Power/Day

A two-way factorial design, shown in Table 1, was used to assess two different profiles at two different parking orientations. For the purposes of this study, the profiles acted as fixed arrays while they are exposed to daily sunlight. The North/South and East/West orientations represent the extreme possible parking scenarios. An East/West orientation was exposed to sunlight through the course of the day with an unfavorable AOI. Being oriented in a North/South orientation allowed for an optimal AOI for the part of the curved profile facing south. The other half faced north and had to rely on midday solar radiation as well as diffuse radiation.

An additional copy of each profile was used, resulting in a replicate for each treatment. This was done so that both the curved and flat profiles were facing both orientations during each blocking period resulting in a complete randomized block. There were four total structures (two flat and two curved), which were randomly assigned to either of the orientations. A complete randomized block was used (see Table 2), which assigns two profiles to the North/South orientation and two to the East/West orientation. Each orientation had to have both a curved and a flat profile when testing during each two-day time interval. In other words, there cannot be three profiles facing one direction and one profile facing the other. Such an arrangement of the profiles was tested for two consecutive days to account for day-to-day changes in weather.

Table 2. Assignment of profiles to East/West (EW) or North/South (NS) over the two-day intervals (blocks). Each profile is randomly assigned to be profile one or two

Profile	Days 1-2 (Block 1)	Days 3-4 (Block 2)	Days 5-6 (Block 3)	Days 7-8 (Block 4)
Curved 1	EW	NS	EW	NS
Flat 1	EW	NS	EW	NS
Curved 2	NS	EW	NS	EW
Flat 2	NS	EW	NS	EW

These directions were chosen to represent the extreme cases of a potential parking situation. With each of the profiles being fixed in one of the orientations for a two-day interval, they simulated many fixed-plate collectors. A fixed array that is aligned in a North/South/south direction has access to the highest yearly average solar irradiation in the Northern hemisphere. This is due to that fact that during the winter months when the sun is lowest on the southern horizon it is more beneficial to be facing south. An East/West orientation is exposed to a different quantity of solar irradiation. Initially, the flat profiles were randomly assigned to one of the two orientations. By default, the curved profiles were placed in the alternate direction. During each day of the two-day interval, measurements of power were taken with the data logger that was connected to and powered by a laptop computer. Following this two-day interval, the profile orientations were reassigned and the same measurements were taken over the same two-day period.

Shown in Figure 4, each of the four profiles had five total solar modules, and the five different sections were wired in series. Sized in 50x16.5x3 cm^3, the amorphous solar panels used in this experiment could operate between -40° and

176°F and had a maximum output of 1.8W. All entry points were sealed using clear silicon to prevent moisture. The PV panel-holding structures were constructed in 2x2 and 2x3 Douglas fir. The series wiring of these solar panel resulted in each of the profiles having a maximum voltage rating of 80 volts (16V x 5) and a maximum current rating of 125mA. It must be pointed out that while each panel was rated for 12V, they actually produced between 13V and 16V, depending on the amount of solar irradiation available and the temperature.

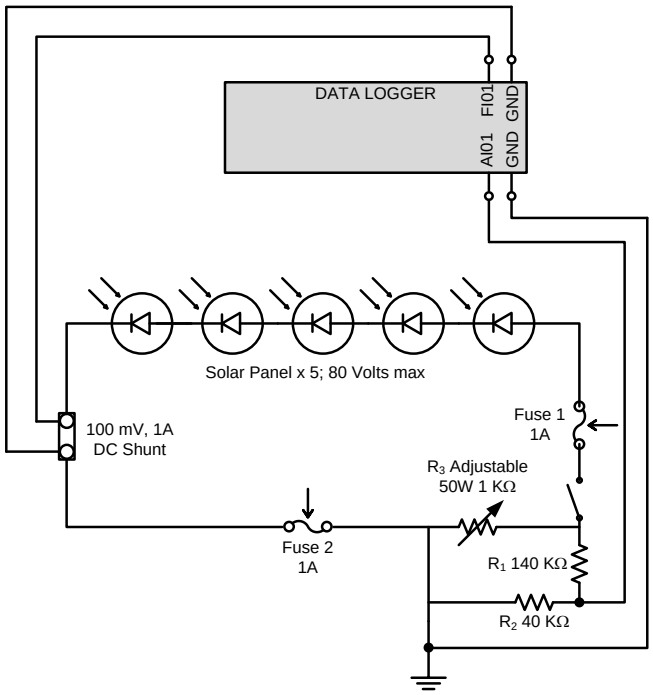

Figure 4. Schematic diagram for the measurement system

Measurement of both current and voltage was accomplished with the use of a Labjack data logger and a Dell laptop. The laptop used the software provided by Labjack called DAQ Factory to record both the current and voltage. The data logger is comprised of 16 channels. Four of these channels are high voltage channels (0 – 20V) and were used for measuring the maximum 80V generated by each profile. Because these channels can only handle a maximum of 20V, a voltage divider circuit was used to reduce the voltage entering each channel. The voltage was reduced from the 80V generated by each profile to below the 20V maximum specified on the data logger's channel. This did not, however, have an effect on the readings generated by the data logger; it only changed the scaling of what was entering each channel to avoid component failure.

Four of the remaining twelve low-voltage channels (0 - 2.5V) were dedicated to measuring current. This was done by the use of an electrical shunt. The shunt (a very precise resistor) was wired in series with each profile before it reached the data logger. The data logger then received a voltage reading based on the voltage drop across the shunt and recorded it on the laptop. The voltage reading was then converted into a current reading and corresponding energy collection was calculated in watt-hours. Both the data logger and computer were housed in a sealed plastic box to protect them from weather. Four of these circuits were constructed, one for each profile. Attribute measurements showed these four circuits performed very similarly with the largest difference of less than 0.5%. Thus, no variation was associated with the measurement circuit.

The observatory at La Lomita Ranch (35.24, -120.62) was used for testing. This site was chosen because it has access to power, which is necessary for running the laptop computer and data logger. It also provides exposure to sunlight during the 8am – 5pm testing period. The experiment was conducted from April 14 to May 7, 2009. Each day after testing was complete, the computer was shut down and the components were covered with a tarp until the next day. In the mornings, all of the materials were once again uncovered for data collection.

The four profiles at the two orientations were analyzed using a two-way factorial design, as presented in Table 1. The statistical method of blocking was used to account for potential variations in weather during each of the two-day testing intervals. Both peak solar irradiation and daily high temperature were used as covariates in the analysis. Each block consisted of each of the possible treatments. Both variables were recorded and could be used as covariates in the analyses if they were deemed significant.

An 8-day pilot study was done prior to the primary experiment. The purpose of this study was necessary for two reasons: To find out any unforeseen problems, as well as to determine the sample size needed to make the analysis statistically powerful. It examined the following potential problems: Robustness of the solar panels, the measurement circuits, the laptop's ability to record measurements, the data recording software and functionality of the wooden structures. This pilot study also provided enough data to do an initial analysis of the first 8 days in Minitab. A significance level of 5% was chosen in the analysis. With the results from the pilot study, issues such as voltage and current measurement as well as equipment resolution were fixed by modifying the measurement system.

With these issues fixed, the primary experiment proceeded for sixteen days. Data from the 16 days was then analyzed. Based on the data, it was clear that the sample size was large enough, because the independent variables were indeed significant at the 5% significant level. An indicator of insufficient sample size would have been that the majority of

independent variables were insignificant. Because this was not the case, a power analysis was not necessary.

Prior to analysis, the raw data had to be converted into usable numbers for two reasons: (1) A voltage-divider circuit was used and (2) the data was collected solely in voltage. To get the correct current reading, the equation ((raw voltage number – 0.4)*10)/201 was used. The amplifier's default offset quantity was 0.4. The multiplication of 10 was done based on the 1–amp, 100mV rating of the shunt. The gain factor of the LJ Tick Amplifiers was 201. The voltage numbers were converted based on the voltage-divider ratio of 0.222 (e.g. 40/180) between the true number of volts and the reading on the computer. Total energy collection can be represented in watt-hours, which was the area under the power curve.

Results and Discussion

Figure 5 illustrates examples of the typical energy collection patterns of the profiles studied during the test period. The vertical axis represents the power in watts for a specific time period between 8am and 5pm. Day 4 depicts completely sunny conditions. This graph is very smooth, with each of the profiles exhibiting unique power generation sequences over the course of an 8-hour exposure. Day 5 exhibits a different scenario. The early morning shows a very undulated and uneven pattern, which was a result of morning clouds ultimately burning off leaving sunny conditions. When compared with Day 4's result, it is obvious that there was much less solar irradiation available on Day 5. Finally, Day 6 offers the most unique power-generation sequences. Day 6 is graphed on the same scale as previous days, which highlights how much less total daily power was generated. This entire day was cloudy and only offered roughly a third of the total solar irradiation of a completely sunny day.

The main effects and interactions between independent variables were determined by examining group means of different treatments. Table 3 indicates that there were main effects of profile, orientation, and set toward the daily power collection. During the 16-day experiment, flat profiles on average collected more energy than curved profiles. In the mean time, profiles parked in North/South orientation on average collected more energy than profiles parked in East/West orientation. Finally, set 2 on average collected more energy than set 1.

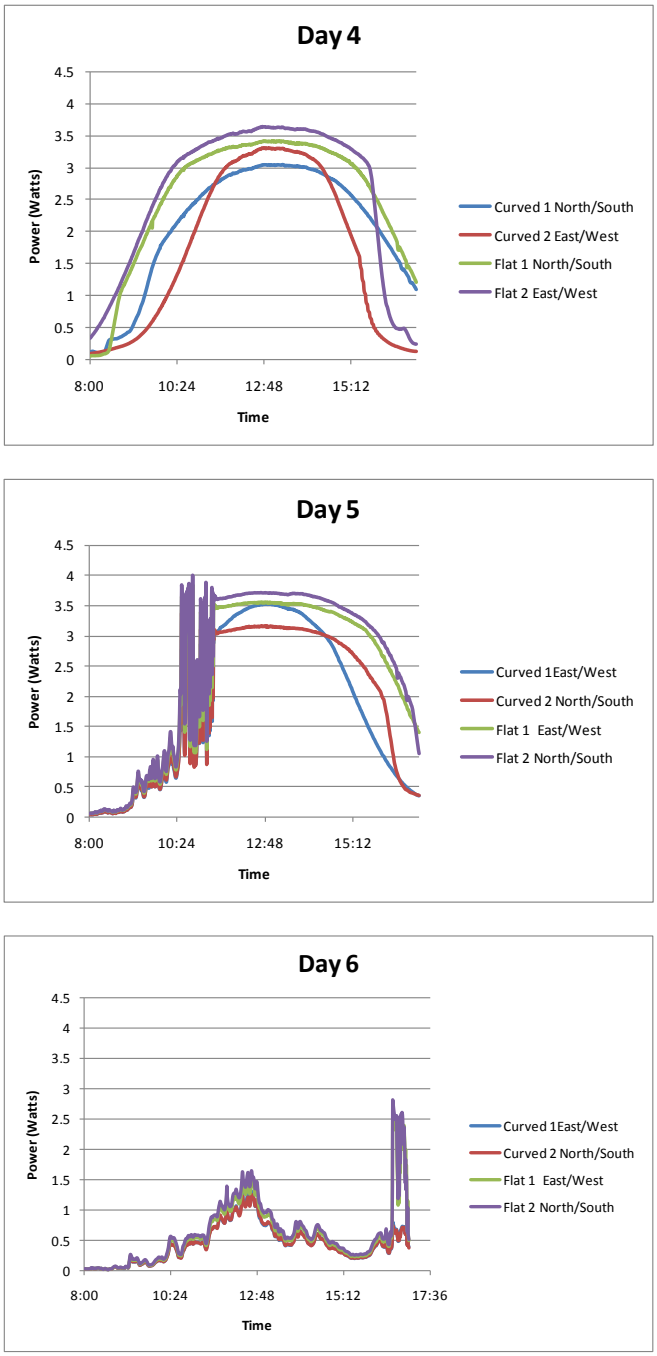

Figure 5. Graphs of time vs. power from days 4, 5, and 6. Solar irradiation was 974, 835, and 346 watts/m^2 respectively, and the high temperature was 72.5, 70.0, and 60.1 °F respectively

Table 3. Group means of power (Watts) collected per day: Main effects of Profile, Parking Orientation, and Set

Profile	Parking Orientation		Group Average
	EW	NS	
Curved	1891.74	2088.98	1990.36
Flat	2606.23	2624.02	2615.12
Group Average	2248.99	2356.50	

Profile	Set		Group Average
	1	2	
Curved	1999.58	1981.15	1990.36
Flat	2547.11	2683.14	2615.12
Group Average	2273.34	2332.15	

Figure 6 illustrates the interaction between profile and orientation, and between profile and set. In examining the profile*orientation plot, it is clear that there was a difference in total daily power generation between curved profiles parked in East/West and curved profiles parked in North/South orientations. There was much less difference between the total daily energy generated by flat profiles parked in either orientation. In both orientations, flat profiles generated more total daily energy than curved profiles. As seen in the Profile*Set interaction plot, there was a difference in the amount of total daily energy collected between different profiles within both set 1 and set 2. Profiles in set 1, however, had much less difference in daily energy collection than profiles in set 2.

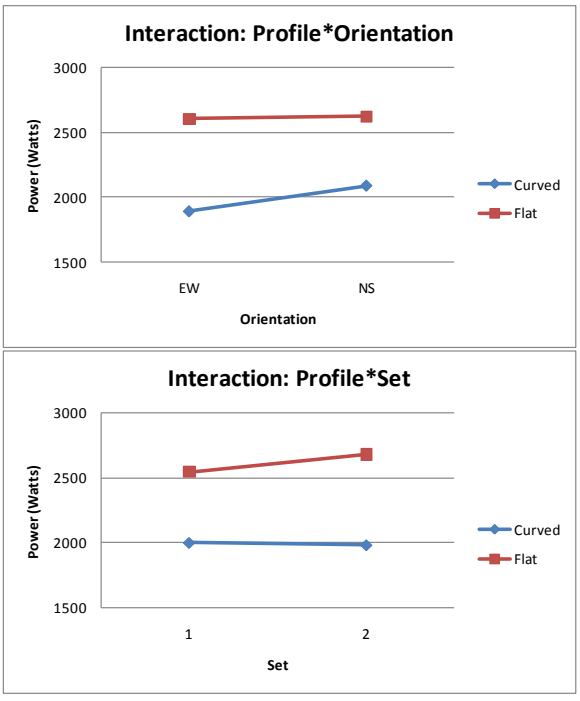

Figure 6. Interaction between Profile and Orientation (top) and interaction between Profile and Set

To determine the significance of main effects and interaction between independent variables, experimental data was analyzed in a two-way ANOVA, shown in Table 4. According to the comparative statistical results, at the 5% significance level the main effects profile, orientation, and day all have significant main effects on total power collection. Nevertheless, there was no significant main effect of the set (e.g. curved 1/flat 1 vs. curved 2/flat 2) on the daily total energy collection at the 5% level. At the 5% significance level, both interactions, profile*orientation and profile*set, significantly affected the daily total energy generation. According to the r-squared adjusted, 94.59% of the variation in the total power output could be explained by the profile, orientation and day. This shows a good linear relationship between the dependent and independent variables used in the study.

Further analysis was done using Tukey pairwise comparisons to minimize both Type I and Type II errors. The following outlines the results from the study:

Table 4. ANOVA General Linear Model results for 16 full days of testing. Daily total power outputs were used in the analysis, which did not look at individual time intervals during the day

Source	Degrees of freedom	Type III sum of squares	Mean square	F Value	*p* Value
Profile	1	6245245	6245245	279.81	0.000
Orientation	1	184931	184931	8.29	0.006
Profile*Orientation	1	128818	128818	5.77	0.021
Set	1	55328	55328	2.48	0.123
Profile*Set	1	95436	95436	4.28	0.045
Day	15	18312885	1220859	54.7	0.000
Error	43	959734	22319		

- When looking at all pairwise comparisons among levels of profile, a level of 95% confidence can be used to state that flat profiles produce between 549.4 and 700.1 more watts per day than the curved profiles.

- When looking at all pairwise comparisons among levels of orientation, a level of 95% confidence can be used to state that a North/South orientation produces between 32.2 and 182.8 more watts per day than an East/West orientation.

The interaction between profile and orientation was also analyzed using Tukey pairwise comparisons:

- When looking at all pairwise comparisons among levels of profile*orientation, a level of 95% confidence can be used to state that a curved profile in a North/South orientation produces between 56.1 and 338.4 more watts per day than an curved profile in an East/West orientation.

- When looking at all pairwise comparisons among levels of profile*orientation, a level of 95% confidence can be used

to state that a flat profile in an East/West orientation produces between 573.3 and 855.7 more watts per day than an curved profile in an East/West orientation.

- When looking at all pairwise comparisons among levels of profile*orientation, a level of 95% confidence can be used to state that a flat profile in a North/South orientation produces between 591.1 and 873.5 more watts per day than an curved profile in an East/West orientation.

- When looking at all pairwise comparisons among levels of profile*orientation, a level of 95% confidence can be used to state that a flat profile in an East/West orientation produces between 376.1 and 658.4 more watts per day than an curved profile in a North/South orientation.

- When looking at all pairwise comparisons among levels of profile*orientation, a level of 95% confidence can be used to state that a flat profile in a North/South orientation produces between 393.9 and 676.2 more watts per day than an curved profile in a North/South orientation.

- Finally, there is no significant difference between in the total power generated by flat profile in an East/West orientation, or flat profile in a North/South orientation.

The test of hypotheses is discussed in the following:

H_1: During an 8-hour interval, there is a significant difference in the amount of total daily power produced by the curved and flat profiles.

a. **H_o: $\mu_{curved} = \mu_{flat}$**
   H_a: $\mu_{curved} \neq \mu_{flat}$
b. At the 5% significance level, H_o is rejected and, therefore, the profile shape is associated with a significant difference in the amount of total daily power produced.

H_2: During an 8-hour interval, there is a significant difference in the amount of total daily power produced between curved profiles parked in East/West and in North/South orientations.

a. **H_o: $\mu_{east/west} = \mu_{north/south}$**
   H_a: $\mu_{east/west} \neq \mu_{north/south}$
b. At the 5% significance level, H_o is rejected and, therefore, the orientation is associated with significant difference in the amount of total daily power produced by the curved profile.

H_3: During an 8-hour interval, there is a significant difference in the amount of total daily power produced between flat profiles parked in East/West and in North/South orientations.

a. **H_o: $\mu_{east/west} = \mu_{north/south}$**
   H_a: $\mu_{east/west} \neq \mu_{north/south}$
b. At the 5% significance level, H_o is not rejected and, therefore, it is not fair to conclude that orientation impacts significantly the amount of total daily power produced by the flat profile.

H_4: During an 8-hour interval, there is a significant difference in the amount of total daily power produced by the solar profiles between different weather patterns.

a. **H_o: $\mu_{day} = 0$**
   H_a: $\mu_{day} \neq 0$
b. At the 5% significance level, H_o is rejected and, therefore, day is associated with a significant difference in the amount of total daily power produced

Limitations and Implications

Three major limitations of this study, namely weather pattern, angle of incidence, and parking location, are discussed in this section.

(1) The Change of Weather Pattern: There were many changes in weather during the experiment. While many of the days were sunny, there were a few days that started with early morning clouds. Since there were not many days that offered complete cloudiness over the course of 8 hours, definite conclusions cannot be drawn on how well different profiles performed in completely cloudy conditions. It also implies that the application of this research is limited by its geographic location and the time of operation. In addition to the weather conditions that may change from time to time, the daily solar energy collection by vehicles deployed will be quite different because solar irradiation will be different at different latitudes and in different months of the year.

While all components were sealed to prevent water destruction, they were not built to be waterproof. With the high cost of the materials, and a limited window of opportunity to complete the experiment, no data collection was done during rainy days; no conclusion can be drawn regarding the performance of different profiles during rainy conditions. Ideally, both cloudy and rainy conditions should be tested more thoroughly before a specific profile of a solar commuter vehicle can be determined.

(2) "Optimal" Angle of Incidence (AOI): As indicated in this study, for these two specific profiles, a flat shape is more effective in daily energy collection than a curved shape. The idea that the curved profile will have the best AOI at all times during the day is valid, but only applies to certain panels. As this study shows, the flat profiles still collected more power during the morning and evening hours. While having a less than optimal AOI during those two periods, the flat profile has the same light exposure on all of its panels. This appears to be superior in power generation to the curved

profile where just one, two, or even three out of the five panels experienced optimal AOI, and the others having little to no solar exposure at all.

The curved profiles' weakness is visible during the middle of the day when peak solar irradiation is available. This is an important window of time that needs to be maximized to improve total daily power generation. With a proper tilt angle, the flat profile is able to fully utilize this time frame, making the curved profile inferior in power generation. It was the thinking that the curved profile could possibly make up for this inferiority during peak solar irradiation by maximizing morning and afternoon sunlight, as well as the direct and diffuse components of the solar irradiation during the course of a day. The finding of this study, however, was not able to confirm such thought.

(3) Parking Location: Parking the vehicle also becomes a critical element in determining the best profile. In order to collect solar energy, the proposed vehicle must be parked in a location that is directly exposed to the sun. In urban areas where such personal commuter vehicles might be deployed, parking structures usually do not provide large uncovered parking lots, not to mention that the shadow of nearby buildings could block the direct sunlight. Some may argue that commuters in such urban areas would take public transportation instead, but the low probability of always being able to park under the sun is a substantial limitation.

As the data shows, orientation has a significant impact on the curved profile's total daily power generation, with the extreme of North/South providing the best energy collection. While the flat profile did not exhibit any significant difference when parked in the two different extreme orientations, it is also known that avoiding a flat design is crucial to providing the comfort and cargo space sought after in a commuter vehicle. It appears that the ultimate solution lies somewhere between the two. Nevertheless, worrying about parking orientation is likely to be the last thing a daily commuter wants to be concerned with. Traffic and simply finding a parking spot are likely to be more serious concerns, especially in a highly-populated area. Thus, reducing the parking orientation's impact on the vehicle's ability to collect power should be seriously considered.

Conclusions and Future Research

While this specific combination of varying angles and coverage was not as efficient as one would have hoped, it has provided valuable insight as to the effects of creating a more curved profile shape. As stated previously, the half-egg shape is just one of the many combinations of angles and percent coverage possible. For this specific research, such a combination proved to be inferior to the flat shape that entrants into the solar car race strive for. Its inferiority does not mean a future solar commuter vehicle is unattainable. What it does suggest is that when increasing the tilt angle to allow for a more spacious commuter vehicle, the designer is sacrificing the vehicle's ability to generate power while it is parked. In recognizing this fact, the designer must try to maximize the flat area on the commuter vehicle that can be parallel with the earth.

Because of the restrictions on design, building an aesthetically pleasing solar commuter vehicle will be a challenge. While future research should investigate designs with solar panel tilt angles and percent coverage that fall in-between the two tested in this study, the designers should also consider other options to reduce the impact of AOI. Aside from changing the quantity of different angles used, the researcher should also consider changing the percent coverage of varying angles. This study used a symmetrically-shaped curved profile in an attempt to track the sun. Such a methodology did not prove as beneficial as one would have hoped. Because of this, future research should look at creating asymmetrical designs to test their effectiveness. While it may not address issues such as parking location or weather pattern, it could increase the overall energy collection making it a worthwhile tradeoff.

While future research should investigate designs with angles and percent coverage that fall in-between the two tested in this study, researchers should also consider other options for minimizing the effects of AOI. Using modular arrays or hidden panels that are deployed only during parking should not be ruled out. Such a design could allow for an aesthetically pleasing appearance while still being able to maintain high levels of power generation. Designers should keep in mind that focusing on functionality is the most important aspect to the success of such a vehicle. Building the ultimate solar commuter vehicle will require that the designer carefully balance the efficiency of the solar array, the comfort of the operator, as well as the safety of the vehicle on the road. The proper combination does exist and can only be exposed with further research.

References

[1] Lundstrom, M. (1995). Forward. In L. Partain (Ed.), Solar cells and their applications (pp. xxi-xxiii). New York: Wiley-Interscience Publication.

[2] Zweibel, K. (1990). Harnessing solar power. New York: Plenum Publishing Corporation.

[3] American solar challenge (2010), Retrieved October 10, 2010, from http://americansolarchallenge.org/events/asc2010/.

[4] Riordan, C. (1995). Solar resource characteristics. In L. Partain (Ed.) Solar cells and their applications (pp. 443-468). New York: Wiley-Interscience Publication.
[5] Schwartz, A. (2010). University of Michigan Solar Car Team Wins American Solar Challenge | Inhabitat - Green Design Will Save the World, Retrieved October 1, 2010, from http://inhabitat.com/2010/06/29/university-of-michigan-solar-car-team-wins-american-solar-challenge/.
[6] Martin, N., Ruiz, J. M., (2000). Calculation of the PV modules angular losses under field conditions by means of an analytical model. Solar Energy Materials & Solar Cells, 70, 25-38.
[7] Nelville, R. (1978). Solar energy conversion: The solar cell. New York: Elsevier/North Holland Inc.
[8] Nann, S., Riordan, C., (1990). Solar spectral irradiance under clear and cloudy skies: measurements and semiempirical model. Journal of Applied Meteorology, 30, 447-462.
[9] King, D.L., Boysen, W. E., Kratochvil, J. A., (1997). Measuring solar spectral and angle-of-incidence effects on photovoltaic modules and solar irradiance sensors. 26th PVSC, 1113-1116.
[10] King, D. L., (2002). Photovoltaic module and Array performance Characterization methods for all system operating conditions. Proceeding of NREL/SNL Photovoltaics Program Review Meeting, 1-22.
[11] Ahmad, G. E., Hussein, H .M. S., El-Ghetany, H. H., (2003). Theoretical analysis and experimental verification of PV modules. Renewable Energy, 28, 1159-1168.
[12] Tang, R., Wu, T. (2004). Optimal tilt-angles for solar collectors used in China. Applied Energy, 17, 239-248.
[13] Arsie, I., Marotta, M., Pianese, C., Rizzo, G., Sorrentino, M., (2005). Optimal design of a hybrid electric car with solar cells. Proceeding of 1st Autocom Workshop on Preventative and Active Safety Systems for Road Vehicles, 1-12.

Biography

YI-HSIANG CHANG is an assistant professor in Industrial Technology at California Polytechnic State University. He received a B.S degree in Mechanical Engineering from Tatung Institute of Technology in Taiwan, a M.S. degree in Mechanical Engineering from Carnegie Mellon University, a M.S. degree in Industrial Engineering and a Ph.D. degree in Technology from Purdue University. Dr. Chang's research interests are in Sustainable Design, Spatial and Cognitive Learning, and Product Lifecycle Management. Dr. Chang may be reached at ychang03@calpoly.edu.

CELLULAR AUTOMATA AND STATE SPACE REPRESENTATION APPLIED TO URBAN LAND-USE MODELING: NORFOLK

Thongchai Phairoh, Virginia State University; Ayodeji Demuren, Old Dominion University; Keith Williamson, Virginia State University

Abstract

The combination of cellular automata (CA) and system dynamics were used to predict the evolution of individual components in urban growth. Feasibility was also considered for use in the study of industrial or commercial growth development. Numerical simulations were performed using the city of Norfolk, Virginia, as a test case. The simulation results show that industrial activities are distributed around the railroad.

Introduction

Urban change is a complex spatial phenomenon controlled by many factors. The geographical conditions of area, socio-economic status, infrastructure supply, demographic features and the potential of population growth, planning and zoning constraints, environmental protection regulations as well as group and individual behavior, all play a role in the process of urban development. The development of a predictive science of urban structure has been characterized by a multitude of approaches from a variety of disciplinary perspectives. Different approaches are dependent on how to treat urban structure and urban change in terms of space and time. One interesting method is the use of cellular automata (CA).

Cellular automata have two characteristics that make them inherently attractive for application to geographical problems. The first is that they are, as noted, intrinsically spatial; the second is that they can generate very complex forms by means of very simple rules. CA was combined with fuzzy logic control to predict urban growth [1]. Fuzzy logic control was used to calculate the development of each cell. Calibration is a time-consuming process in CA. To overcome this, neural network was utilized with CA to reduce the time requirement [2].

This study used the combination of CA and a linear state space model to predict the development of housing, industrial, and commercial activities in the area of interest. CA was used to find the transition possibility of the considered cell as functions of its own state and the state in neighborhood cells. The linear state space equation represents the dynamics of each component in the area under consideration.

Cellular Automata

White and Engelen [3] used CA to predict the evolution of land-use development. The area was divided into small sub-regions referred to as cells. Each sub-region had its own state, which could be changed by effects of its present state and those of neighborhood cells. For example, an area is divided into a rectilinear grid. The size may be varied from 10 to 500 meters. Smaller sizes have smaller error in state representation, but higher computational times would be required. Cell states most commonly represent land cover and land use, but they may also be used to represent any spatially-distributed variable. In keeping with the spirit of the simplicity of CA, applications most often adopt either the Von Neumann neighborhood (consisting of the four cells directly adjacent to the sides of the cell), or the Moore neighborhood (the eight adjacent cells), as shown in Figure 1.

The transition rules are the heart of CA. They represent the logic of the process which is being modeled and, thus, determine the resulting spatial dynamics. Since they are as varied as the processes they represent, it is difficult to generalize them. They may be simple, as in the "Game of Life" or spatial voting models where a cell takes the state of the majority state in its neighborhood, or complex; in the limit the rule may consist of an entire sub-model. Rules developed to apply to neighborhoods with a large cell radius will typically represent local spatial processes that include a distance-decay effect. For example, a rule relating the future land use of a cell to the actual land use within an eight-cell radius will represent the attraction and repulsion effects of the various land uses in the neighborhood, but with an attenuation of the effect of the more distant cells. In models of human systems, it is usually appropriate, or even necessary, to introduce a stochastic element into the transition process in order to capture the effects of imperfect information and differences among individuals.

Again, noting the simplicity of CA, applications most often adopt spatial modeling. In CA models, time is normally discrete, with a simultaneous updating of all cell states after the rules have been applied to each cell using the current configuration. For many applications, the appropriate time

step is a matter of convenience; e.g., iterations representing 1 year may be adequate in a model of land use change.

Component Development

The changing of each component in the urban model was considered in this study. As well, Markov chain and linear state space methods were utilized to predict the number of each component. Weng [4] used the first-order Markov chain to predict the land use in the Zhujiang Delta of China, and Lopez et. al., [5] used it to predict the land-use changes in Moelia City, Mexico. Aaviksoo [6] compared the first- and second-order Markov chain to predict the plant cover and land-use types. The changing of components in the cellular-automata analysis is controlled by either Markov chain or linear state space systems.

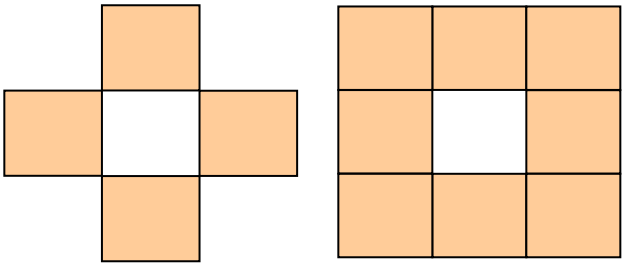

Von Neumann Neighborhood **Moor Neighborhood**

Figure 1. Neighborhood Cell

Urban growth is considered in its own state by how developed it is; i.e., is it urban, suburban, or rural? The factors of interest are: distance between any given cell and whether it is urban or suburban, a road, expressway or railroad; if there are neighborhood states; and, its agricultural suitability.

Markov Chain

Markov chains are stochastic processes that can be parameterized by empirically estimating transition probabilities between discrete states in the observed systems. For a Markov chain of the first order, the next state depends only on the present state. In a Markov chain of second or higher order, the next state depends on the present state and one or more of the previous states. The first order transition matrix can be represented [4];

$$P = \begin{bmatrix} p_{11} & p_{1,2} & \cdots & p_{1,m} \\ p_{21} & p_{2,2} & \cdots & p_{2,m} \\ \vdots & \vdots & \ddots & \vdots \\ p_{m,1} & p_{m,2} & \cdots & p_{m,m} \end{bmatrix} \quad (1)$$

$$[p_1 \;\; p_2 \;\; \cdots p_m]_{futu} = [p_1 \;\; p_2 \;\; \cdots p_m]_{pres} P$$

The transition probabilities, p_{ij}, of any state vary between 0 and 1. The summation of transition probabilities in a row equals 1.

Linear State Space Model

The evolution of various components in the city, e.g., housing, industrial, and commercial developments, are represented by the Lotka-Volterra model:

$$\dot{x}_i = k_i x_i + \sum_j g_{ij} x_i x_j$$

where

x_i = population i

$k_i x_i$ = the growth ability of population i

$g_{ii} x_i x_i$ = environmental pressure or resource on population i

$g_{ij} x_i x_j$ = the influence of population j on population i

g_{ij} = the properties of the influence are varied by time

$g_{ij} > 0$ has promotional effects on population i, and if

$g_{ij} < 0$ then the action is inhibited.

For more applicability, the extended Lotka-Volterra model can be represented [7], [8] as

$$\dot{x}_i = k_i x_i + \sum_j g_{ij} x_i x_j + \sum_k \alpha_{ik} x_i u_k$$

where

u_k represents a forcing function on the compartments

α_{ik} is coefficient varied by time

The linearization model will be

$$\dot{z} = Az + Bu$$

where

$$a_{ii} = k_i + \sum_j g_{ij} x_{j0} + \sum_k \alpha_{ik} u_{k0}$$

$$a_{ij} = \sum_j g_{ij} x_{i0} \delta x_j, i \neq j$$

$$b_{ij} = \sum_k \alpha_{ik} x_{i0}$$

a_{ii} is the growth ability of population i, environment pressure or resource on population i, and the influence of popula-

tion j on population i; a_{ij} is the influence of population j on population i; b_{ij} is depended on the population.

As a discrete model, it can be written as

$$z(k+1) = Fz(k) + G\mathbf{u}(k) \qquad (2)$$

The state will be number of housing, industrial, and commercial units. This study used the Markov chain of Equation (1) and the extended Lotka-Voltera model from Equation (2) to control the population in the area under consideration. The state status of each cell was calculated using the CA.

State Transition

The next state of each cell was calculated using the transition potential [9];

$$P_{ij} = s_j a_j S\left(1 + \sum_{h,k,d} m_{kd} I_{hd}\right) + H_j$$

where

P_{ij} = the transition potential from state i to state j

m_{kd} = the weighting parameters applied to cells in state k in distance zone d

h = the index of cells within a given distance zone

I_{hd} = 1, if the state of cell $h = k$, otherwise $I_{hd} = 0$

s_j = suitability of the cell state for j, $0 \le s_j \le 1$

a_j = accessibility by transportation $a_j = \left(1 + \frac{D}{\delta_j}\right)^{-1}$

δ_j = the coefficient expressing the importance of accessibility for desirability of the cell for land use j

D = Euclidean distance from the cell to the nearest cell of the network.

H_j = inertia parameter, $H_j > 0$ *if* $i = j$

S = a stochastic disturbance term

$$S = 1 + (-\ln R)^{\alpha}$$

where $0 < R < 1$ uniform random variation, α is a parameter that allows control of the size of the stochastic perturbation.

The stochastic S has a highly skewed distribution so that most values are near unity, and much larger values occur only infrequently. Most of the potentials, P_{ij}, are close to their unperturbed deterministic values; i.e., the transition parameters dominate the determination of the transition potentials. As $P_{ij} \ge 1$, every cell in the array has a nonzero chance of transition. In general, cells within the neighborhood are weighted differently depending on their state and also on their distance from the reference cell, and the m_{kd} may be specified to represent, for example, a standard negative exponential distance-decay relationship. Vacant cells do not receive a weight and, thus, do not contribute directly to the transition potential.

At each iteration, sufficient cells are converted to each use so that the net increase in the number of cells in each non-vacant state is equal to the exogenously specified increase, N_i ($i = H, I, C$). The cells converted to each state are those with the highest potentials for that state. To begin with commerce, the N_c cells with the highest potentials for commerce are identified. If some of these cells are also in the lists of the cells with the highest potentials for industry or housing, then those cells will change to commercial. If for industry, some of the cells are also in the lists of the cells with the highest potentials for housing, then those cells will change to industrial.

Numerical Simulations

The city of Norfolk was the test case for the study. The aerial photo is divided into a 62×100 square grid. The railroad, road, bridge and river are mapped in the grid, as shown in Figure 2. The transition weighting parameters are the same as those found by White et. al., [9]. The simulations were performed using MATLAB.

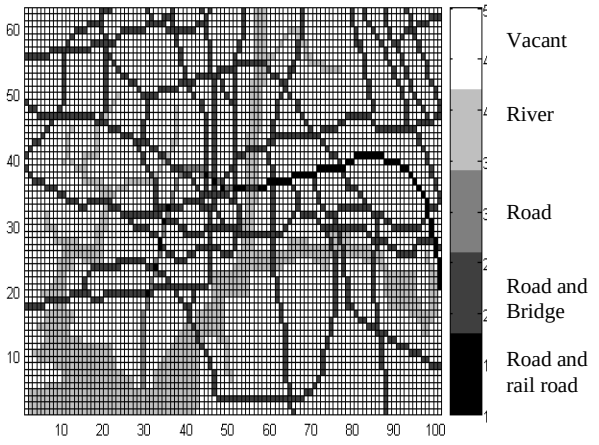

Figure 2. Railroad, Road, Bridge, and River

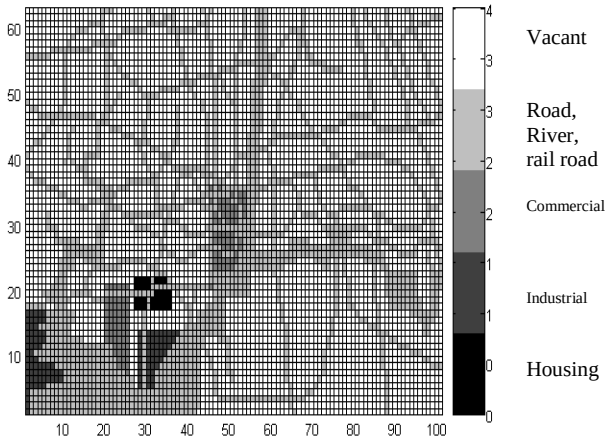

Figure 3. Initial Condition

The first-order Markov chain transition matrix is

$$P = \begin{bmatrix} 0.9 & 0.06 & 0.03 & 0.01 \\ 0.0 & 0.8 & 0.1 & 0.1 \\ 0.0 & 0.5 & 0.4 & 0.1 \\ 0.0 & 0.6 & 0.32 & 0.08 \end{bmatrix}$$

The results of these simulations are the same as for the linear system representation.

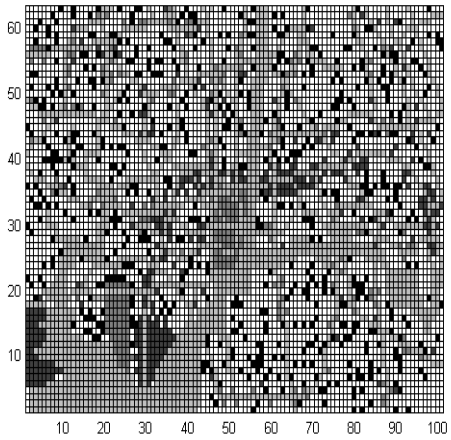

Figure 4. 20th Iterations

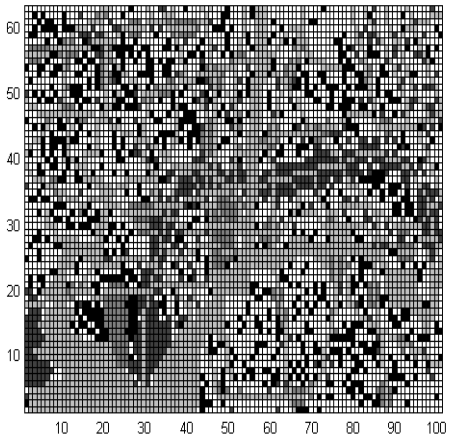

Figure 5. 50th Iterations

For the linear system representation, the linear system parameters are

$$F = \begin{bmatrix} 0.94 & .01 & 0 \\ .05 & 0.9 & 0 \\ 0 & 0 & 0.94 \end{bmatrix}, \quad G = \begin{bmatrix} 50 \\ 15 \\ 20 \end{bmatrix}$$

Numerical simulation results are shown in the Figures 3-7. Figure 3 is the initial condition for simulation. Figures 4, 5, and 6 show the distribution of housing, industrial, and commercial sites at the 20th, 50th, and 100th iteration, respectively. One iteration represents a one-year change of the compartment. Figure 8 shows the number of each compartment's history.

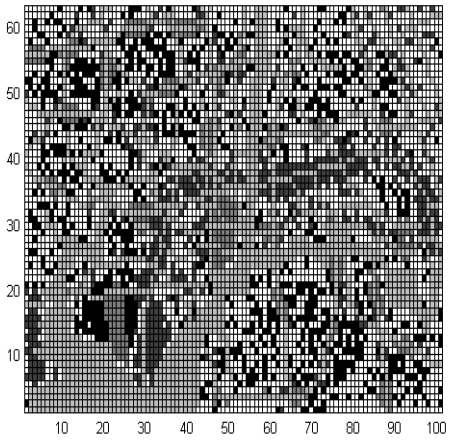

Figure 6. 100th Iterations

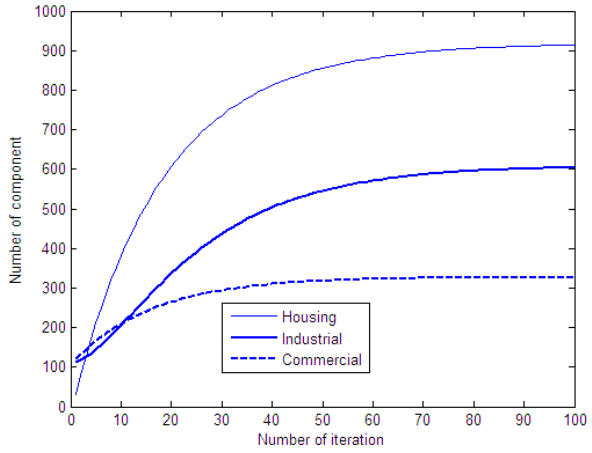

Figure 7. Simulation time history of number of housing, industrial and commercial

Conclusions

Urban land-use dynamics can be divided into two parts: cell state change, which is dependent on neighborhood cells, and the total land use of each compartment. The linear state space model is more flexible to use than the Markov chain model for the prediction of the past growth data. For linear state model representation, it is easy to change the new equilibrium of the state of each compartment. In this study, cellular automata were used to predict the area of each cell and state space to represent the number of each compartment at each point in time. When it becomes necessary to change the equilibrium points, the state space equation is easier to manipulate than the Markov chain. If more accurate predictions are needed, the identification should be done to find parameters used in the CA and state space equations.

References

[1] Liu Y. and Phinn S. R., 2003. Modelling urban development with cellular automata incorporating fuzzy-set approaches, Computers, Environment and Urban Systems, Vol.27, pp 637-658.

[2] Li, X. and Yeh, A. G. O., 2001. Calibration of cellular automata by using neural networks for the simulation of complex urban systems. Environment and Planning A, 33(8), pp. 1445-1462.

[3] White R., and Engelen G. 1993. Cellular automata and fractal urban form: a cellular modeling approach to the evolution of urban land use patterns, Environment and Planning A, 25, pp1175–1199.

[4] Weng Q., 2002. Land use change analysis in the Zhujiang Delta of China using satellite remote sensing, GIS and stochastic modeling, Journal of Environmental Management, Volume 64, Issue 3, pp 273-284.

[5] López E., Bocco G., Mendoza M., and Duhau E., 2001. Predicting land-cover and land-use change in the urban fringe: A case in Morelia city, Mexico. Landscape and Urban Planning, Volume 55, Issue 4, pp 271-285.

[6] Aaviksoo K., 1995. Simulating vegetation dynamics and land use in a mire landscape using a Markov model, Landscape and Urban Planning, Volume 31, Issues 1-3, February 1995, pp 129-142.

[7] Huang J., Systems Evolutionary Analysis for Urban Industry System, Systems, Man, and Cybernetics, 1998 IEEE International Conference, 11-14 Oct 1998, San Diego, CA , USA

[8] Magyar A., Szederkenyi G., Hangos K.M., Globally stabilizing feedback control of process systems in generalized Lotka–Volterra form, Journal of Process Control 18 (2008) pp80–91.

[9] White R., Engelen G., and Uljee I. 1997. The use of constrained cellular automata for high-resolution modeling of urban land-use dynamics, Environment and Planning B, 24, pp323–343.

Biographies

THONGCHAI PHAIROH received the B.Eng. and M. Eng. degree in Mechanical Engineering from the King Mongkut's Institute of Technology North Bangkok, Thailand, in 1986, and 1997 respectively, and the Ph.D. degree in Mechanical Engineering from the Old Dominion University, Norfolk, VA 2006. Currently, He is an Assistant Professor of Technology at Virginia State University. His research areas include instrumentation, control systems, system modeling and system identification. Dr. Phairoh may be reached at tphairoh@vsu.edu.

AYODEJI O. DEMUREN received the B.Sc. and the Ph.D. degree in Mechanical Engineering from the Imperial College London in 1975 and 1979 respectively. Currently, He is Professor of Mechanical Engineering at Old Dominion University. His research areas include computational fluid dynamics and heat transfer. Dr. Demuren may be reached at ademuren@odu.edu.

KEITH WILLIAMSON received the BS, MS, and Ph.D. all in Mechanical Engineer from Bucknell University in 1983, Northeastern University in 1989, and Tuft University in 1998 respectively. Currently he is Professor and Associate Vice President, Research and Innovation at Virginia State University. His research involves thermo-mechanical processing and mathematical modeling. Dr. Williamson may be reached at kwilliamson@vsu.edu.

AUTOMATIC FACIAL EXPRESSION RECOGNITION USING 3D FACES

Chao Li, Florida A&M University; Antonio Soares, Florida A&M University

Abstract

Automatic facial expression recognition has gained much attention during the last decade because of its potential application in areas such as more engaging human-computer interfaces. Automatic facial expression recognition is a subarea of face analysis research that is based heavily on methods of computer vision, machine learning, and image processing. Many efforts either to create a novel or to improve existing face expression recognition systems are, thus, inspired by advances in these related fields. This study explored the automatic recognition of facial expressions using 3D range images. In this paper, the development of an algorithm designed to distinguish between neutral and smiling faces is outlined, along with a summary of its experimental verification with a database containing 30 subjects, who posed for both neutral and smiling expressions. As a comparison with 2D facial expression recognition, a PCA algorithm was used to exact features from 2D images to be used for expression recognition. Results show that 3D facial expression recognition outperforms 2D ones.

Introduction

In human-to-human dialogue, the articulation and perception of facial expressions form a communication channel that is supplementary to voice and which carries crucial information about the mental, emotional and even physical states of the conversation partners [1]. As a basic mode of nonverbal communication among people, the facial expression of another person is often the basis by which we form significant opinions on such characteristics as friendliness, trustworthiness and status. Facial expressions convey information about emotion, mood and ideas.

Ekman and Friesen [2] proposed six primary emotions. Each emotion possesses a distinctive content together with a unique facial expression. These prototypical emotional displays are also referred to as basic emotions. They seem to be universal across human ethnicities and cultures. These six emotions are happiness, sadness, fear, disgust, surprise and anger. Together with the neutral expression, these seven expressions also form the basic prototypical facial expressions.

Facial expressions are generated by contractions of facial muscles, which result in temporally deformed facial features such as eyelids, eyebrows, nose, lips and skin textures, often revealed by wrinkles and bulges. Typical changes of muscular activities for spontaneous expressions are brief, usually between 250ms and 5s. Three stages have been defined for each expression: onset (attack), apex (sustain) and offset (relaxation). In contrast to these spontaneous expressions, posed or deliberate expressions can be found very commonly in social interactions. These expressions typically last longer than spontaneous expressions.

Automatic facial expression recognition has gained more and more attention recently. Face expression recognition deals with the classification of facial motion and facial feature deformation into abstract classes that are purely based on visual information [3]. It has various potential applications in improved intelligence for human-computer interfaces, image compression and synthetic face animation. Automatic face recognition can be used to build an intelligent tutoring system [4]. Facial expression recognition can also be used to detect drowsiness of a driver to prevent car accidents [5].

Currently, all existing face expression analysis and recognition systems rely primarily on static images or dynamic videos. A number of techniques were successfully developed using 2D static images or video sequences, including machine vision techniques [6-8]. Although some systems have been successful, performance degradation remains when handling expressions with large head rotation, subtle skin movement, and/or lighting change with varying postures [9]. Recently, with the development of 3D imaging technology, fast and cheap 3D scanners became available. 3D scans do not have the inherent problems cited above for 2D images. Therefore, the extraction of features from the faces is expected to be more robust, which will make the final expression recognition more reliable. In this study, 3D range images were used to assess the practicability of 3D facial expression recognition.

Also in this study, one specific facial expression, social smile, was used to test a 3D expression recognition system. In our experiment, the authors sought to recognize social smiles, which were posed by each subject, in their apex period. Smiling is the easiest of all expressions to find in photographs and is readily produced by people on demand. 3D range images were used for smiling recognition. In order to compare 3D facial expression recognition with 2D facial

expression recognition, a 2D facial recognition algorithm was also employed for the database.

Data Acquisition and Processing

For purposes of this study, a database including images from 30 subjects was built. In this database were included smiling faces, as well as neutral faces from the same subjects. Each subject participated in two data-acquisition sessions, which took place on two different days. In each session, two 3D scans were acquired; one, a neutral expression, the other a happy (smiling) expression. At the same time, 2D images were also obtained from the same subjects. The 3D scanner used was a Fastscan 3D scanner from Polhemus Inc. [10]. The accuracy of this scanner is specified as 1mm. The resulting database contained 60 3D neutral scans and 60 3D smiling scans for the 30 subjects. There are also corresponding 2D images for each 3D scan. Figure 1 shows an example of the 3D scans obtained using this scanner.

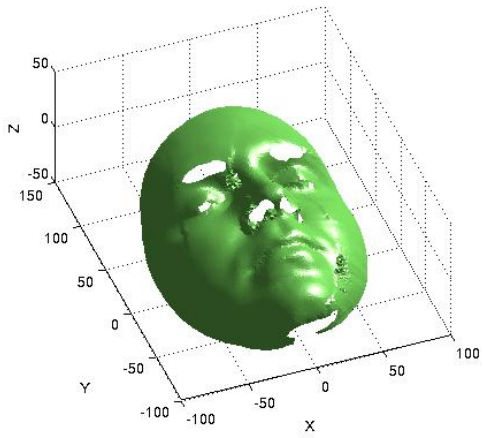

Figure 1. 3D Face Surface Acquired by the 3D Scanner

In 3D facial expression recognition, registration is a key pre-processing step. In this experiment, a method based on the symmetric property of the face was used to register the face image. In converting the 3D scan from a triangulated mesh format to a range image with a sampling interval of 2.5mm, trilinear interpolation was used [11]. Unavoidably, the scanning process will result in face surfaces containing unwanted holes, especially in the area covered by dark hair, such as the eyebrows. To circumvent this problem, the cubic spline interpolation method was used to patch the holes [11]. An example of the resulting 3D range image is shown in Figure 2.

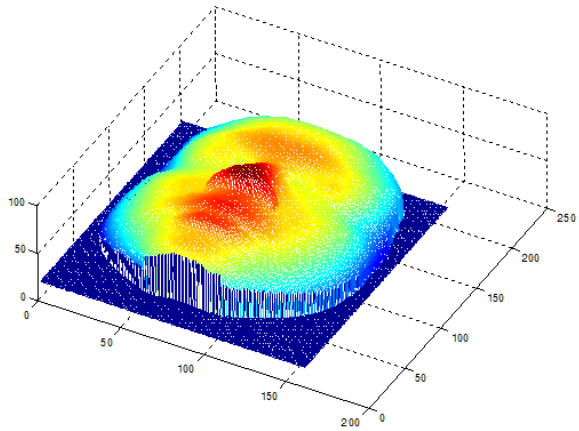

Figure 2. Mesh Plot of the Converted Range Image

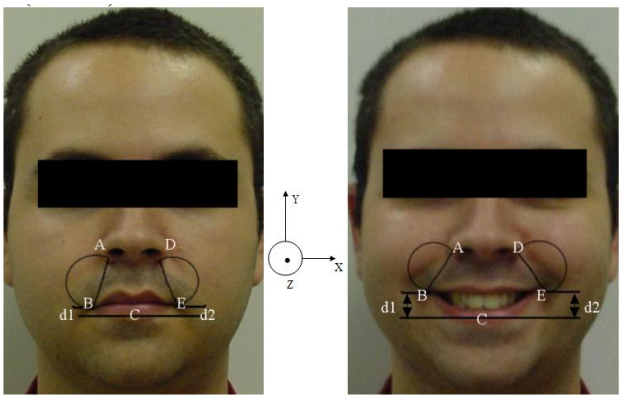

Figure 3. Illustration of the Features of a Smiling Face

Feature Extraction and Classification

The smile is generated by the contraction of the Zygomatic Major muscle. The Zygomatic Major originates in the cheek bone (Zygomatic arch) and ends near the corner of the mouth. This muscle lifts the corner of the mouth obliquely upwards and laterally, producing a characteristic "smiling expression". So the most distinctive features associated with a smile are the bulge of the cheek muscle and the uplift of the corner of the mouth, as can be seen in Figure 3. The line on the face generated by a smiling expression is called the nasal labial fold, or smile line.

The following steps are followed to extract the features for the smiling expression from a 3D range facial image:

- An algorithm is developed to obtain the coordinates of five characteristic points (A, B, C, D and E) in the face range image, as shown in Figure 3. A and D are at the extreme points of the base of the nose. B and E are the

points defined by the corners of the mouth. C is in the middle of the lower lip.

- The first feature is the width of the mouth, BE, normalized by the length of AD. Obviously, while smiling the mouth becomes wider. The first feature is represented by *mw*.
- The second feature is the depth of the mouth (the difference between the Z coordinates of points BC and EC) normalized by the height of the nose to capture the fact that the smiling expression pulls back the mouth. This second feature is represented by *md*.
- The third feature is the uplift of the corner of the mouth, compared with the middle of the lower lip, d1 and d2, as shown in the Figure 1, normalized by the difference of the Y coordinates of points AB and DE, respectively, and represented by *lc*.
- The fourth feature is the angle of AB and DE with the central vertical profile, represented by *ag*.
- The last two features are extracted from the semicircular areas, which are defined by using AB and DE as diameters. The histograms of the range (Z coordinates) of all the points within these two semicircles are calculated.

Figure 4 shows the histograms for the smiling face and the neutral face of the subject shown in Figure 3.

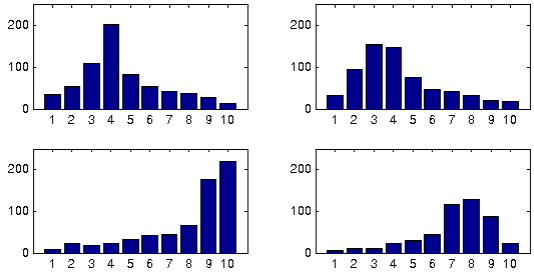

Figure 4. Histogram of range of cheeks for neutral and smiling face

The two figures in the first row are the histograms of the range values for the left cheek and right cheek of the neutral face image; the two figures in the second row are the histograms of the range values for the left cheek and right cheek of the smiling face image.

From the above figures, one can see that the range histograms of the neutral and smiling expressions are different. The smiling face tends to have large values at the high end of the histogram due to the bulge of the cheek muscle. On the other hand, a neutral face has large values at the low end of the histogram distribution. Therefore, two features can be obtained from the histograms: One is called the 'histogram ratio', represented by *hr*, the other is called the 'histogram maximum', represented by *hm*.

$$hr = \frac{h6 + h7 + h8 + h9 + h10}{h1 + h2 + h3 + h4 + h5} \tag{1}$$

$$hm = i \qquad i = \arg\{\max(h(i)\} \tag{2}$$

In summary, six features—*mw*, *md*, *lc*, *ag*, *hr* and *hm*—are extracted from each face for the purpose of expression recognition. After the features have been extracted, this becomes a general classification problem. Two pattern-classification methods are applied to recognize the expression of the incoming faces.

1. Linear discriminant classifier: (Linear Discriminant Analysis-LDA)

LDA tries to find the subspace that best discriminates different classes by maximizing the between-class scatter matrix, S_b, while minimizing the within-class scatter matrix, S_w, in the projective subspace. S_w and S_b, are defined as follows,

$$S_w = \sum_{i=1}^{L} \sum_{\vec{x}_k \in X_i} (\vec{x}_k - \vec{m}_i)(\vec{x}_k - \vec{m}_i)^T \tag{3}$$

$$S_b = \sum_{i=1}^{L} n_i (\vec{m}_i - \vec{m})(\vec{m}_i - \vec{m})^T \tag{4}$$

where $\vec{m}_i$ is the mean vector for the individual class, n_i is the number of samples in class X_i, $\vec{m}$ is the mean vector of all the samples and L is the number of classes.
The LDA subspace is spanned by a set of vectors, W, satisfying

$$W = \arg\max \left| \frac{W^T S_b W}{W^T S_w W} \right| \tag{5}$$

2. Support Vector Machine (SVM):

Support vector machine is a relatively new technology for classification. It relies on preprocessing the data to represent patterns in a high dimension, typically much higher than the original feature space. With an appropriate nonlinear mapping to a sufficiently high dimension, data from two categories can always be separated by a hyperplane [12]. In this study, the LIBSVM program package [13] was used to implement the support vector machine.

In order to compare the 3D facial expression algorithm with the 2D facial expression algorithm, the corresponding 2D images were used for expression recognition. First, 2D images were cropped to just keep the face part, eliminating the hair and other artifacts in the 2D image. Then, instead of extracting features from 2D images intuitively, as in 3D face expression recognition, Principal Component Analysis (PCA) was used to extract the "feature" from 2D images [14].

PCA

PCA seeks a projection that best represents the data in a least-square sense. In PCA, a set of vectors are computed from the eigenvectors of the sample covariance matrix, C,

$$C = \sum_{i=1}^{M} (\vec{x}_i - \vec{m})(\vec{x}_i - \vec{m})^T \quad (6)$$

where $\vec{m}$ is the mean vector of the sample set. The eigen space, Y, is spanned by k eigenvectors $u_1, u_2, \cdots, u_k$, corresponding to the k largest eigen values of the covariance matrix, C.

$$\vec{y}_i = (\vec{x}_i - \vec{m})^T [\vec{u}_1 \vec{u}_2 .... \vec{u}_k] \quad (7)$$

The dimensionality of vector $\vec{y}_i$ is *K (K<<M).*

These K Eigen values serve as the "features" in 2D images. Then, the same LDA and SVM methods are used for facial expression recognition.

Experiments and Results

Because the size of the database was relatively small, the leave-one-out cross validation method was used to test the facial expression recognition algorithm. The images of 29 subjects were used to train the classifier, which was used to recognize the expression of the one remaining subject. The results of recognition hits shown below are correct expression recognition (either neutral or smiling), divided by the total number of trials.

Discussion and Conclusion

From Figure 5, it can be seen that both classifiers (LDA & SVM) achieve very good facial expression recognition rates for 3D images; both being more than 90%. Otherwise, for 2D images, the recognition for both classifiers is around 80%. 3D images have achieved significantly better recognition rates than 2D images. This result is in line with the authors' assumption that because of the advantages of 3D images, a 3D facial expression recognition system should perform better than its 2D counterpart.

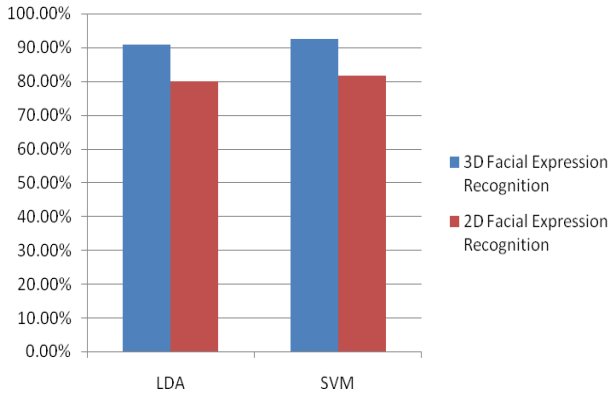

Figure 5. Facial Expression Recognition Result

It should also be noted that this experiment, as implemented, pursues the recognition of "absolute facial expressions". This means that the recognition is being attempted without prior knowledge of the neutral facial expression of a subject. It is always more difficult to recognize absolute facial expressions, without referring to the neutral face of a given subject. In many real scenarios, the knowledge of the neutral expression of a subject could be incorporated and the algorithm modified in order to achieve better performance.

References

[1] Whitehill, J., "Automatic Real-Time Facial Expression Recognition for Signed Language Translation", Master thesis, University of West Cape, South Afirca, 2006.

[2] Ekman, P., and Friesen, W, "Constants across cultures in the face and emotion", Journal of Personality and Social Psychology 17(2): 124-129, 1971.

[3] Fasel, B., Luettin, J., "Automatic facial expression analysis: a survey", Pattern Recognition **36**: 259-275, 2003.

[4] Whitehill,J, Bartlett,M and Movellan,J, "Automatic Facial Expression Recognition for Intelligent Tutoring Systems", Proceedings of the CVPR Workshop on Human Communicative Behavior Analysis, 2008.

[5] Vural,E, Cetin,M, Ercil, A, Littlewort, G,Bartlett, M and Movellan,J ,"Automated drowsiness detection for improved driving safety". Proc. Int'l Conf. Automotive Technologies. 2008.

[6] Donato,G, Bartlett, M, Hager,J, Ekman, P and Sejnowski, T, "Classifying facial actions", IEEE Trans. PAMI, 21(10):974-989, 1999.

[7] Lyons, M et al. "Automatic classification of single facial images", IEEE Trans. PAMI, 21(12):1357-1362, 1999.
[8] Essa I, and Pentland, A. "Coding, analysis, interpretation, and recognition of facial expressions", IEEE Trans. PAMI, 19(7), 1997.
[9] Yin, L. et al. "A 3D Facial Expression Database For Facial Behavior Research" Proceedings of the 7th International Conference on Automatic Face and Gesture Recognition, FGR06, Southampton, UK, 10-12 April 2006
[10] http://www.polhemus.com
[11] Li, C., Barreto, A., "Profile-Based 3D Face Registration and Recognition", Lecture Notes on Computer Science **3506**: 484-494. 2005
[12] Duda, R., Hart, P., Stork D., Pattern Classification, 2001.
[13] Chang, C and Lin, C. *LIBSVM: a library for support vector machines*. http://www.csie.ntu.edu.tw/~cjlin/libsvm/, 2001.
[14] Turk, M and Pentland, A. "Eigenfaces for Recognition", Journal of Cognitive Neuroscience, vol 3, pp71-86, 1991.

Biographies

CHAO LI is an assistant professor in Electronic Engineering Technology Program in Florida A&M University. He got his PhD in Electrical Engineering from Florida International University. He worked for telecommunication and electronics industry for five years before he entered academia. He may be reached at
chao.li@famu.edu

ANTONIO SOARES received a Bachelor of Science degree in Electrical Engineering from Florida Agricultural and Mechanical University in Tallahassee (FAMU), Florida in December 1998. He continued his education by obtaining a Master of Science degree in Electrical Engineering from FAMU in December of 2000 with focus on semiconductor devices, semiconductor physics, Optoelectronics and Integrated Circuit Design. He then worked for Medtronic as a full-time Integrated Circuit Designer until November 2003. Antonio started his pursuit of the Doctor of Philosophy degree at the FAMU in January 2004 under the supervision of Dr. Reginald Perry. Upon completion of his PhD, Dr. Soares was immediately hired as an assistant professor (Tenure Track) in the Electronic Engineering Technology department at Florida A&M University. He may be reached at
antonio.soares@famu.edu

PHOTOVOLTAIC ENERGY SYSTEMS: A FEASIBILITY STUDY

Youakim Kalaani, Georgia Southern University; William Nichols, Georgia Southern University

Abstract

The Industrial Revolution has brought an enormous increase in the use of fossil fuels, specifically oil, coal and natural gas. The combustion of these fuels releases many gases that are harmful to humans and the rest of the ecosystem. Therefore, increasing energy efficiency including the use of renewable energy is heralded as the most effective strategy to reduce air pollution and hinder anthropogenic climate changes.

In this study, the viability of photovoltaic (PV) systems was investigated via a case study involving a shopping center. Engineering, environmental, and economic aspects were thoroughly examined and, as a result, a grid-connected PV system was designed to satisfy various system constraints. Engineering factors such as optimal array orientations, shading effects, module sizing, and compatibility issues were analyzed using the PV Watts method. The environmental analysis took into account not only the amount of pollution avoided over the lifetime of the system but also the energy extended during the manufacturing process. Additionally, various capital budgeting and sensitivity analyses were presented including the grid-parity technique for optimal conditions. Finally, advances in smart-grid technologies for integrating distributed energy sources were suggested for further studies.

Introduction

Renewable energy, including the use of Photovoltaic (PV) systems, has extensively been discussed in the literature. However, most of the studies [1-20] dealing with the design and applications of PV systems, were limited in scope and, therefore, did not cover all of the underlying issues involved in the process. In this study, the feasibility of PV systems was thoroughly investigated, taking into consideration not only engineering aspects, but also economic and environmental factors, thus providing a more comprehensive approach to the study of PV systems. Although PV systems do not emit any pollution during their operation, manufacturing its various components does require a substantial amount of energy. Thus, the environmental study presented here takes into account the amount of pollutants avoided over the lifetime of the system and also the time it takes to recover the energy that went into the manufacturing process.

For the economic analysis, capital budgeting techniques were utilized to determine the net present value and internal rate of return based on estimated cash flows over a 30-year period. Furthermore, the market analysis provided techniques to predict the cost and performance of PV systems such as inverter lifespan, future inverter costs, and module degradation. These estimates, along with the expected trends in electricity costs, were incorporated into the cash-flow analysis in order to provide a more realistic solution. In this paper, several design-optimization strategies to reach grid parity at certain government incentive levels are proposed.

Case Study

The viability of photovoltaic (PV) systems to produce clean electricity was investigated via a case study involving a shopping center located in the southeastern region of the Untied States. This case study was conducted to address key factors involved in the planning and designing of large PV systems such as optimal array orientations, shading effects, and compatibility issues between the PV arrays and inverters under various weather conditions. Different capital budgeting techniques were also investigated to determine if installing PV systems in this part of the country is feasible under the prevailing environment and economic conditions. For the purposes of this study, solar data was obtained from the National Renewable Energy Laboratory (NREL) software [2], PVWatts (V2), based on analysis of the National Solar Radiation Data Base (NSRDB). While calculations are based on historical data, the actual performance of the PV system will be valid within 10 to 12% of the calculated values [3].

Engineering Aspects

Solar irradiation is the total amount of solar energy collected on an area over time and is typically expressed in kWh/m^2. At most locations on Earth, solar irradiation will peak around $1kW/m^2$ every day around solar noon. Insolation is the term used to gauge the solar energy that reaches the Earth's surface over the course of a day. It is usually expressed in $kWh/m^2/day$. PV modules should ideally be facing the sun to collect maximum power. This can be achieved by using a sun-tracking system that automatically orients the array to the position of the sun. However, sun-tracking is usually used for smaller applications and rarely roof mounted, as it may cause structural problems [7].

The proposed site for the PV installation was a shopping center served by a 3-phase, 480-volt feeder. The shopping center operates 24 hours a day, 7 days a week. Its electricity use over a five-year period is shown in Figure 1.

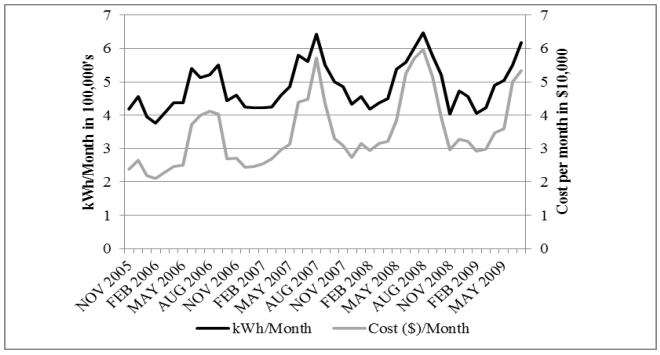

Figure 1. The Energy Profile for the Shopping Center

The cost of energy incurred by the facility fluctuates throughout the year, costing more in summer than other months during the year. The cost per kWh is depicted in Figure 2.

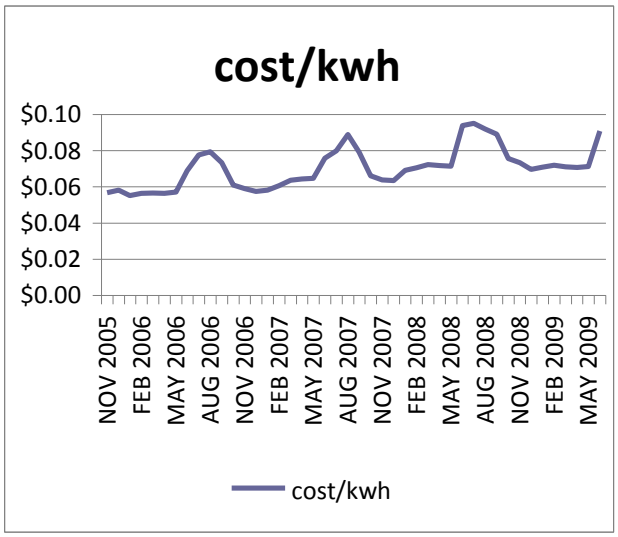

Figure 2. The Energy Cost for the Shopping Center

The solar insolation received for fixed arrays facing due south at various tilt angles is shown in Table 1. Since the best of these array angles changes throughout the year, it may be more economicaly feasible to mount the modules on an adjustable platform and adjust the tilt angle as needed. This arrangement should allow the array to be tilted at 32.3° during March, at 17.3° from April to September, and at 47.3° between October and February, resulting in about 7.2% energy increase over a fixed-array arrangement.

Table 1. Available Solar Insolation in kWh/m^2/day

	17.3°	32.3°	47.3°	Best of
JAN	3.68	4.17	4.42	4.42
FEB	4.51	4.91	5.03	5.03
MAR	5.46	5.67	5.56	5.67
APR	6.42	6.29	5.80	6.42
MAY	6.19	5.78	5.08	6.19
JUN	6.27	5.74	4.93	6.27
JUL	6.29	5.83	5.07	6.29
AUG	5.51	5.28	4.79	5.51
SEP	5.51	5.58	5.35	5.58
OCT	5.09	5.46	5.52	5.52
NOV	4.03	4.55	4.81	4.81
DEC	3.61	4.17	4.49	4.49
YEAR	5.22	5.29	5.07	5.52

Rack systems manufactured by IronRidge were considered in this study with mount models UNI-GR/12H and UNI-GR/14H capable of holding 7 and 8 PV arrays, respectively. Shading on PV modules can cause a significant drop in energy production. The Solar Pathfinder, a popular instrument to measure shading, was used in this study. It contains a convex transparent dome placed over a sun-path chart. When properly oriented, the reflection of the dome provides a comprehensive solar/shade evaluation for the entire year.

The cost of energy incurred by the facility fluctuates and several pictures were taken by the Pathfinder from different sites of the proposed locations. Each picture was then analyzed by the Solar Pathfinder Assistant program to determine the site efficiency for each location. The site efficiency is a measure of how well each site will collect solar energy after factoring in the dates and times of possible shading. This includes any losses that may occur if the proposed site happened to deviate from the optimal orientation defined at a tilt angle of 32.3° and an azimuth angle of 0° (due south).

For example, a site with optimal orientation will have 100% efficiency if no shading occurs throughout the entire year. Three locations on the roof of the building were selected for analysis with the results shown in Table 2. As depicted, all three areas were considered excellent PV sites for their near-optimal shading efficiency.

Table 2. Shading Evaluation by the Solar Pathfinder

	# of readings	Shading Factor
South Side	8	99.38
Center	11	99.3
North Side	11	98.67

Table 3. Array Spacing Calculation

array tilt angle	47.3°	32.3°	17.3°
module length (m)	1.65	1.65	1.65
array height (m)	1.21	0.88	0.49
mount length (m)	1.12	1.40	1.58
solar alt angle	20°	20°	20°
shadow length (m)	3.33	2.42	1.35
solar azimuth angle	45°	45°	45°
distance between rows to prevent shading (m)	2.61	1.90	1.06
total space need for row (m)	3.74	3.30	2.63

PV systems are designed so that the operating voltage of each module string always falls within the maximum power point tracking (MPPT) voltage range of the inverter. Most inverters are equipped with MPPT circuits to ensure that arrays produce maximum power under varying temperatures and solar irradiance. The maximum number of modules in a string can be found by the quotient of the MPPT input voltage of the inverter, Vmax (INV) and the open-circuit voltage of the module (V_{OC}) at the coldest operating temperature.

The minimum number of modules is found by rounding up the quotient of the inverter minimum input voltage at MPPT and model voltage at the maximum expected temperature. The DC input current of the inverter is the sum of the currents of all the strings or, more simply, the product of the number of strings and module current. The maximum number of strings is found by dividing the maximum input current of the inverter by the module short-circuit current at the maximum module operating temperature [4].

The ratio of the PV array power to the nominal AC power output of the inverter is called the inverter sizing ratio. The ideal sizing ratio is typically greater than 1 to account for any module mismatch, soiling, aging, and wiring losses. An inverter ratio around 1.15 is very common in the PV industry [5]. When a system has an inverter sizing ratio higher than 1.3, there will be significant energy losses and premature aging of the inverter. An inverter sizing ratio that is too small will make overloading the inverter less likely, but having too few modules could harm the economic performance of the system. However, it has been found that the economic performance of PV systems with inverter efficiencies around 98% is less sensitive to variations in inverter sizing ratio [6].

Due to space limitations, a PV system rated at a 286.44kW was originally designed to fit the site location. However, a smaller system rated at 152.5kW was found to reach the grid parity resulting in a more attractive return on investment. Both options were considered in this study to provided a comparison between the two systems. Arrays sizing are presented in Table 4.

Table 4. Arrays Sizing Calculation

Hottest Day (°C)	40.6	40.6
Coldest Day (°C)	-16.1	-16.1
temp rise coef (°C/kW/m^2)	20	20
max solar irradiance (kW/m^2)	1.3	1.3
module temp at hottest day	66.6	66.6
Inverter Model	SC250U	Satcon
Nominal AC output	250	135
max input voltage	600	600
maximum MPP voltage	600	600
minimum MPP voltage	330	310
max DC input current	800	454
inverter efficiency	97.0%	96.5
Voc at coldest temp	25.70	25.70
max power at hottest temp	15.25	15.25
Isc at hottest temp	12.36	12.36
string Voc at coldest temp	565.5	565.5
string max power at hottest temp	335.6	335.6
max # of series connected modules	23.3	23.3
min # of series connected modules	21.6	20.3
# of modules in series	22	22
max # of strings	64.72	36.7
# of series strings	62	33
total # of modules	1364	726
inverter sizing ratio	1.15	1.13

The method for estimating the performance of PV systems is discussed in this section. It is based on the PVWatts (V2) program developed by NREL [2]. Various losses associated with PV systems are shown in Table 5. According to NREL, PV modules should be derated by 1% each year after installation [8]. Energy and revenues generated by the 286.44kW system are shown in Table 6.

Table 5. Derate Factors used for Calculations

Component Derate Factors	PV Watts Default	NREL suggested Range	Derate Factor
PV module nameplate rating	0.95	0.80–1.05	.95
Inverter and transformer	0.92	0.88–0.98	.97
Mismatch	0.98	0.97–0.995	.98
Diodes and connections	0.995	0.99–0.997	.995
DC wiring	0.98	0.97–0.99	.98
AC wiring	0.99	0.98–0.993	.99
Soiling	0.95	0.30–0.995	.95
System availability	0.98	0.00–0.995	.98
Shading	1	0.00–1.00	.9934
Sun-tracking	1	0.95–1.00	1
Age	1	0.70–1.00	1
Total	.77		.806

Table 6. PV Watts Analysis for the 286.44 kW System

Month	Insolation (kWh/m2/day)	kWh produced	Value $
Jan	4.17	28,581	$2,239
Feb	4.91	30,467	$2,387
Mar	5.67	38,190	$2,992
Apr	6.29	40,141	$3,145
May	5.78	36,890	$2,890
June	5.74	34,646	$2,715
July	5.83	36,472	$2,858
Aug	5.28	33,197	$2,601
Sep	5.58	34,296	$2,687
Oct	5.46	35,474	$2,779
Nov	4.55	29,682	$2,326
Dec	4.17	28,682	$2,247
Year	5.29	406,719	$31,866

Financial Analysis

A review of the literature revealed a range of assumptions that go into estimating the engineering and financial performance of PV systems. For instance, yearly electricity price inflations between 6.7% [9] and 7% [10] may be used for financial analysis. Module degradation rates may vary between 0.5% and 1.0% per year [8]. PV modules have life expectancies of up to 40 years [10] but inverters need to be replaced every 5 to 10 years [11]. The price of inverters is expected to decrease by 35% in 10 years and by 50% in 20 years [11]. The typical weighted average cost of capital for such a facility is around 7.04% [12] and an appropriate discount rate for PV systems is 4% to 6% [13]. A study conducted in 2008 by the Lawrence Berkeley National Laboratory [14] set the average cost of rack-mounted PV systems (>100kW) to $7.20 per installed watt capacity or $7.28 in today's dollars [15]. At this rate, the price of the 286.44kW, PV system is about $2,085,283 but would only cost $959,698 after the 30% federal tax credit and the 35% state tax credit [11] have been applied.

The financial analysis conducted was based on Brigham and Ehrhardt's capital budgeting methods [16]. The cash-flow estimates were based on a yearly electricity price inflation of 6.7%, module degradation of 1.0% per year, 30-year system life with the inverter replaced every 10 years, and a 7.0% capital cost. The net present value (NPV) is the amount of money saved or spent as a result of investing in the PV system. Sensitivity analysis is a powerful tool that provides alternative scenarios as assumptions are varied. For the base-case scenario presented in Figure 3, the NPV and the internal rate of return (IRR) were found to be -$218,214 and 5.19% respectively.

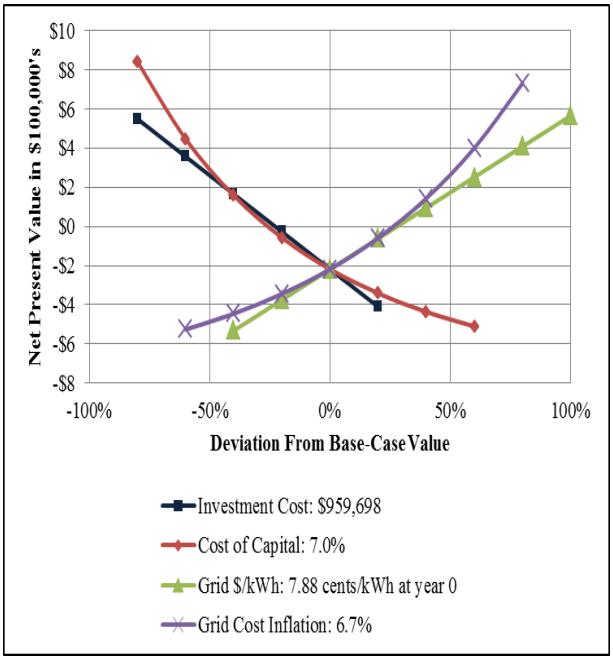

Figure 3. Sensitivity Analysis for the 286.4 kW System

The PV energy presented in Table 6 is very conservative in nature and may as well be the worst-case scenario for this case. Another important factor to consider is the cost of elec-

tricity. Currently, the state average kWh price of 8.44¢ is relatively low compared to the rest of the country. Many states have higher electricity prices such as California (13.1¢) and New York (15.4¢), which make PV systems more attractive investments to undertake [18].

Optimal Conditions

The sensitivity analysis (Figure 3) determined that the project return is not sufficient to cover the cost of capital investment even after all of the government incentives were utilized. The fact that the NPV is negative suggested that this particular PV system is not optimal since it has not reached grid parity, where the cost of photovoltaic electricity is equal to or less than the price of electricity [17]. However, this result should not imply that the system is not feasible since small deviations in the sensitivity analysis may lead to different conclusions. For instance, a 12% energy increase under favorable weather conditions could lead to a positive NPV, rendering the system profitable.

Under the current circumstance, it is feasible to design an optimal PV system if the government incentives cover at least 64.4% of the total cost. The government incentives for the 286.4kW system, including the state tax credit, amounted to only 54% of the system cost. Therefore, it was determined that a smaller system with a DC rating of 152.5kw would achieve the optimal results. The sensitivity analysis for this case is provided in Figure 4 in which the NPV and IRR were found to be + $3,682 (positive) and 7.07%, respectively.

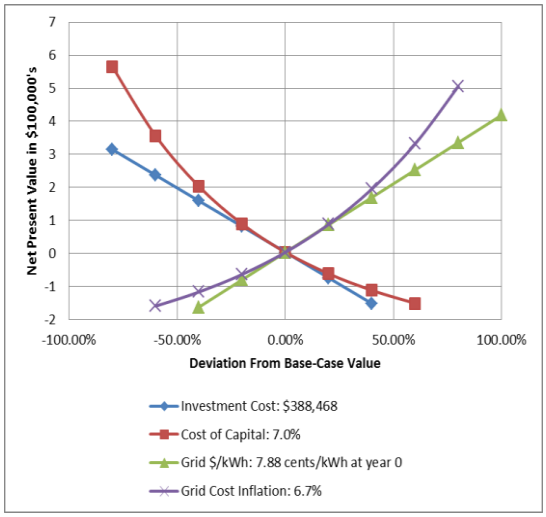

Figure 4: Sensitivity Analysis for the 152.5kW System

Environmental Analysis

Two aspects were considered for this environmental analysis: the energy payback and the amount of pollutants avoided over the lifetime of the PV systems. Photovoltaic systems do not emit any pollution or carbon dioxide during their operation. However, manufacturing the components of PV systems does require a substantial amount of energy. The amount of time that it takes for a PV system to recover the amount of energy that went into manufacturing the components is called the energy payback per years.

The Evergreen ES-A-210 module, made from multi-crystalline silicon, has a minimum efficiency of 13.4% and requires no more than 650kWh/m^2 of energy to manufacture [19]. Here, the received solar energy is about 1,932kWh/m^2/year. Therefore, the energy payback for the ES-A-210 module is calculated to be around 2.51 years. The module frames and the other components typically have an energy payback period of 1.8 years; thus, the proposed 152.5kW system is expected to have a total energy payback period of 4.31 years.

Conventional power generation plants use fossil fuels that release various pollutants and greenhouse gasses. The amount of chemicals emitted for every 1MWh of electric energy produced has been published by the Environmental Protection Agency (EPA) for various regions of the United States. Table 7 shows the amount of each chemical released in the SERC region, which includes the State of Georgia [20].

Table 7. EPA Pollution Data

Chemical	lbs/MWh
CO2	1490.0
CH4	0.02627
SO2	8.87
NOx	2.06

The PV system is expected to produce 4,698.7MWh of electricity during its 30-year lifetime. Table 8 shows the amount of emissions avoided after accounting for the 4.31 energy payback time.

Table 8. Estimated Emission Offset of the 152.5kW System

	Pollution from conventional electricity	Lifetime 4,698.7MWh	Yearly average of 156.6MWh
Chemical	lbs/MWh	offset in lbs	offset in lbs
CO2	1,490.0	7,001,063.0	233,368.8
CH4	0.02627	123.43	4.80
SO2	8.87	41,677.47	1,622.32
NOx	2.06	9,679.32	376.77

Future Studies

This study did not particularly deal with net-metering, which can be an integral part of any grid-connected PV system. However, future studies would examine recent advances in smart-grid technologies and their impact on distributed energy sources including the use of renewable energy. Further studies could also examine other design options such as taking time-of-use pricing for electric utilities and other considerations. Another expansion is to study the use of concentration lenses and ventilation methods to reduce temperatures, thus increasing the efficiency of PV systems. The other aspect of this study is to bring renewable energy into education. For this purpose, a pre-engineering course is under development to incorporate student projects involving the use of a PV system to calculate efficiency as a function of solar irradiance and temperature. Future work would also involve using a prototype PV system to verify the theoretical results presented in this paper.

Summary

In this study, the feasibility of photovoltaic systems as a renewable energy source was investigated via a case study involving a shopping center. Several factors that went into the design process, including engineering, economic, and environmental aspects, were presented and discussed. The PV Watts method for estimating the energy production of the PV system was used to perform the financial analysis, including government and state incentives. Capital budgeting techniques were utilized to determine the net present value and internal rate of return based on estimated cash flows over a 30-year system lifetime. The market analysis provided techniques to predict the cost and performance of PV systems such as inverter lifespan, future inverter costs, and module degradation. These estimates, along with the expected trends in electricity costs, were incorporated into the cash-flow analysis to provide a more realistic solution. Design options to reach grid parity at certain government incentive levels were shown to provide optimal results. The environmental analysis conducted in this study takes into account the amount of pollutants avoided over the lifetime of the system as well as the time it takes to recover the energy that went into the manufacturing process.

Although PV systems are still expensive and not very efficient to use in this part of the country, they nevertheless offer valid long-term investment if uncertainties regarding fuel prices and environmental regulations are taken into considerations. Further studies involving smart-grid integration with distributed energy sources is suggested.

Acknowledgements

This study was funded in part by the Sustainability Incentive Grant at Georgia Southern University. Special thanks and gratitude was also extended to the management of the shopping center for providing support and unlimited access to their facility.

References

[14] Dunlop, Jim. *Photovoltaic Systems.* Homewood, IL : American Technical Publishers, 2007.

[15] PV Watts. *PV Watts.* [Online] [Cited: March 4, 2010] http://rredc.nrel.gov/solar/calculators/PVWATTS/version1/US/Georgia/Savannah.html.

[16] Cautions for interpreting the results. *PV Watts.* [Online] NREL. [Cited: March 16, 2010.] http://rredc.nrel.gov/solar/calculators/PVWATTS/version1/i nterp.html.

[17] German Solar Energy Society. *Planning and Installing Photovoltaic Systems: A Guide for Installers, Architechs and Engineers.* Sterling, VA : Earthscan, 2008.

[18] Gregg, Allan. Sizing Ratio Should Optimize Specific Yield. *Solar Pro.* 2010, April/May.

[19] *Solar Energy.* Mondol, J.D., Yohanis, Y.G., & Norton, B. 80, Amsterdam : Elsevier, 2006.

[20] Perez, R. To track…or not ot track. *Home Power* 2004, June/July.

[21] How to Change PVWatts Parameters. *PV Watts.* [Online] NREL. [Cited: March 22, 2010.] http://www.pvwatts.org/.

[22] Economics of Solar Electric Systems for Consumers: Payback and other Financial Test. *OnGrid.* [Online] July 2009. [Cited: March 21, 2010.] http://www.ongrid.net/papers/PaybackOnSolarSERG.pdf.

[23] Gevorkian, P. *Solar Power in Building Design: The Engineer's Complete Design Resource.* New York, NY : McGraw-Hill Professional Publishing, 2007

[24] Navigant Consulting Inc. A review of pv inverter cost and performance projections. *NREL.* [Online] January 2006. [Cited: March 6, 2010.] http://www.nrel.gov/pv/pdfs/38771.pdf.

[25] Galvin, C.N., Muniz, L. Cost of capital of walmart. *CSUFullerton.* [Online] Dec 7, 2006. [Cited: March 20, 2010.] http://business.fullerton.edu/finance/yunpark/Files/fin332/Project/Cost%20of%20Capital%20of%20Walmart_Muniz%20and%20Galvin.pdf.

[26] Evaluating return on solar investments. *Solar Today.* [Online] American Solar Energy Society, October 12, 2009. [Cited: March 12, 2010.]

http://www.ases.org/index.php?option=com_content &view=article&id=860&Itemid=2.
[27] Wiser, R., Barbose, G., Peterman, C., & Darghouth, N. (2009). Tracking the sun ii: the installed cost of photovoltaics in the u.s. from 1998-2008. Lawrence Berkeley National Laboratory, Retrieved from http://eetd.lbl.gov/EA/emp/reports/lbnl-2674e.pdf
[28] Bureau of labor statistics, *Cpi inflation calculator*. Retrieved from http://www.bls.gov/data/inflation_calculator.htm
[29] Brigham, E.F., & Ehrhardt, M.C. (2008). *Financial management*. Mason, OH: South-Western Cengage Learning.
[30] McGrath, D. Analyst: Solar approaching grid parity in U.S. *EET Times.* [Online] July 13, 2009. [Cited: March 14, 2010.] http://www.eetimes.com/news/semi/showArticle.jhtml?artic leID=218500156
[31] Average Retail Price of Electricity to *Ultimate Co*nsumers by End-Use Sector, by State. *U.S. Energy Information Administration*. [Online] March 15, 2010. [Cited: March 30, 2010.] http://www.eia.doe.gov/cneaf/electricity/epm/table5_6_a.html
[32] What is the energy payback for PV? *NREL.* [Online] January 2004. [Cited: March 14, 2010.] http://www.nrel.gov/docs/fy04osti/35489.pdf.
[33] eGrid2007 Version 1.1. *EPA.* [Online] Dec 2008. [Cited: March 20, 2010.] http://www.epa.gov/cleanenergy/documents/egridzips/eGRID 2007V1_1_year05_SummaryTables.pdf

Biographies

YOUAKIM KALAANI graduated from Cleveland State University with a Doctoral degree in Electrical Engineering with emphasis in power systems. He is a licensed professional engineer, an ABET evaluator, and a member of IEEE, IAJC, and ASEE organizations. He is currently an Assistant Professor at Georgia Southern University. Dr. Kalaani may be reached at yalkalaani@gerogiasouthern.edu

WILLIAM NICHOLS graduated from Georgia Southern University in May 2010 with a Master of Science in Applied Engineering. His graduate research focused on the design of both grid direct and off-grid photovoltaic systems and photovoltaic system monitoring. Mr. Nichols may be reached at wtn918@gmail.com

DEVELOPMENT OF A COMPACT THREE-PHASE INDUCTION MOTOR DRIVE SYSTEM WITH DISCRETE COMPONENTS

Shiyoung Lee, The Pennsylvania State University Berks Campus

Abstract

Growth in the high-volume market in variable-speed drives (VSDs) is expected due to emerging applications in both home appliances and process industries. VSDs greatly improve efficiency in those applications. Almost all of these applications do not require precise positioning or speed control and, hence, are of low-performance types. The inverter-controlled induction motor drive (IMD) is a strong competitor for such applications due to the low-cost of the motor and its inherent features such as simplicity of control requiring no sensors in these low-performance applications. It is brushless, as it has no slip rings, thus making it truly almost maintenance-free and robust.

This study addresses issues of design and development of such a low-cost inverter and its controller in order to obtain a one-horsepower variable-speed IMD. In addition, an implementation of VSD with analog and discrete components is thoroughly discussed. The various issues addressed in detail are: specifications, appropriate control strategy and drive configuration, design of control circuits, and their switching and conduction losses and tuning. Results from a fully-tested one-horsepower experimental inverter-controlled induction motor drive system are presented to correlate the key design aspects and design specifications. The proposed VSD for the three-phase induction motor is implemented mostly with analog and discrete components; it will be very useful to students in electric motor drive courses to get an insight into a three-phase inverter and hands-on experiences in building and testing such a system.

Introduction

Emerging high-volume VSD applications have the stringent requirements of low-cost and compact packaging for the electronic inverter and its controller to induce the conversion of many fixed-speed applications to VSD operations with very little added cost due to the extra electronic components. The presentation of various studies would enhance the design and development concepts leading to the achievement of low-cost and compact drives for the motor drives market.

Such a study of the design and development of a one-horsepower inverter and its controller for an IMD achieving the specified requirements is presented in this paper. Furthermore, the proposed VSD for the three-phase induction motor is implemented mostly with analog and digital discrete components to gain insight into a three-phase inverter system and hands-on experience in building and testing a VSD for electric motor drives courses.

The induction motor is essentially a constant speed machine if a constant voltage and frequency source is connected [1]. When the load torque increases, the induction motor speed drop will be minimal, which is the advantage for constant-speed applications. Many single-chip microprocessor or digital signal controller (DSC) solutions to design a three-phase inverter for induction-motor-based VSDs involve a lot of software design; thus, they are not suitable solutions for this study [2], [3]. However, the software control of a VSD is desirable for providing flexibility of control and tuning without tinkering with hardware components, but it may not be sufficient to deal with details of VSD system implementation without a background in specific software language programming skills. The exposure of the major functional subsystems of the VSD to students is very important to the understanding of the overall system requirements and the design circuitry to meet the system requirements. The design philosophy in this study was to use as many commercial off-the-shelf (COTS) discrete analog and digital components as possible in order to provide rich insight into the IMD system and plenty of hands-on opportunities for the students to understand, analyze, and build it [3-15].

The highlights of this study are as follows: The specifications of the drive system and the rationale for choosing a drive system control strategy are explained first. Then, the subsystems of the proposed IMD are functionally identified. The design concepts of various subsystems and their implementation are explained. The outlines of the drive losses which lead to the selection of cooling arrangement satisfying the cost and packaging requirements are explained. The layout and final assembly of the power and control circuits are described along with the packaging details including that of the enclosure. Experimental results from the prototype inverter-fed IMD are presented to validate the design and conformity to specifications. In conclusion, various teaching topics for electric motor drives courses are suggested, based on the proposed IMD system.

Drive System Specifications and Selection of a Control Strategy

System Specifications

The induction motor considered for the development of the inverter and its controller was one-horsepower with three-phase windings and two poles, even though the number of poles does not affect the general design and development approach outlined in this paper. The ac input available was single-phase either with 50 or 60Hz and 240V. The design was modifiable for 120Vac input, hence the power rating of the inverter, without any modification, may be considered as 0.5hp.

The following general requirements and desirable features are the starting points for consideration of an IMD system design strategy: first quadrant operation capability, which means motoring operation only, variable stator voltage and variable stator frequency (VVVF), variable voltage with pulse-width modulation (PWM) at a low frequency to enhance efficiency of the overall IMD system, soft starting, current-limiting feature for the protection of the inverter, variable PI speed-controller gains, and provision for operation with and without tachogenerator feedback. In addition to these requirements, the following specifications, summarized in Table 1, were considered satisfactory for fan/pump types of loads.

Table 1. Target Specifications of the Proposed IMD

Power Source	Single-Phase, 240Vac, 50/60Hz
Output Power	1-hp maximum, three-phase
Output Voltage Range	0 to 220Vrms (line-to-line)
Output Frequency Range	0.1 to 86Hz
Commanded Speed Reference Voltage	5V for the rated speed
Measured Speed Input Voltage	50V maximum at rated speed
Modulation Method	Sine-triangular PWM (SPWM)
Carrier Frequency	2.78kHz
Protection Features	Current and torque limitation with undervoltage operation prevention
Adjustments	Soft start controller time constant, proportional and integral speed controller gains, torque limit, offset voltage, V/Hz ratio, and dc bus current limit
Ambient Temperature	0 to 40^{o}C (70^{o}C with derated output power)
Cooling Method	Forced air cooling
Target Package Volume	100 cubic inches

The parameters of the single-phase equivalent circuit of an induction motor are obtained by these measurements [1]: After running the motor until it was warmed up, the stator resistance, R_s , was determined from three dc resistance measurements between each pair of motor phases, and the obtained data were averaged and divided by two.

Other measurements were undertaken with the no-load test at the synchronous speed (3,600rpm) and the locked-rotor test at rest. The induction motor ratings and measured and calculated parameters are listed in Table 2.

Table 2. Induction Motor Ratings and Measured Parameters

Ratings of the Induction Motor under Test	1-hp, 230V, 3 phase, 60Hz, 3A, 3450rpm, 2-pole, Y-connected
Measured and Calculated Induction Motor Parameters at 60 Hz	R_s=2.355Ω, R_r=2.055Ω, L_m=183.4mH, L_{ls}=L_{lr}=7.388mH

Selection of a Drive Control Strategy

Based on the drive specifications, the most important first step is to identify the appropriate control strategy for the inverter-fed induction motor drive. The volts-per-hertz (V/Hz) control strategy was selected because it has sufficient performance from the point of view that it requires simple control circuitry [1]. It keeps the flux magnitude in the motor approximately constant by maintaining the voltage-to-frequency ratio constant except for a small resistive voltage offset. It is also not dependent on feedback signals for open-loop operation, requires very simple tuning in the form of its offset trimming and the change of voltage-to-frequency ratio.

As the frequency decreased at low speed, the voltage drop across the stator resistance can no longer be neglected; thus, an offset or boost voltage is necessary to provide the rated flux at low speeds. The effect of the offset voltage is negligible at higher frequencies. That even stator current measurement and feedback are not essential to this strategy is an important factor to be noted. All other control strategies, such as vector control, constant air gap flux control, and slip control, involve a greater use of control circuitry and feedback sensors, though they offer much more precise control of torque and speed. Since these control strategies involve rigorous code development efforts with a microprocessor or DSC, they were, therefore, not considered in this study in order to implement a simple controller with discrete analog and digital components.

Overall Drive System

The simplified block diagram of the proposed IMD incorporating the V/Hz control strategy is shown in Figure 1. The

speed reference, ω_m^*, is processed through a soft-start circuit, whose time constant can be adjusted externally with a potentiometer. The output of the soft-start circuit provides the modified speed command from which the filtered speed feedback signal is subtracted to provide the speed error. The speed error is amplified and processed through a proportional-plus-integral (PI) controller resulting in the

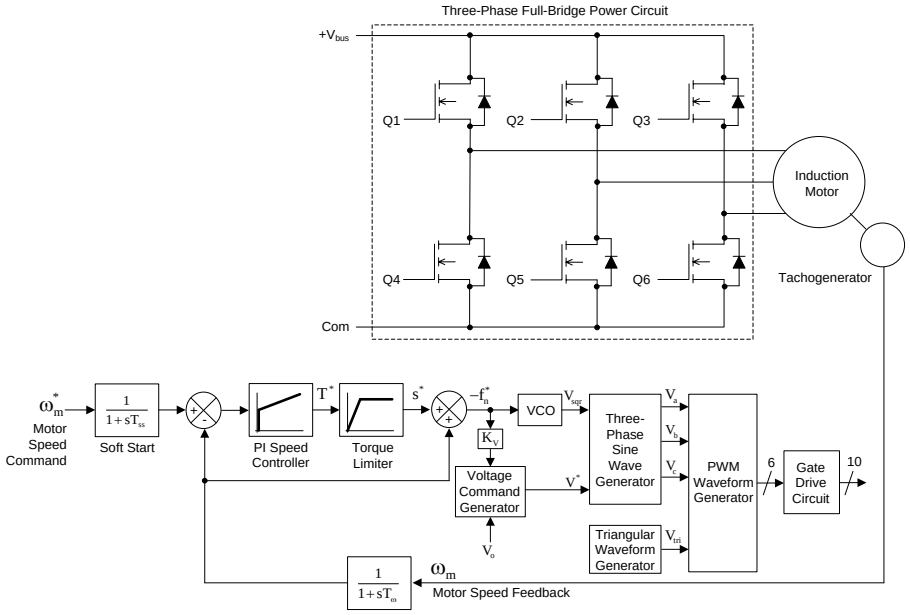

Figure 1. Block diagram of the proposed IMD incorporating the constant V/Hz technique

torque command, T^*, which is further processed through a torque limiter. The torque limiter constrains the torque to be within the stable region of the steady-state torque slip region and, in the process, also limits the currents to be within the permitted levels.

In the stable operating region the torque is proportional to the slip speed; hence, the output of the torque limiter could be taken as slip speed command, s^*. The slip speed command is added to the filtered normalized rotor speed, obtaining the normalized stator angular speed command or normalized stator frequency command, f_n^*. The stator frequency is multiplied by the voltage-to-frequency ratio and added to the stator offset voltage, V_o, to provide the stator voltage command. The offset voltage is intended to overcome the reduction of the air gap voltage and, hence, in the weakening of the magnetizing current due to the large stator resistive voltage drop at low speeds.

The stator frequency and voltage commands are then fed to a sine wave generator block to generate the three-phase stator voltage commands. These phase voltage commands are translated to actual phase voltages through SPWM with a triangular carrier frequency and obtaining a set of gate drive signals to the inverter bridge. The dc input voltage to the inverter is obtained through a diode full-bridge rectifier fed from a single-phase ac supply. It can be any dc voltage source, such as a solar panel and a wind generator with or without a front-end boost converter to control the dc bus voltage level.

Drive System Design and Realization

Design of an IMD System

The various major subsystems shown in Figure 1 were considered for design and implementation in this section. The schematic of each block and the realization with discrete analog and digital components may lead to application-specific integrated-circuit (ASIC) packaging if this design is to be adopted for manufacturing. But at this stage of prototype verification, it was decided to avoid the costs associated with such a development. Furthermore, the implementation of such a drive system with a microprocessor is not an option in this study to provide an insight of the drive system, which consists of discrete components only. Either a microprocessor (microcontroller) or DSC solution to implement a drive system usually involves a significant software development effort.

For the PWM signal generation in this study, the sine-triangular carrier modulation method was selected due to its simplicity for implementation. It consists of a carrier wave, which is basically a high-frequency triangular waveform,

and a sinusoidal modulation signal, whose amplitude varies depending on the speed command. These two signals were compared to generate a desired PWM output. The width of each PWM pulse is weighted by the amplitude of the sine wave at that instant. Therefore, the rms value of the voltage applied to the motor phase can be controlled by varying the duty cycle of the PWM signal. A voltage of 5V is selected to represent 1 p.u. value.

Soft-Start Circuit

The developed soft-start circuit consists of a difference amplifier (IC1:D) and an integrator (IC1:C). They are cascaded together to get a slow-rising voltage ramp. Figure 2 shows the soft-start circuit and has a transfer function of

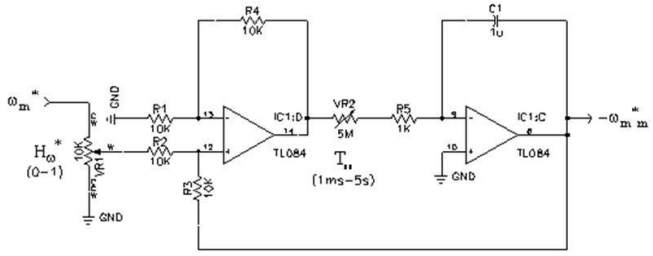

Figure 2. Soft-start circuit

$$G_{ss}(s) = \frac{1}{1 + T_{ss} \cdot s} \tag{1}$$

where

$$T_{ss} = (VR2 + R5) \cdot C1 \tag{2}$$

is the soft-start time constant that can be varied with VR2 from 1ms to 5s. VR1 adjusts the commanded normalized speed input gain, H_ω^*. When VR1 is turned to its maximum position, the 5V input commands the rated speed. In order to command the rated speed with a higher voltage, VR1 should be decreased accordingly.

PI Speed Controller

The PI speed controller shown in Figure 3 consists of IC2:C and IC2:D. Its transfer function is

$$G_c(s) = K_P + \frac{K_I}{s} \tag{3}$$

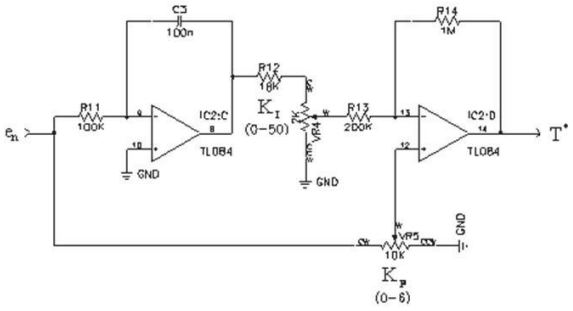

Figure 3. PI speed controller circuit

It produces the torque command, T^*. VR5 varies the proportional gain, K_P, from 0 to 6, and VR4 varies the integral gain, K_I, from 0 to 50. Since there is no simple way to determine these gains with the motor parameters, they should be adjusted empirically.

Torque Limiter

The torque limiter limits the torque and, consequently, the motor current to a safe level and prevents the motor from operating in the unstable region. The implemented torque limiter circuit is shown in Figure 4. It is formed around IC2:B and IC2:A. D1 does not allow the input voltage to exceed the voltage at the wiper of VR6, and, therefore, VR6

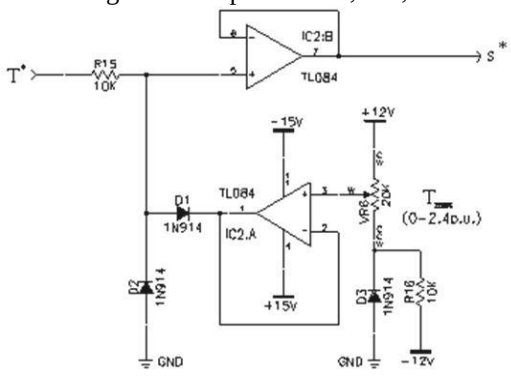

Figure 4. Torque limiting circuit

adjusts the torque limit from 0 to about 2.4 p.u.. D2 does not allow negative input voltages, since this is a one-quadrant drive and torque cannot be negative. The torque is proportional to the slip; the output of this circuit is the commanded slip speed in a normalized unit, s^*.

Voltage Command Generation Circuit

The voltage command generation circuit is implemented with an inverting amplifier IC3:B and is shown in Figure 5.

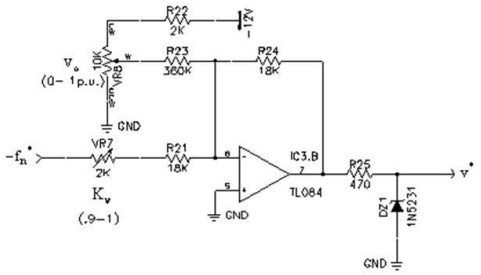

Figure 5. Voltage command schematic

It produces the commanded normalized voltage from the commanded normalized synchronous frequency using the formula

$$v^* = v_o + K_v \cdot f_n^* \tag{4}$$

where v_o is the normalized offset voltage and K_V is the normalized frequency to normalized voltage constant. VR8 varies v_o from 0 to 0.1 p.u., and VR7 varies K_V from 0.9 to 1. At the output of this block, there is a 5.1V zener diode, which prevents commanded voltages higher than the rated level of 5V. This causes the motor to operate in the flux-weakening region for speeds higher than the rated one.

Voltage-controlled Oscillator

Figure 6 shows the voltage-controlled oscillator (VCO), which is implemented with IC4 (XR 2207). The difference amplifier consists of IC3:C, and IC3:D brings the input voltage to a value suitable for IC4. This block produces a TTL level square wave, v_{sqr}, with a frequency of f_a given by

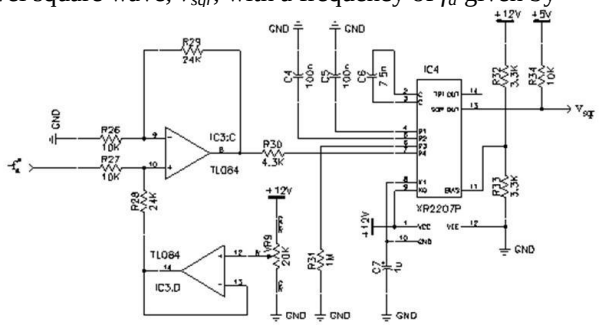

Figure 6. VCO schematic

$$f_a = \frac{1}{R31 \cdot C6} \cdot \left[1 - \frac{(V_c - 6) \cdot R31}{6 \cdot R30} \right] \tag{5}$$

where V_c is the voltage at the output of IC3:C, and is given by

$$V_c = 2.4 \cdot V_{in} + 12 \cdot \frac{VR9_W}{VR9} \tag{6}$$

where $VR9_W$ is the resistance from the pot wiper to its end. VR9 adjusts the frequency to be 1024 times the commanded value.

Three-Phase Sine Wave Generation Circuit

The three-phase sine wave generation circuit produces three-phase sinusoidal waveforms according to the commanded normalized synchronous frequency and the commanded normalized voltage. Figure 7 shows the sine wave generator block.

The signal from the VCO feeds a 12-stage ripple counter, IC5. The outputs of the counter's first ten stages, or $1024=2^{10}$, form a 10-bit address bus for a 16-bit output EPROM, IC6, where the sine waves for phases A and B are stored with 8-bit resolution for each phase. IC7 and IC8 are multiplying 8-bit DACs that produce negative voltages down to -5V. The amplitude and offset of the generated sine waves vary according to the commanded voltage signal so that

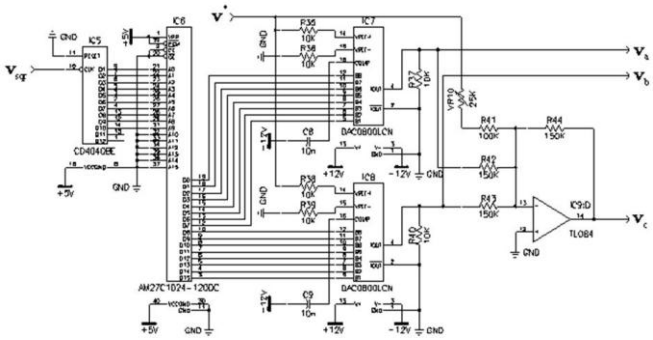

Figure 7. Sine wave generator circuit

$$v_a = -v^* \cdot \frac{1 + \sin(2\pi \cdot f_s^* \cdot t)}{2} \tag{7}$$

$$v_b = -v^* \cdot \frac{1 + \sin(2\pi \cdot f_s^* \cdot t - \frac{2\pi}{3})}{2} \tag{8}$$

where f_s^* is the commanded synchronous frequency. The voltage for the phase C is produced from the inverted summing amplifier circuit with IC9:D, as

$$v_c = -\tfrac{3}{2} v^* - (v_a + v_b) \tag{9}$$

VR10 balances the three-phase system eliminating any undesirable offset voltage from IC9:D.

Triangular Waveform Generation Circuit

The three-phase inverter was designed to operate at a switching frequency of f_S = 2.78kHz. Therefore, the output of a carrier frequency generation circuit has the same frequency. Figure 8 shows the triangular carrier waveform generator circuit, which is formed around IC11.

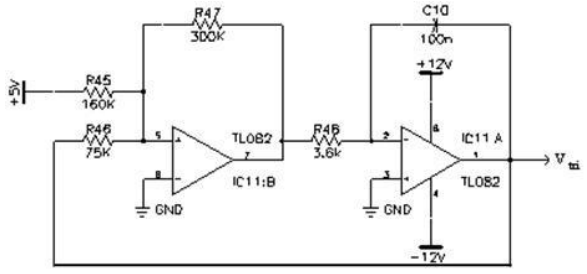

Figure 8. Triangular wave generator schematic

This circuit produces a triangular waveform, v_{tri}, with a frequency of f_b , which is given by

$$f_b = \frac{R47}{4 \cdot R46 \cdot R48 \cdot C10} \tag{10}$$

And has a peak-to-peak amplitude, V_m , given as

$$V_m = 2 \cdot V_{max} \cdot \frac{R46}{R47} \tag{11}$$

where V_{max} is the maximum output voltage of IC11 with 10V, and an offset of V_{of}

$$V_{of} = 5 \cdot \frac{R46}{R45} \tag{12}$$

which matches the output voltage range of the DAC0800.

Three-Phase PWM Generation Circuit

Figure 9 shows the three-phase PWM block comprised of IC10, IC9:B and IC9:C. Each of the three-phase sine waves is compared with the common triangular carrier waveform with two complementary comparators to produce the three-phase PWM signals: IC10:C and IC10:B for v_a, IC10:D and IC10:A for v_b, and IC9:C and IC9:B for v_c. The outputs of the comparators are v_{L1} - v_{L3} for the low-side and v_{H1} - v_{H3} for the high-side drive signals for the succeeding gate drive circuit.

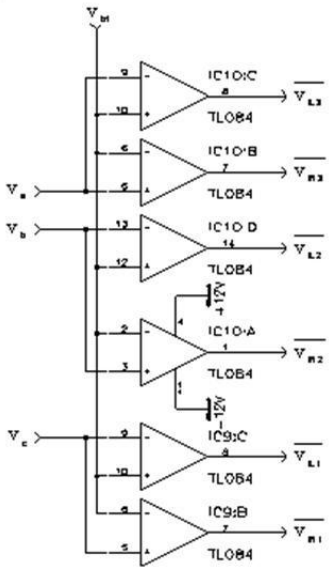

Figure 9. Three-phase PWM generation circuit

The Multisim circuit diagram for the simulation of the SPWM technique is shown in Figure 10. The schematic diagram shows the single phase only. The triangular carrier signal is common to all three-phase PWM generation circuitry. R1 and R2 are dummy loads to monitor resulting PWM signals. The simulation result which depicts the three-phase SPWM technique is shown in Figure 11(a) with the three-phase sine waves and triangular carrier waveform. The generated high-side PWM signal for the following gate drive IC, IR2130, is shown in Figure 11(b).

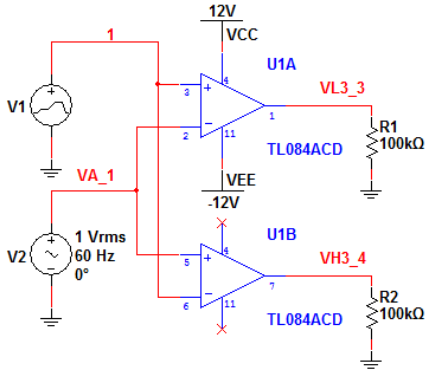

Figure 10. Multisim three-phase SPWM generation circuit (single phase only)

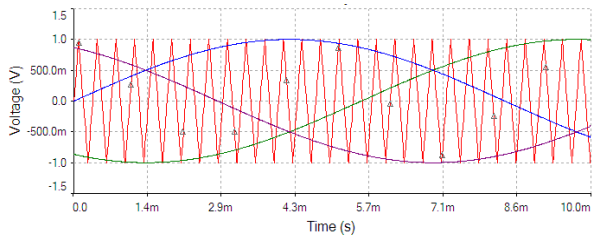

(a) Multisim simulation result with three-phase sine waves (60 Hz) and triangular carrier waveform (2.78 kHz)

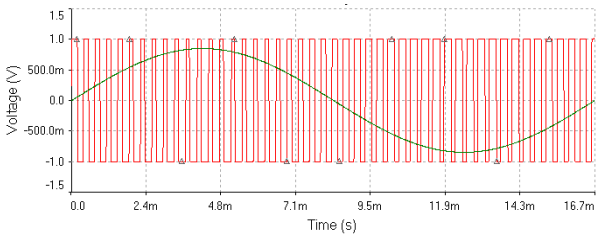

(b) Three-phase SPWM signal for the phase A

Figure 11. Multisim simulation result of the normalized three-phase PWM signals with SPWM technique

Gate Drive Circuit

A high-voltage three-phase gate driver IC, IR2130 from International Rectifier, is used for interfacing gate drive signals with MOSFET power switches. Figure 12 shows the gate drive circuit which is implemented with IC12 (IR 2130). The PWM signals are limited to a 0-5V range, and fed to the gate driver circuit, IC12, which interfaces them to the power-switching devices. IC12 contains three floating and three ground-referenced drivers, and provides dead time between the high and the low sides, as well as current limiting. VR11 adjusts the dc bus current limit value from 2A. It should be adjusted so that the instantaneous bus current does not exceed the rated instantaneous switching power device current. v_{G1} - v_{G6} are

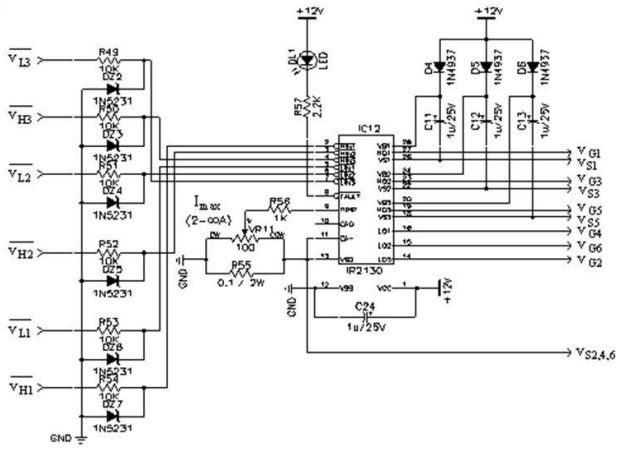

Figure 12. Gate drive circuit

connected to the gate terminals of the power switching devices, and v_{S1} - v_{S6} to the power devices' source terminals. In this study, the three-phase inverter circuit consists of six IRF840 Power MOSFET devices. But integration of those power devices by replacing them with an intelligent power module, which encases the dedicated gate drive circuit and protection circuit, may provide better thermal management, a smaller footprint, and less electromagnetic interference (EMI) noise emission.

Loss Evaluations and Cooling Design

Losses in the Converters

The inverter operates at a switching frequency of f_S = 2.78kHz. The resistors that are in series with the devices' gates set the switching time to about 0.5μs. Assuming the dc bus voltage is constant at

$$V_{BUS} = 230 \cdot \sqrt{2}\ V \tag{13}$$

the three-phase inverter losses are modeled as:

$$\begin{aligned} P_{INV} &= 3 \cdot (\tfrac{1}{2} \cdot V_{BUS} \cdot I_M \cdot f_S \cdot (t_r + t_f) + \\ &\tfrac{1}{2} \cdot V_{BUS} \cdot I_M \cdot f_S \cdot t_{rr} + {I_M}^2 \cdot R_{DS}) \\ &= 1.98 \cdot I_M + 3.57 \cdot {I_M}^2 \end{aligned} \tag{14}$$

where I_M is the motor current, t_{rr} the reverse recovery time of the antiparallel diodes of the power MOSFET switching device, and R_{DS} is the ON resistance of the power devices.

The loss model of the front-end full-wave bridge rectifier circuit is:

$$\begin{aligned} P_{BR} &= 2 \cdot V_D \cdot I_{IN} = 2 \cdot V_D \cdot \frac{P_{IN}}{V_{IN}} \\ &= 2 \cdot 0.7 \cdot \frac{P_{IN}}{230} = 0.0061 \cdot P_{IN} \end{aligned} \tag{15}$$

where V_D is the voltage drop across one of four bridge rectifier diodes, I_{IN} is the input current, and P_{IN} is the input power. The drive efficiency is derived from the inverter losses and the bridge rectifier losses. Based on these, the maximum inverter and bridge rectifier losses are estimated to be 40.8 and 6.21W, respectively, giving total losses of 47W.

Cooling Design

Based on the estimation of 47W losses, the compactness requirement in the drive packaging requires the smallest heatsink with forced-air cooling. A compact heatsink, which could satisfy all the requirements including the most crucial one of low-cost until a heatsink with dense small thin fins and allowing a turbulent air flow, is utilized in this design and layout to meet the compactness requirements.

PCB Layout Design and Final Assembly

Based on the heatsink dimension of 2.4 square inches and the final package volume requirement of 100 cubic inches, it became necessary to develop the layout of the power, controller, dc link filter, power supplies, fuses and connector around these specifications. The controller boards were split into two boards with dimensions of 2.45" × 5.1" and the power board connections were arranged in a printed circuit board (PCB) of 2.87 square inches. The drive circuit was divided into three double-sided PCBs, namely control board, driver board, and power board, as shown in Figure 13. The control board and driver board were implemented on the 5.0"× 2.4" PCBs. They contain the housekeeping power supply and the PI controller and the sine wave generator, and the PWM circuit and the gate drive IC, respectively. The power board (2.8"× 2.8") contains the bridge rectifier, the power devices, and the rest of the power circuit. The bridge rectifier and the power devices were mounted on the 2.4"× 2.4"× 0.5" heatsink, which also has a small fan attached to it. The three PCBs were assembled to form a 'Π' with the control board and the driver board at the sides, and the power board at the top, so as to enclose the dc bus electrolytic capacitors. A 6.0"× 4.3"× 2.9" enclosure was designed for the drive as follows: The top two pieces are folded to form two 'L's along the dotted line. When put together, they form a box whose front and back are the other two pieces. There is a hole in the middle of the front piece for mounting a potentiometer, if one is used to give the speed command.

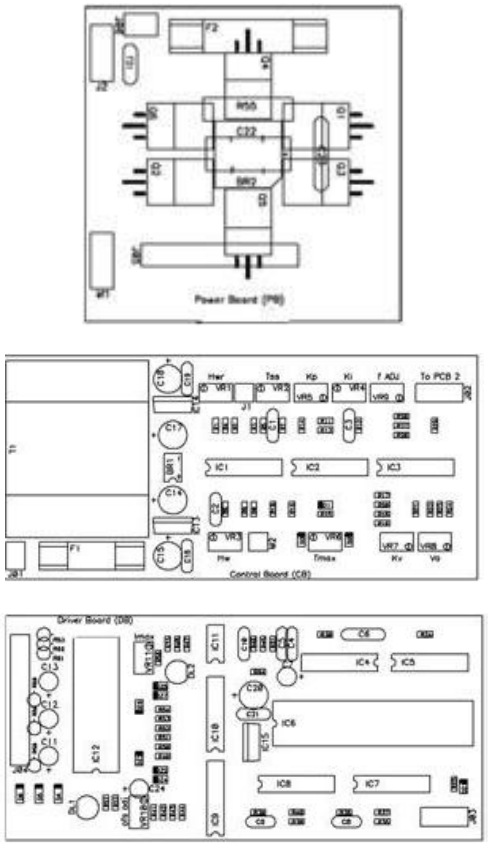

Figure 13. Proposed three PCBs to enclose all electronic circuitry (from top: power, driver, and control boards)

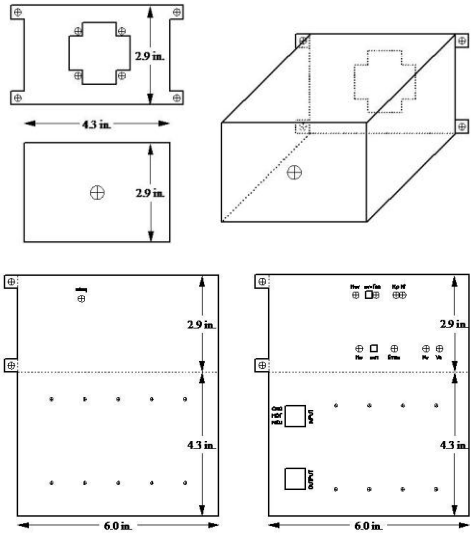

Figure 14. Proposed enclosure design

Figure 15. Comparison of the developed inverter (left) with a commercial one

The four holes at the edges of the rear piece were used for the mounting of the drive. The final enclosure assembly had the dimensions of 4.3"x 2.9"x 7" including heatsink and fan with an overall packaging volume of 87 cubic inches, thus satisfying the packaging specification of less than 100 cubic inches. The proposed enclosure design is shown in Figure 14 and the prototype VSD is compared with Toshiba's VF-SX inverter in Figure 15. The size of Toshiba's inverter is 4.1"x 5.9"x 4.7" (approximately 114 cubic inches) with 1-hp output rating and contains many extra functions, which are not necessary for the low-cost fan/pump applications. The designed inverter is comparable to a commercial one in enclosure size.

Experimental Results

Experimental results on a 1-hp induction motor using the prototype VSD are presented in this section. The measured motor current waveform and its fast Fourier transform (FFT) results are shown in Figure 16. The FFT shows a strong fundamental frequency, 60Hz, component with negligible harmonics. The current ripple in the motor-current waveform can be reduced by increasing the frequency of the PWM. The overall efficiency of the motor drive is both calculated using procedures outlined in [11] and measured as shown in Figure 17 for a fan load. The efficiency of both methods shows a close match over the

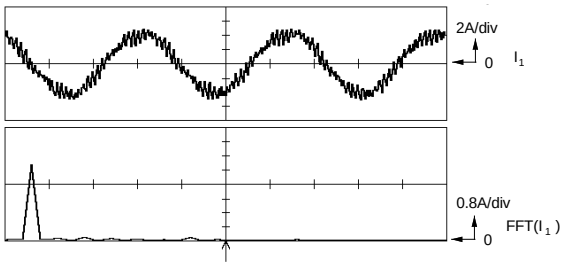

Figure 16. Motor current (Horizontal: 5 ms/div) and FFT (Horizontal: 100 Hz/div)

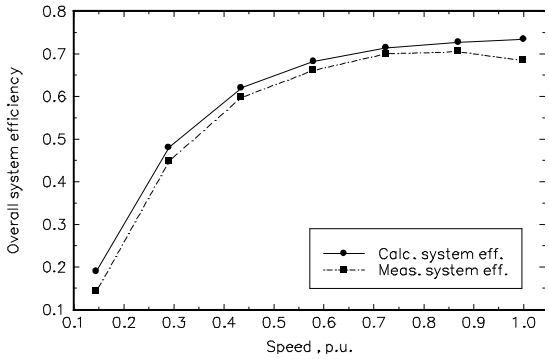

(a) Overall system

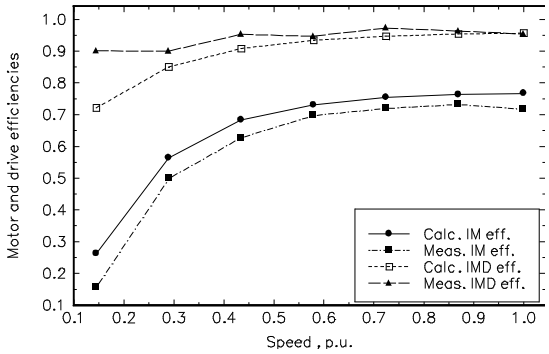

(b) Motor and inverter

Figure 17. Predicted and measured efficiencies

entire speed range. Figure 17(b) shows the predicted and measured induction motor and drive efficiencies that contributed to the system efficiency curves shown in Figure 17(a).

Topics for Electric-Motor Drives Courses

With the prototype IMD, the following topics are valuable for the electric motor drives course: principles and operations of the three-phase rectifier, SPWM, three-phase inverter, V/Hz control technique, three-phase sine wave generation, PI controller, gate drive circuit, soft-start circuit, torque-limiting circuit, VCO, and triangular waveform generation circuit. The layout design of the developed circuitry on PCB to optimize the power dissipation and EMI emission is very useful for the development of a VSD in the real world. Tuning and adjustment of the VSD provides plenty of hands-on experience to the students.

Conclusion

A high-density package of less than 100 cubic inches, 1-hp IMD with discrete analog and digital components have been designed, implemented and tested for emerging high-

volume VSD applications. The design details and considerations of the controller, converters, their layouts and packaging, thermal design and overall packaging were systematically developed to assist in the development of other drives of various sizes. The overall VSD system efficiency and induction motor efficiency are obtained analytically and empirically. Both results were well matched with each other over the entire motor speed range. In conclusion, various teaching components are identified for electric motor drives courses.

References

[1] R. Krishnan, "Electric Motor Drives: Modeling, Analysis and Control," Prentice Hall, 2001

[2] Padmaraja Yedamale, "Speed Control of 3-Phase Induction Motor Using PIC18 Microcontrollers," AN 843, Microchip Technology, 2002.

[3] Dave Wilson and Bill Lucas, "Ready-to Use AC Induction Motor Controller IC for Low-Cost Variable Speed Applications," Freescale Semiconductor White Paper, MC3PHACWP Rev. 0, October 2005.

[4] Ali Keyhani, Mohammad Marwali, Lauis Higuera, Geeta Athalye, and Gerald Baumgartner, "An Integrated Virtual Learning system for the Development of Motor Drive systems," IEEE Transactions on Power Systems, vol. 17, no. 1, pp. 1-6, February 2002.

[5] Carlo Cecati, Antonio Dell'Aquila, and Marco Liserre, "A Novel Three-Phase Single-Stage Distributed Power Inverter," IEEE Transactions on Power Electronics, vol. 19, no. 5, pp. 126-1233, September 2004.

[6] Jacinto Jiménez-Martinez, Fulgencio Soto, Esther de Jódar, Jose Villarejo, and Joaquin Roca-Dorda, "A New Approach for Teaching Power Electronics Converter Experiments," IEEE Transactions on Education, vol. 48, no. 3, pp. 513-519, August 2005.

[7] Robert Balog, Zakdy Sorchini, Jonathan Kimball, Patrick Chapman, and Philip Krein, "Modern Laboratory-Based Education for Power Electronics and electric Machines," IEEE Transactions on Power Systems, vol. 20, no. 2, pp.538-547, May 2005.

[8] S. Shirsavar, Benjamin Potter, and Isabel Ridge, "Three-Phase Machines and Drives – Equipment for a Laboratory-Based Course," IEEE Transactions on Education, vol.49, no. 3, pp.383-388, August 2006.

[9] Erkan Mese, "Project-Oriented Adjustable Speed Motor Drive Course for Undergraduate Curricula," IEEE Transactions on Education, vol.49, no. 2, pp. 236-246, May 2006.

[10] Anibal Almeida, Fernando Ferreira, and Dick Both, "Technical and Economical Considerations in the Application of Variable-Speed Drives with Electric Motor Systems," IEEE Transactions on Industry Applications, vol.41, no. 1, pp. 188-199, January/February 2005.

[11] R. Krishnan, D. Diamantidis and S. Lee, "Impact of Power Factor Correction on Low Power Inverter-Fed Induction Motor Drive System," IEEE Power Electronics Specialists Conference, pp. 593-598, 1995.

[12] J. Zhao and J. Liu, "Modeling, Simulation and Hardware Implementation of an Effective Induction Motor Controller," International Conference on Computer Modeling and Simulation (ICCMS 2009), pp. 136-140, February 20-22, 2009.

[13] L. Xue and J. Liu, "Simulation and Experiment of Induction Motor Controller," IEEE International Conference on Computer and Automation Engineering (ICCAE 2009), pp. 54-58, March 8-10, 2009.

[14] C. Kamble, J. Chaudhari, and M. Aware, "Digital Signal Processor Based V/f Controlled Induction Motor Drive," IEEE Third International Conference on Emerging Trends in Engineering and Technology, pp. 345-349, November 19-21, 2010.

[15] M. Arrofiq, N. Saad and M. Karsiti, "Performance of a PLC-based Hybrid Fuzzy Controller for PWM-driven Variable Speed Drive with Constant V/Hz Ratio," IEEE International Conference on Intelligent and Advanced Systems (ICIAS 2010), pp. 1-6, June 15-17, 2010.

Biography

SHIYOUNG LEE is currently an Assistant Professor of Electrical Engineering at Pennsylvania State University Berks Campus, Reading, PA. He teaches Programmable Logic Controller (PLC), Linear Electronics, Electric Drives, and Electric Circuits Laboratory courses. His research interest is digital control of motor drives and power converters. He is a senior member of IEEE and member of ASEE, ATMAE, and IAJC. Dr. Lee may be reached at sul28@psu.edu.

DYNAMICS OF A VERTICAL TAKEOFF AND LANDING (VTOL) UNMANNED AERIAL VEHICLE (UAV)

Alvaro Vargas-Clara, Arizona State University; Sangram Redkar, Arizona state University

Abstract

The objective of this work was to develop a stop-rotor unmanned aerial vehicle (UAV). This UAV would be capable of vertical takeoff and landing like a helicopter and could convert from a helicopter mode to an airplane mode in midflight. Thus, this UAV could hover as a helicopter and achieve high mission range like an airplane. The term stop-rotor implies that in midflight the lift generating helicopter rotor stops and the rotor blades transform into airplane wings. The thrust in the airplane mode is provided by a pusher propeller. This aircraft configuration presented unique challenges in modeling, aerodynamics, and control. Another important task was to design an autopilot for this configuration that would stabilize the aircraft and allow it to operate in a fly-by–wire mode. In this paper presented the modeling and aircraft design along with a brief discussion of the autopilot architecture of this UAV. Also presented are some experimental "conversion" results, where a stop-rotor aircraft was dropped from a hot-air balloon and performed successful conversions from helicopter to airplane mode and vice versa.

Introduction

For any meaningful payload, speed, or endurance, airplanes need runways. Helicopters, having no need for runways, cannot compare with their fixed-wing relatives for payload, speed, range, or endurance. A vehicle that would not require a runway like a helicopter but enjoy the payload, speed, range, and endurance of an airplane would be an ideal aircraft. The multimode rotors on tilt-rotor vehicles, such as the V-22 Osprey and the TR911D Eagle Eye UAV, are compromised in terms of factors such as blade twist and geometry, due to conflicting requirements depending on the mode of flight. While cruising as a fixed–wing machine, the rotors are far from ideal as a thrust device; and while in helicopter mode, the rotors are likewise far from ideal in the hover mode and particularly in autorotation. Such fundamental compromises will likely make a candidate tilt-rotor small VTOL UAV performance fall well short of the mission range and endurance performance objectives over fixed-wing aircraft (citing the Scan Eagle example) and gain the VTOL capability. For over five decades, the aerospace community has recognized that such an ideal aircraft would likely be of a stop-rotor configuration. For most of those five decades, innumerable stop-rotor concepts and ideas have been advanced. Among recent efforts have been the cancelled Boeing X-50 Canard Rotor Wing and the Sikorsky X-Wing.

In virtually every case known to the authors, the stop-rotor concepts were of a radial-flow conversion category. This is to say the rotor disc is parallel to the airflow during conversion when the rotors are to be slowed and stopped to become wings. Like the critical roll-control issue plaguing airplane developers fifty years since Cayley's experiments, the stop-rotor development progress has been stalled for fifty years mainly over the obstacle of the conversion approach between rotary and fixed-wing modes of flight. What is demonstrably needed in order to resolve this critical issue from hampering stop-rotor development is a departure from the radial-flow conversion approach. A stop-rotor proposed here is the first and only stop-rotor concept where an axial-flow conversion approach is advanced. Axial-flow conversion is analogous to feathering or pitching propellers with the airflow impinging upon the rotor disc plane perpendicularly, aligned with the rotational axis of the rotor. The principal advantage of an axial-flow conversion approach compared to the radial-flow conversion is that the airflow impinging the airfoil does not change direction; as such, the airfoil can have conventional, normal profiles with aeroelastically-stable quarter-chord pitch axes.

The flight Conversion Concept for the stop-rotor is illustrated in Figure 1. It is important to note that the stop-rotor craft can convert between helicopter and airplane modes of flight any number of times during the same flight. The helicopter mode is not just the launch and recovery method that some have misunderstood from this illustration. Really, the point of this illustration is to emphasize the conversion sequence between helicopter and airplane mode of flight for the vehicle.

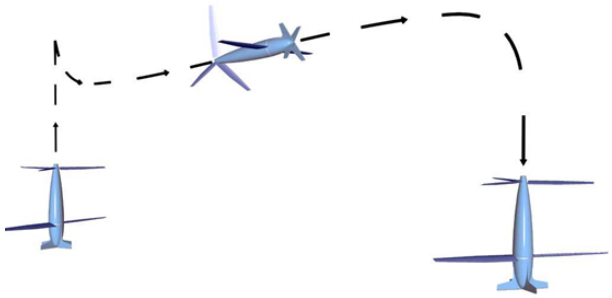

Figure 1. Stop-Rotor Flight Conversion

For example, from the powered helicopter mode, a selectable clutch is released while the wings and tail fins are collectively pitched (analogous to feathering a propeller) until in the airplane-mode position. The wings and tail fins stop rotation solely due to external aerodynamic forces and do not require indexing or braking and/or a locking mechanism of any kind. The selectable clutch engages the propeller drive shaft so that power can be delivered to the pusher propeller for the airplane-mode of flight. The propeller is thus optimized for cruising and not compromised like many other fixed-pitch propeller UAVs for take-off and cruise conditions. In the conversion from airplane to helicopter (from powered airplane) mode, the clutch is released and the wing and tailfins are collectively pitched to the autorotation position. The wings and tail fins spin up solely due to external aerodynamic forces. The selectable clutch engages the tail fin hub and power is then delivered to the tail fin for powered helicopter mode of flight while the collective pitch is increased to provide hovering and normal helicopter-like flight in the usual manner. Thus, the stop-rotor design is an ideal fixed-wing, uncompromised in terms of propulsion and landing mechanism making available higher weight fractions for payload and fuel for longer endurance and greater payload than conventional fixed-wing designs. In helicopter mode, the stop-rotor craft is an ideal rotary-wing vehicle, with efficient, slow turning rotors without a power-robbing tail rotor for anti-torque.

Mathematical Modeling of the Stop-Rotor UAV

Consider the stop-rotor configuration of Figure 2. In order to develop the mathematical model, the stop-rotor structure is divided into the following subcomponents.

a) Tail rotor: The tail rotor is comprised of three identical tail fins. It acts as a rotor in the helicopter mode and generates lift.
b) Wings: The wings provide the lift in the airplane mode and have control surfaces. In the helicopter mode, the wings rotate due to torque reaction.
c) Fuselage: The fuselage houses the electro-optical payload and is stationary during helicopter or aircraft mode.

In this section, the mathematical model of the stop-rotor design is briefly discussed. This model is incorporated in the MATLAB code. The mathematical model is developed using d'Alembert's principle considering dynamic, gravity, and aerodynamic forces [1-3]. For the initial analysis, the stop-rotor tail rotor is assumed to be unpowered and conversion from helicopter mode to airplane mode is achieved by feathering the wings. The following coordinate systems are used to develop the model as shown in Figure 2.

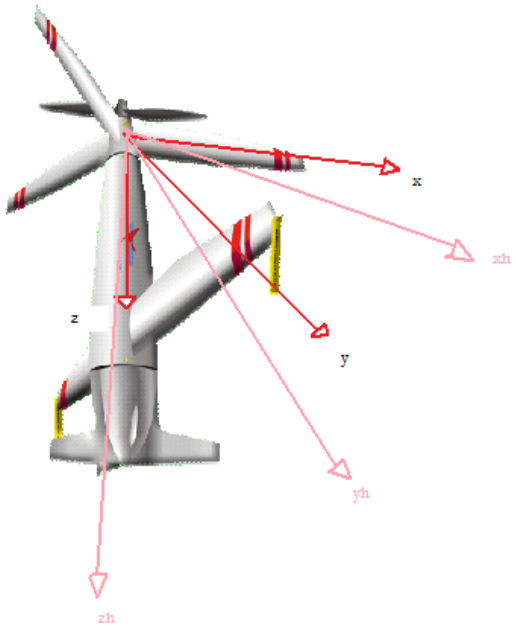

Figure 2. Stop-Rotor Configuration and Coordinate Axes

1. Tail rotor body fixed coordinate system that rotates with tail rotor.
2. Hub coordinate system coinciding with the tail-rotor coordinate system but fixed to hub.
3. Wing coordinate system: wing fixed coordinate system rotating with wing in the helicopter mode.
4. Gravity coordinate system: located on fuselage coinciding with the hub coordinate system but z axis is always pointed downwards aligning itself with the pull of gravity.
5. Ground coordinate system inertial coordinate system located fixed on ground.

In this study, procedures for deriving the equations of motion were similar to those of other studies [1-3]. The gravity coordinate system is translated from the ground coordinate system with $\mathbf{x} = [x_G, y_G, z_G]$; where x_G, y_G, z_G corresponds to distances from the inertial reference frame. The relation between the coordinates in both the systems is given by

$$\mathbf{x}_p = \mathbf{A}(\psi, \theta, \phi)\mathbf{x} \tag{1}$$

where $\mathbf{A}(\psi, \theta, \phi)$ is the generalized rotation matrix and ψ, θ, ϕ are inertial yaw, pitch and roll angles. Equations of motion for the stop-rotor configuration are grouped as

$$\begin{aligned} \mathbf{F}_{TR} + \mathbf{F}_F + \mathbf{F}_W &= 0 \\ \mathbf{M}_{TR} + \mathbf{M}_W + \mathbf{M}_W &= 0 \end{aligned} \tag{2}$$

where $\mathbf{F}_{TR}, \mathbf{F}_F, \mathbf{F}_W$ are the forces acting on the tail rotor, fuselage and wings, and $\mathbf{M}_{TR}, \mathbf{M}_W, \mathbf{M}_W$ are the moments act-

ing on the tail rotor, fuselage and wings. Each element of Equation (2) is comprised of inertia, aerodynamic and gravity parts.

Inertial Loads: The expressions for inertial load, $\mathbf{Q}_{pi}$, is obtained using the conservation of momentum, which can be written in the general form as

$$\mathbf{Q}_{pi} = \mathbf{I}_{pi}(\dot{\mathbf{Y}}_{pi} + \dot{\mathbf{Y}}_{mi}) + (\mathbf{\Omega}_{pi} + \mathbf{\Omega}_{mi})\mathbf{I}_{pi}(\mathbf{Y}_{pi} + \mathbf{Y}_{mi}) \quad (3)$$

where $\mathbf{I}_{pi}$ is the generalized inertia matrix, $\mathbf{Y}_{pi}$ is the state vector comprising the components of velocities and rates. $\mathbf{Y}_{mi}$ is the state vector comprising the relative velocities and rates. $\mathbf{\Omega}_{pi}, \mathbf{\Omega}_{mi}$ are angular velocities and relative angular velocity matrices. The nonlinear parts of Equation (3) contains all acceleration acting on the rotating elements including gyroscopic effects.

Gravity Loads: The vector of gravity acceleration in the gravity coordinate system is given by $\mathbf{g} = [0, 0, g]^T$. The gravity vector can be rotated using the transformation matrix $\mathbf{A}_G(\psi, \theta, \phi)$. The gravity loads on stop-rotor components can be calculated as

$$\begin{aligned} \mathbf{F}_{ig} &= m_i \mathbf{A}_G \mathbf{g} \\ \mathbf{M}_{ig} &= \mathbf{r}_{CG} \times (m_i \mathbf{A}_G \mathbf{g}) \end{aligned} \quad (4)$$

where m_i is the mass of the element/component and $\mathbf{r}_{CG}$ is the position vector from the center of gravity of the element relative to the reference coordinate frame.

Aerodynamic Loads: The differential aerodynamic loads comprising drag, lift and moment on element i, can be expressed in the element coordinate system as

$$\begin{aligned} dD &= \frac{1}{2}\rho c(y) V_a^2 C_D(\alpha) dy \\ dL &= \frac{1}{2}\rho c(y) V_a^2 C_L(\alpha) dy \\ dM &= \frac{1}{2}\rho c^2(y) V_a^2 C_M(\alpha) dy \end{aligned} \quad (5)$$

where $\frac{1}{2}\rho V_a^2$ is the dynamic pressure and $C_D(\alpha), C_L(\alpha), C_M(\alpha)$ are coefficients of drag, lift and moment, respectively. The aerodynamic forces in the element coordinate system can be transformed to the coordinate system corresponding to Equation (2). It is important to note that the tail fin and wing has NACA0012 airfoil, which is widely studied and performance data is available in the literature. However, to characterize fuselage aerodynamic coefficients, CFD modeling, and/or wind-tunnel testing is required.

Design Considerations

In the course of detailed design, Finite Element (FE) Analysis was used. In this section, aerodynamic and FE analysis on the stop-rotor wing is briefly presented [4]. A wing under operating conditions experiences aerodynamic loads. These aerodynamic loads were used to conduct a structural analysis on the wing. The wing was modeled as pin supported at two bearing locations at aluminum spar. The loads that the wing structure experienced were lift force, drag force, and moment. All aerodynamic loads were assumed to be acting at a quarter-chord point and to be constant along the span of the wing.

The first step in conducting this analysis was to determine the aerodynamic loads that the wing structure would experience. These loads were determined by conducting a 2D CFD analysis on a NACA 0012 airfoil. The calculated Reynolds number at which the wing would operate was 483,908 at STP. The CFD analysis was conducted using XFLR 5 [5] software. In doing the CFD analysis, coefficients of lift, drag, and moment were obtained (shown in Tables 1 and 2) at various angles of attack (alpha).

Table 1. Coefficient of Lift, Drag and Moment at Different Angles of Attack [4]

Alpha	CL	CD	CM
0	0	0.00623	0
5	0.6317	0.01049	-0.0134
10	1.0411	0.01955	0.0114
15	1.2194	0.04987	0.0331

Once these coefficients were obtained, the aerodynamic forces were calculated using Equation (5).

Table 2. Aerodynamic Loads at Different Aangles of Attack [4]

Alpha	Lift per unit Span(N/m)	Drag per unit Span (N/m)	Moment per unit Span(Nm)
0	0	0.7196791	0
5	72.97292	1.2117871	-0.41284
10	120.2661	2.2583831	0.35122
15	140.863	5.7608984	1.019769

The next step was to construct the wing structure using Solidworks [6]. The structure is shown in Figure 3 and consists of two major components: an airfoil skin and the aluminum spar. The span of the wing was 47.5 inches and the thickness was assumed to be 0.1 inches. The aluminum spar had a span of 52.5 inches and the thickness of the aluminum spar was measured to be 0.125 inches. The material for both components was assumed to be Aluminum 2014.

The wing structure was then inputted into NX 7 Nastran [7], where mesh, constraints, and loads were applied. The elements selected for this analysis were thin-shell Quad-4, and solid Hex-8. The airfoil skin used the thin shell, while the aluminum spar used solid elements. A 2D mapped mesh was applied on the airfoil skin, while a 3D swept mesh was applied on the aluminum cross-section. This resulted in a uniform mesh in the aluminum spar and airfoil, as shown in Figure 3. A face split was used on the top surface of the airfoil to create a single contact point with the aluminum spar. At this location, the spar and airfoil shared common nodes along the span-wise direction.

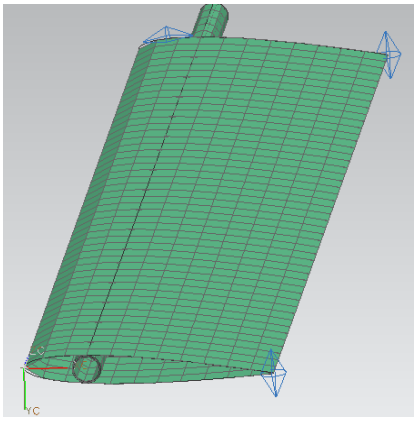

Figure 3. Wing structure and FE mesh [2]

The last step in setting up the analysis was to input the loads and constraints. The edge created by the face split was used to apply the lift and drag forces. The lift force was applied on the top surface of the airfoil skin in the negative y-direction, while the drag force was split in half and applied to the top and bottom of the spar in the x-direction. The moment was applied to the inner surface of the tube in the z-direction. The constraints used for this analysis were pinned constraints at the aluminum spar. These constraints were selected to simulate the mounting structure of the wing. The method of applying these constraints was using a user-defined constraint. This was done by fixing the translations in the x, y, and z directions for selected nodes at the locations where the bearing supports would be located.

For this structural analysis, the results obtained were for deflection, Von Mises stresses, and vibration of the wing structure. This analysis was conducted using the maximum values of lift, drag, and moment forces previously obtained. The wing structure had a maximum magnitude deflection of 0.167 inches located at the tip of the wing (as shown in Figure 4). The minimum deflection was 0 inches, situated at the constraints.

The maximum and minimum deflections in the x and y directions are given in Table 3:

Table 3. Maximum and Minimum Deflection in x and y Directions [4]

Direction	Maximum	Minimum
X-direction	0.002243 in.	-0.00029 in.
Y-direction	0.1672 in.	-0.00675 in.

The maximum Von-Mises stress was found to be 5,421 psi located next to the pinned constraint, while the minimum Von-Mises stress was 1.931 psi at the tip of wing. These results are presented in Figure 5.

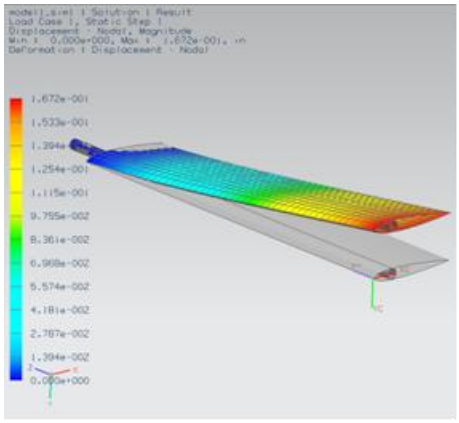

Figure 4. Magnitude Deflection of wing structure [4]

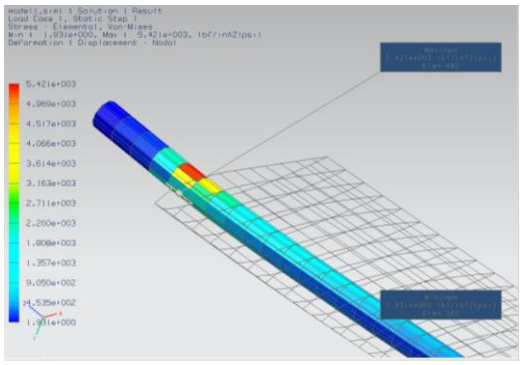

Figure 5. Von Mises Stress in entire wing structure [4]

The maximum Von-Mises stress occurred at the bottom and top of the spar right after the constraints; this is understandable since the wing structure is mostly experiencing a bending due to the lift. As well, the maximum stress of 5,421 psi is well within the yield strength of Aluminum 2014, which is 60,000 psi. This relatively low Von-Mises value is due to the weak loading conditions the structure experienced. The aerodynamic forces were calculated using the assumption that the maximum velocity the wing would experience would be 26.82m/s, which is a qualified small velocity. So, the aerodynamic forces were small. The results obtained from vibration are realistic because they illustrated all of the deformations that are expected under vibration.

The stop-rotor wing exhibits the following modes, as shown in Table 4. These modes are depicted in Figure 6.

Table 4. Vibration Deformations [4]

Vibration Frequency	Deformation Type
Mode 1: 15.9 Hz	Bending
Mode 2: 19.6 Hz	Lead or Drag
Mode 3: 71 Hz	Torsion
Mode 4: 112.5 Hz	Second Bending
Mode 5: 168.3 Hz	Second Torsion

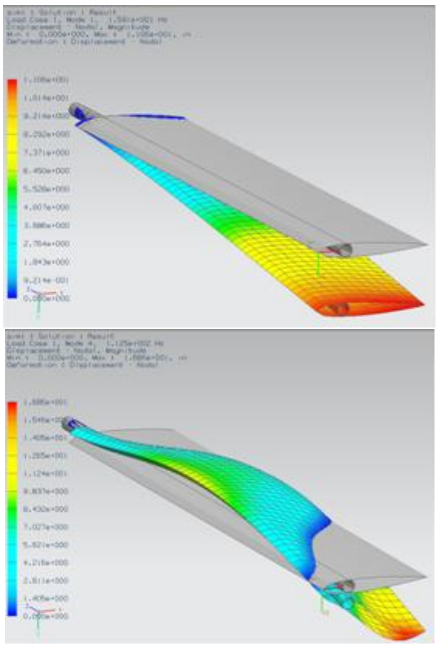

Figure 6. Stop-Rotor Wing Vibration Modes [2]

Airframe Fabrication and Autopilot

After design validation, a test stand and airframe was fabricated in collaboration with local industry, as shown in Figure 7.

Figure 7. Stop-Rotor Test Stand

Collective feathering of the wing is the most important aspect of this design that enables the aircraft to transition from rotary-wing to fixed-wing configuration and vice versa. The wing collective control is obtained by two independent motor controllers. Each controller is powered by a separate battery pack. An RC interface is provided for collective and aileron control.

In order to log the data from the test instrumentation based on an open-source autopilot, Ardupilot was used [8]. This instrumentation is comprised of an autopilot that has static and pitot pressure sensors, thermopiles and GPS. This autopilot used in the data-logging mode, along with Zigbee wireless transmitter and receiver, and a ground station, is shown in Figure 8. It is anticipated that this instrumentation will later be used as an autopilot for the stop-rotor UAV.

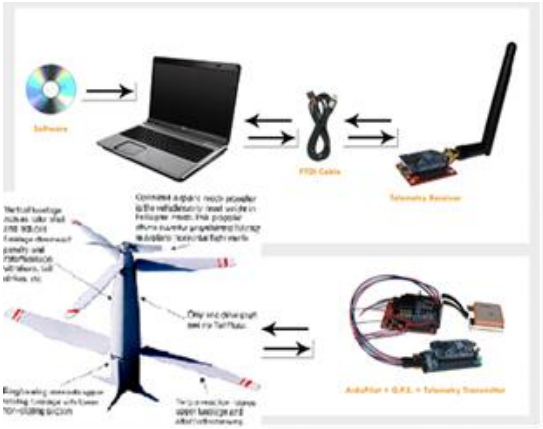

Figure 8. Ardupilot [8] Interface for the Stop-Rotor Design

The ground station interface was implemented using open-source software [8]. However, the Labview interface was modified to incorporate data-logging capability, as shown in Figure 9. This ground station interface shows airspeed, GPS location, attitude, and altitude of the aircraft.

Figure 9. Ground Station Interface for Stop-Rotor [8]

Experimental Validation of Stop-Rotor Conversion

In order to demonstrate the conversion, a "big drop" test was scheduled. In this drop test, an unpowered stop-rotor test specimen was dropped from a hot-air balloon with the wings and tail fins pitched for helicopter mode (for autorotation), then dump the collective (feather) to an airplane-mode position for the wings and tail fins, pull out of the dive and glide before pushing over and pitching the wings and tail fins back into their previous helicopter mode positions and land, as shown in Figure 10. The ardupilot [8] was used for data logging and a simple mathematical model for computation of rotor speed in helicopter autorotation mode was used [1].

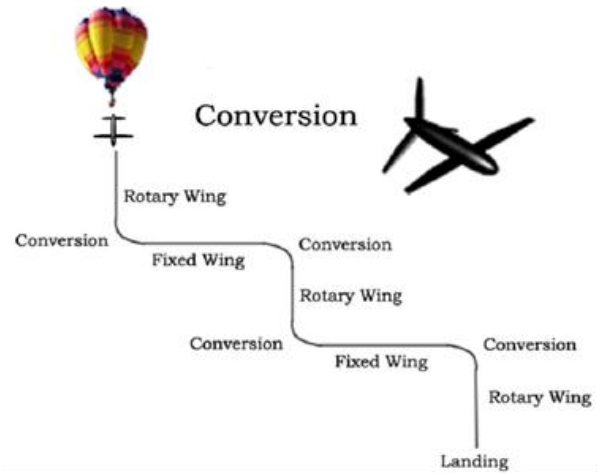

Figure 10. Stop-Rotor Big-Drop Test

It should be noted that the big drop was unpowered and that the expression for rotor speed in autorotation can be directly used to compute rotor RPM and velocity [1]. Thus, from Drier [1], the first-order equation for rotor speed was assumed to be

$$\mathbf{J}\dot{\Omega} = \mathbf{Q}_{eng} - \mathbf{Q}_{rotor} \tag{5}$$

where $\mathbf{J}$ is the inertia, $\dot{\Omega}$ is the angular velocity, and $\mathbf{Q}_{eng}, \mathbf{Q}_{rotor}$ are the engine torque and the rotor torque, respectively. The rotor torque, $\mathbf{Q}_{rotor}$, and thrust, $\mathbf{T}$, can be modeled as

$$\mathbf{Q}_{rotor} = \left(\frac{\Omega}{\Omega_0}\right)^2 \mathbf{Q}_0 \tag{6}$$

$$\mathbf{T} = \left(\frac{\Omega}{\Omega_0}\right)^2 \mathbf{W} \tag{7}$$

where Ω_0 is the initial speed and $\mathbf{W}$ is the weight. During the unpowered big drop, engine torque $\mathbf{Q}_{eng} = 0$ and the rotor speed equation is given by

$$\mathbf{J}\dot{\Omega} = -\left(\frac{\Omega}{\Omega_0}\right)^2 \mathbf{Q}_0 \tag{8}$$

This is called Bernoulli's equation with the closed form solution

$$\Omega(t) = \frac{\Omega_0}{1 + \dfrac{\mathbf{Q}_0 t}{\mathbf{J}\Omega_0}} \tag{9}$$

The equation of vertical motion during the big drop (i.e., free fall) is given by

$$\ddot{y} = g\left(1 - \frac{\mathbf{T}}{\mathbf{W}}\right) = g\left[1 - \left(\frac{\Omega}{\Omega_0}\right)^2\right] \tag{10}$$

Equation (9) is substituted into Equation (10) and integrated numerically once for velocity $\dot{y}$ and twice for position y determination. The simulation results by numerically integrating dynamic equations of motion; the experimental results are shown in Figure 11. It should also be noted that initially from time t=2 seconds, when the stop-rotor device is in the autorotation mode, results are comparable. However, the difference between experimental RPM and simulation RPM increases as the time increases. The difference between simulation and experimental results can be attributed to approximate aerodynamic modeling, approximate mathematical model for the stop-rotor, inability to specify exact initial conditions during conversion and numerical integration error.

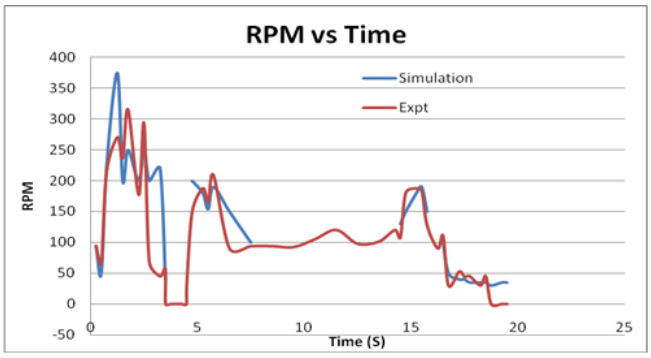

Figure 11. Comparison of simulation and experimental results

It can further be noted that during the drop from time t= 7 to14 seconds, the stop-rotor vehicle has undergone an uncontrolled roll in the fixed-wing mode that results into the discontinuity in simulation RPM from time t=7 to14 seconds (see Figure 12).

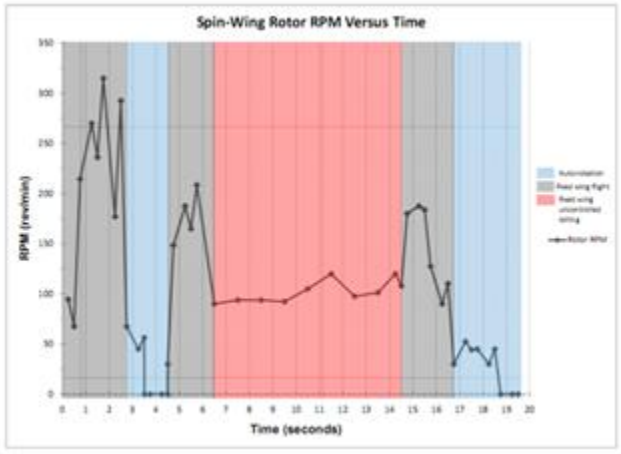

Figure 12. Stop-Rotor Flight Modes During the Big Drop

Conclusion

In this work, modeling, analysis and drop-test results on a novel stop-rotor UAV is presented. A low-cost, open-source autopilot was used in a data-logging mode to acquire flight data. The results from a simple mathematical model of the drop test were compared with the experimental data. A successful helicopter–to-fixed-wing-flight conversion was demonstrated during the drop test. Currently, researchers at ASU are working on modifying modeling and simulation to yield more accurate fidelity with measurements.

References

[34] M. Drier, Introduction to Helicopter and Tiltrotor Flight Simulation Published by AIAA, 2007, 1st Edition, ISBN-10: 1-56347-873-0, ISBN-13: 978-1-56347-873-4

[35] Kendoul, F. Fantoni, I. Lozano, R. "Modeling and Control of a Small Autonomous Aircraft Having Two Tilting Rotors"Robotics, IEEE Transactions on Volume: 22 Issue: 6, Dec. 2006 pp 1297 - 1302 ,

[36] Ghiringhelli G.L; Masarati P.; Mantegazza P; Nixon M.W. " Multi-Body Analysis of a Tiltrotor Configuration", Nonlinear Dynamics, Volume 19, Number 4, August 1999 , pp. 333-357(25)

[37] Vargas-Clara, "Finite Element Analysis of Stop-rotor" Class Project Report, Spring 10.

[38] http://xflr5.sourceforge.net/xflr5.htm Retrieved on 3/15/2011

[39] www.solidworks.com Retrieved on 3/15/2011

[40] www.Siemens.com/NX Retrieved on 3/15/2011

[41] http://www.pololu.com/catalog/product/1393 Retrieved on 3/15/2011

[42] http://diydrones.com/notes/ArduPilot Retrieved on 3/15/2011

Biographies

ALVARO VARGAS-CLARA, Alvaro Vargas-Clara is a graduate student in the Department of Engineering Technology at ASU Poly. He can be reached at vargasc@asu.edu

SANGRAM REDKAR, Sangram Redkar is an assistant professor in the Department of Engineering Technology at ASU Poly. His research interests include inertial measurement, MEMS dynamics, control, and nonlinear dynamics. He can be reached at sredkar@asu.edu.

Acknowledgements

The financial support from the US Navy is gratefully acknowledged.

GREEN PLASTICS: AN EMERGING ALTERNATIVE FOR PETROLEUM-BASED PLASTICS

Zaki Kuruppalil, Ohio University

Abstract

Plastics are referred to as "green" if they exhibit one or more of the following properties: source renewability, biodegradability/compostability at end of life, and/or environmentally friendly processing. World plastics production and consumption is increasing every year and so is a growing concern about its impact on the environment. The vast majority of plastics today originate from petroleum-based hydrocarbons and therefore are made from non-renewable resources. Even though less than 5% of all petroleum is used in plastics manufacturing, the renewability of the source is often a concern. Separation of different types of petroleum-based recyclable plastics from other solid wastes is a difficult and labor-intensive process; hence only a very small percentage of plastics are recycled. The inability of petroleum-based plastics to biodegrade is also criticized by environmentalists. As a response to these issues, there has been an increasing interest in what are called "green plastics."

Green plastics are being widely publicized as a possible solution for concerns regarding the use of traditional petroleum-based plastics. Materials such as polylactic acid (PLA) are examples of renewable plastics used for plastic products that are traditionally made using petroleum-based plastics such as polyethylene terephthalate (PETE), polystyrene (PS), and polypropylene (PP). Several challenges could be faced in an attempt to replace petroleum-based plastics with green plastics. Physical properties, chemical resistance, processing, and recycling are just a few potentially problematic areas. This paper is an investigation into facts about green plastics, their current status, advantages, shortcomings, and other related issues. The conclusion reached would comment on the future of green plastics and whether they can replace petroleum-based plastics.

Introduction

"Green," "sustainable," and "renewable" are some of the most frequently heard buzzwords nowadays. In the United States and the rest of the world, advertisements and campaigns from different businesses, organizations, and governmental agencies meant to educate people about advantages of going green have become commonplace. The corporate world is trying to show its commitment to and investment in sustainability. As most people may agree, one of the most common targeted materials when it comes to sustainability is plastics. The impact of the plastic industry on the US economy is significant. According to the Society of the Plastics Industry (www.plasticsindustry.org), the trade association based in Washington, D.C., plastics is the nation's third largest manufacturing industry. Since 1980, the plastics industry has grown at a rate averaging 3.4 percent. US plastics companies employ 1.1 million workers and provide nearly $379 billion in annual shipments [1].

Along with growing plastics production and consumption is a growing concern about impact on the environment. The source for most commercial plastics is petroleum, which is considered a non-renewable resource. Even though less than 5% of all petroleum is used in plastics manufacturing, the renewability of the source is a concern, as it takes millions of years for fossil fuels to be replenished. In addition, most commodity plastics (bottles, cups, etc.) made out of petroleum are non-compostable and non-biodegradable. Separation of different types of petroleum-based recyclable plastics from other solid wastes is a difficult and labor-intensive process; hence only a very small percentage of such plastics are recycled, leaving the rest in landfills. Most of the commodity plastic materials are used for food packaging and therefore are either contaminated or difficult to clean for recycling. In addition, it costs more to recycle common commodity plastics such as polyethylene terephtalate (PET) than to produce new plastics from scratch [2]. As per Environmental Protection Agency (EPA) statistics, plastics waste is one of the fastest-growing sectors in the Municipal Solid Waste (MSW) segment, and the majority of plastic wastes originate from packaging materials [3]. The amount of solid plastics waste generated in 2007 was estimated to be approximately 30.7 million tons, which accounts for almost 12.7% of the total MSW. The amount of plastic waste after recovery was almost 28.6 million tons, meaning that just less than 7% was recovered while aluminum and paper were recovered at rates of 33.8% and 54.5% respectively [3]. Plastics manufacturers have been trying to reduce the flow of solid waste with source reduction, recycling at source, etc. All such methods have their own limitations and can only address the solid waste generation to an extent.

History

Green plastics made from naturally occurring renewable resources are being widely publicized as a possible solution for concerns regarding the use of traditional petroleum-based

plastics. Bioplastics materials such as polylactic acid (PLA) are often projected as replacement for traditionally-made petroleum-based plastics such as polyethylene terephthalate (PETE), polystyrene (PS), and polypropylene (PP) in commodities manufacturing. The history of plastics made from non-petroleum resources goes back to 1868 when John W. Hyatt invented celluloid [1]. Celluloid was made from wood pulp, plant fibers (cellulose), or cotton fibers treated with nitrogen and camphor. Soon cellophane and rayon were invented by treating cellulose with other acids and solvents. In 1907 with the invention of the first petroleum-based plastics, Phenol Formaldehyde (Bakelite) by Leo Bakeland, the history of bio-based plastics took a twist. Since then, bioplastics became sidetracked in favor of petroleum-based plastics. In the 1920s, in an effort to find applications for agricultural surplus, Henry Ford experimented with manufacturing automobile parts from plastics made out of soya beans [4]. The resin for soy plastics was not completely plant-based; part of it was composed of phenol formaldehyde. Ford's soy plastic idea did not survive for a variety of reasons, including lack of molding technology for manufacturability of complex parts and noticeable formaldehyde odor from the parts [4]. After the industrial revolution following World War II, the only non-petroleum-based plastic that was steadily growing in consumption was cellophane.

Definition of Green Plastics

The definition of green plastics has changed from the days of Ford's soy-based plastics. Plastics are referred to as "green" if they exhibit one or more of the following properties: source renewability; biodegradability/compostability after life; and/or environmentally friendly processing, lifecycle, and afterlife disposal [4]. The term "bioplastics" is often used in books and articles referring to green plastics, and the terminology could be confusing. Bioplastics could be biodegradable plastics (those which degrade) or bio-based plastics (synthesized from renewable biomass) [5]. Not all biodegradable plastics are bioplastics (some oil-based plastics are biodegradable), and not all bio-based plastics are biodegradable. Biodegradability of a material mostly depends on its chemical structure [6]. Plastics being polymers, most oil-based plastics have a strong carbon-carbon single bond which is difficult to break, hence making it non- degradable. For example, polyethylene (developed by Braskem, a Brazilian petrochemical company) made from renewable masses such as sugarcane is not biodegradable but is recyclable [7]. Green plastics are also referred to as biopolymers. These natural polymers are inherently biodegradable because of the oxygen or nitrogen atom in their polymer backbones, as opposed to the carbon-carbon single bond in petroleum-based polymers. According to the American Society for Testing and Materials (ASTM), in order for a biodegradable plastic to be classified as compostable, it should yield carbon dioxide, water, and inorganic compounds at a rate consistent with other known compostable materials. In essence, a biodegradable plastic degrades from the action of naturally occurring microorganisms such as bacteria, whereas a compostable plastic undergoes biological processes to yield carbon dioxide, water, and other inorganic compounds which are non-toxic [8].

Previously, renewability of materials mostly pointed toward the renewability of the source, whereas now it is redefined in terms of the carbon footprint the material leaves. For example, when comparing corn to sugarcane, both being sources for ethanol, corn uses more fertilizer than sugarcane. The manufacture of fertilizers consumes natural gas, thereby causing corn to have a large carbon footprint [9]. "Environmentally friendly nature" refers to the direct and indirect impact the plastic has on the environment. This could be direct impacts during processing such as the usage of water or the amount of solid waste generated after life, or indirect impacts such as the amount of electricity consumed, the additional cost in transportation because of higher specific weight, etc.

Several challenges could be faced in an attempt to replace petroleum-based plastic products with green plastics. Physical properties, chemical resistance, processing, recycling, and cost are just a few potentially problematic areas. These limitations have set the application of bioplastics to certain niche markets accounting for 0.3% of global plastic production (according to 2007 estimates) [2]. But organizations such as the industry association European Bioplastics foresee a 37% annual growth rate in the bioplastics market by 2013 [2]. Still, critics are skeptical about the ability of green plastics to serve as an alternative for petrochemical-based polymers. This paper is a review of the current status of green plastics, major developments in the area, and challenges faced. The conclusions reached would comment on the future of green plastics and whether they can replace petroleum-based plastics.

Green Plastics Classification

E. S. Stevens classifies modernday green plastics into three categories [4]:

(i) Polymers extracted directly from biomasses (plants or animals), with or without modification. (Referred to as Type I hereafter.) For example, polysaccharide starch modified polymers and polymers derived from cellulose.

(ii) Polymers processed directly by microorganisms through large-scale fermentation processes. (Referred to as Type II hereafter.) For example, polyhydroxyalcanoates (PHA), copolymers of Polyhyrodxybutyrate and hydroxyvalerate (PHBV).

(iii) Polymers obtained from resins (monomers) produced with renewable and naturally occurring raw materials. (Referred to as Type III hereafter.) For example, polyesters such as polylactic acid (PLA) processed from naturally occurring lactic acid monomers.

Table 1 is a snapshot and description of all three types of plastics mentioned above, and their advantages and disadvantages. Of the three categories in Table 1, the polymers that are produced from naturally occurring monomers are widely gaining popularity because of their physical, chemical, and biological properties as well as their cost effectiveness in mass production. Polylactic acid (PLA), co-developed by Nature Works LLC, a subsidiary of Cargill, is one of such polymers finding increased attention. PLA is finding widespread applications for a short product life, with low-performance disposable packaging production. PLA usage has been significantly growing since 1998 [10]. Estimated production of PLA by 2013 is approximately 450 thousand tons per year. Some 70% to 80% of PLA is utilized for packaging purposes such as cups, trays, etc. [11]

Table 1. Green Plastics Materials and Properties

Type	Origin	Examples	Products	Utility	Disadvantages	Advantages
I	Extracted directly from biomass	Polysaccharides (Starch)	Non-Durable Goods: packaging	Medium	Modest strength, poor water resistance	Low cost
II	Polymer from large scale fermentation of biomass	PHBV	Durable Goods: toiletry and office accessories	Low	Synthesizing cost, Narrow melting range	Superior physical properties, good water resistance
III	Monomer extracted from biomass	PLA	Non Durable goods: Disposable plates, cups, boxes, film wraps	High	Low thermal resistance, brittleness, high specific weight	More cost effective than Type II, optical clarity, good moisture resistance

Processing Green Plastics

Products made of biodegradable plastics must be stable during processing. Most green plastic materials are processed by methods such as thermoforming, injection molding, blow molding, and extrusion [12]. These processes demand certain mechanical and physical properties such as melt strength, flow, elongation, temperature resistance, and elasticity. Most green plastic materials have modest strength, low water and temperature resistances, lower impact strength, etc. Therefore these materials require improvement and modification, and hence most commercial bioplastics are composed of several chemicals such as additive stabilizers, colorants, etc. which makes it almost impossible for them to be manufactured from 100% renewable resources (most bioplastics now contain 50% renewable resources) [13]. These additives must meet standards for compostable plastics such as ASTM D6400. Therefore, the bioplastics industry sees a shift in the marketplace from compostability to renewability partly due to lack of facility infrastructure here in the United States [14].

Higher specific weight of commonly used bioplastics materials such as PLA is always an issue. PLA, often used in packaging, has a high specific weight (1.24g/cc) compared to PP (.90g/cc) and PS (1.04g/cc), which implies more material usage and processing cost for a given packaging. PLA also has less resistance to prolonged temperature exposure over 130°F [15]. The low impact resistance of PLA and its low melting point is another downside of it being used in packaging applications. Athena Institute International, a nonprofit research and development firm, compared sixteen-ounce drink cups, deli containers, envelop window film, foam trays, and twelve-ounce containers made using PLA with ones made using equivalent PET and PP [16]. The study observed total energy consumed, solid waste generated, and greenhouse gases emitted during the manufacture of the abovementioned products. From fabrication to grave, most of the PLA packaging generated more solid waste and consumed more energy for production. The greater energy consumption was due to the fact that PLA underwent extra processing steps (more cooling time) as well as required more material to make a given size product. The study found that PLA is difficult to degrade in household compost pits and would emit an amount of greenhouse gases comparable to that of traditional oil-based plastics. The study also noted that possible mixing of PLA with PET in the existing recycling system could end up harming the reusable PET. At the same time, advocates argue that the additional crops cultivated to produce green plastics would remove a substantial amount of carbon dioxide from the atmosphere.

Most biopolymers seem to be tough to process because there is a small window between processing temperature and

decomposition point. Injection molding has large application in bioplastics products starting from durable goods such as toys, tools, bathroom accessories, etc. to non-durable goods such as packaging. The biggest challenges in injection-molding bioplastics are heat, moisture, and degradation caused by excessive temperature, shear or residence time [17]. Modifications need to be made to barrel temperature profile, mold temperature, screw speed, screw back pressure, and injection speed [18]. Materials such as PLA tend to hold heat for a longer time, and therefore would require higher cooling time. PLA also tends not to flow well over long distances. Materials such as PHA tend to respond better to slower injection speed which means higher cycle time. Increasing pressure would increase shear which can cause it to break down [17]. Unmodified biopolymers resins are hygroscopic and if not dried properly (as low as 250ppm) can result in decreased molecular weight and dropped melt viscosity, generating more flash and trim wastes. Even though most of the bioplastics resin manufacturers endorse using traditional thermoplastic machinery, they recommend avoiding high-shear screws and hotspots in the barrel. Also most of the bioresins cannot be left at the machine at the end of the work day to prevent excessive degradation. Extruding bioplastics with general purpose polyolefin screw may be less efficient due to lack of drive because of the inferior flow property [11]. The higher specific weight necessitates sturdier roll handling equipments and reinforced hoppers. Also, the cooling rolls after extrusion need to remove more heat compared to materials such as PS [11]. One of the major difficulties in thermoforming PLA is its narrow softening range which makes the process very hard to control. PLA's higher tensile strength and lower elongation properties could make thermoforming difficult [19]. Other obstacles while thermoforming PLA include its low melt strength which could cause shearing when stretched.

Recycling Issues

Plastics recycling falls into two categories: pre-consumer and post-consumer [20]. Pre-consumer recycling involves waste generated during manufacture of the product, such as trim wastes after thermoforming or runner and sprue waste from post-injection molding. Most manufacturers are focused on recycling the pre-consumer waste at the source itself. The problem arises with post-consumer recycling of bioplastics after its end use. Recycling post-consumer waste is a tedious and expensive process as it involves a considerable amount of cleaning and sorting. With petroleum-based plastics, it is not easy to determine the differences between similar plastics such as PE or PP. One of the major hurdles in recycling is that these different polymers are not mixable. Mixing of bioplastics with petroleum-based plastics could contaminate the oil-based plastic feed generated from recycling. A mixture could result in inferior properties leading to a recycled plastic that is unusable for many processes. This is very likely to happen as consumers may not differentiate between different plastic types. Therefore, bioplastics should be from identifiable sources that will allow for sorting. In the United States, little infrastructure currently exists to collect bioplastics in sufficient quantities, and consumers do not have a clear picture on its recyclability. Another way to deal with post-consumer plastics is composting. It should be noted that one of the biggest myths about landfills is that they are giant compost pits, which is not true. In fact, anything that goes into a landfill (bioplastics or oil-based plastics) that lacks exposure to sunlight and air will not decompose properly. Therefore, bioplastics composting needs additional infrastructure and settings to handle the volume. Commercial bioplastics such as PLA can compost only in municipal and industrial compost settings [21]. Therefore, the composting sector has to expand to accommodate the growing waste generated from bioplastics.

Synthetic Blending

A large amount of green plastics' shortcomings are overcome by synthetic blending. For example, Novamont, Europe's largest bioplastics producer, produces Mater-Bi which is a blended bioplastic composed of starch and other fully biodegradable synthetic polymers[22]. Blending can overcome property shortcomings such as water resistance, strength, and elasticity. BASF's Ecovio, which is fully biodegradable, is another example of synthetic blending where 45%Naturework's PLA (made from lactic acid) is combined with 55%Ecoflex (made from petrochemicals). Combining Ecoflex, which is softer with higher elongation properties, and PLA, which is rigid with higher tensile strength, resulted in Eco-Vio, which falls in between two points, making it a suitable material for packaging and other non-durable goods. Starch-based biopolymers have poor water resistance and modest strength. In order to overcome these shortcomings, it is mixed with polyethylene or totally biodegradable polyvinyl alcohol [4]. Sometimes starch-based polymers are coated with PHBV to obtain better water resistance. Teknor Apex Co, another blender, is targeting on producing alloys of thermoplastic starch with materials such as PLA, PHA, and PP. Professor Richard Larock at Iowa State University has been successful in simply combining natural oils (up to 85%) with conventional plastic monomers to produce a synthetic blend which is claimed to have better thermal properties and shape memory properties [2]. A question arises whether some of the synthetic materials may have a non-renewable source, resulting in less than 100%-green plastics.

Standards and Certifications

In the United States, ASTM D-6400 specifications for compostable plastics covers plastics and products made from plastics that are designed to be composted in municipal and industrial aerobic composting facilities [23]. The ASTM D-6868 specification covers biodegradable plastics and products (including packaging), where plastic film or sheeting is attached (either through lamination or extrusion directly onto the paper) to substrates and the entire product or package is designed to be composted in municipal and industrial aerobic composting facilities [22]. Similar standards exist elsewhere, such as the German (DIN-54900), European (EN-13432), and international (ISO-14855) standards. Professional associations such as the Biodegradable Products Institute (BPI), which comprises key individuals and groups from government, industry, and academia, promotes the use and recycling of biodegradable polymeric materials (via composting). They have an established series of specifications, and standards for compostability (based on ASTM D6400 and D6868), which if met will allow the product to display the BPI logo. Similarly, in Japan, Japan Bioplastics Association (JBPA) has started the BiomassPla certification to distinguish products made from biomasses [24]. Certification in other countries includes EcoLogo (Canada) and Vincotte (Belgium). These endorsements and certifications could boost consumer confidence regarding biodegradability of a given product. Consumer certainty is critical to the growth of the bioplastics industry, as studies in Europe and Japan have shown that consumers are willing to spend the extra dollar for sustainable products [25].

Cost Factor

Cost is a significant factor when it comes to most plastics applications, especially disposable ones such as packaging. For example, if a small bag of chips from a vending machine costs $1.00, then the cost of the bag should not be a significant portion of it. The cost per pound for bioplastics has dropped significantly in recent years. For example, PLA, which cost $3/lb in the 1990s has dropped to 90 cents/lb in 2010. The rise in the price of oil has made bio-based plastics prices comparable to the price of oil-based commodity thermoplastics. Still, additional cost incurred due to increased processing steps, high specific weight, and several other factors could be impediments to bioplastics usage. Along with growing concerns regarding utilizing agricultural land for production of raw bio materials such as corn, one of the other obstacles for growth of bioplastics is the increasing price due to competition from the food industry [10]. However, some critics argue that this is not the case. According to Blackburn, the land mass necessary to produce 500,000 tons of PLA is less than 0.5% of the annual US crop [26]. Currently, with bioplastics being only less than 1% of the total plastics used, the concern regarding agricultural land usage may not be an issue. But according to Evans, if bioplastics usage grows to 10%, 5 billion pounds of starch will be required, which could make an impact on agriculture. Also, the increased use of crops such as corn in the production of ethanol has caused prices to double in the past year [2].

Conclusions

Current market trends regarding the growth of bioplastics look promising. Significant growth has been observed in patents deposits for bioplastics such as PLA, which had 20 patents deposited in 1998 versus 330 in 2005[10]. Bioplastics demand is expected to hit an annual production level of 2% of global thermoplastics production, which is approximated at 250 million tons annually. Major manufacturers and even governments are focusing on renewability of plastics. For example, the Japanese government has set a target for the year 2020 to produce 20% of their plastic from renewable sources. Toyota targets making 20% of their interior trims from renewable sources by 2020. Ford is currently using soy-based polyurethane on the seats of twenty-three of its models. Consumer products giant P&G has a long-term goal set to make all of its packaging renewable or recyclable, and replacing 25% of its packaging materials with "sustainably sourced material" [27]. Wal-Mart, the world's biggest retailer, is demanding packaging made from renewable resources [28]. All these steps could be real indications of an existing commitment and an upcoming demand.

The green plastics industry is still in its infancy and may not be ready to replace the petrochemical-based plastics. At the same time, this sector is preparing for growth and getting ready to meet increased demand. Still, there are challenges in processing, material properties, and recycling to be faced when attempting to replace the petrochemical-based plastics. Most bioplastics are currently utilized for non-durable goods such as packaging. Plastics such as PHA have properties comparable to their petroleum-based counterparts and could be used for durable goods. The fermentation step in processing makes the raw material expensive. Research is underway in processing such polymers without fermentation [22]. Green plastics with a wide range of properties that could allow them to be processed like conventional plastics need to be developed. One real problem that exists is in defining and identifying green plastics. There needs to be a better understanding of what constitutes "greenness." A venture between governments, industry, and society (such as BPI) could play an extensive role in educating society on what "greenness" truly means. Standardizations and certifications of sustainability should be publicized extensively. A globally accepted system of standards for green plastics

could help manufacturers and producers focus their efforts toward a common goal. Infrastructure for collection and composting of degradable plastics needs to be improved. Governmental incentives such as tax cuts and rebates could also help promote greenness. Diversification of feed stocks from food crops to alternative biomass materials could have a positive impact on the cost as well as alleviate concerns regarding use of agricultural land. There seems to be a lot of enthusiasm in society, industry, and government regarding greenness. If the trend continues, and the motivation for innovation in this field persists, the results could be promising.

References

[43] Kuruppalil, Z. November 2010.. Plastics packaging: The challenge of going green. Accepted for publishing in *The First International Conference on Green and Sustainable Technology* conference proceedings, University of North Carolina A & T.

[44] Evans, J. 2010. Bioplastics get growing. *Plastics Engineering, 66(2):*, 14-20.

[45] Municipal solid waste in the United States: 2007 facts and figures. 2008. United States Environmental Protection Agency. Retrieved from http://www.epa.gov/osw/nonhaz/municipal/pubs/msw07-rpt.pdf.

[46] Stevens, E.S. 2003. What makes green plastics green? *BioCycle*, *44*(3): 24,4.

[47] Tokiwa, Y., Calabia, B.P., Ugwu, C.U., & Aiba, S. (2009). Biodegradability of plastics. *International Journal of Molecular Sciences*, *10*(9): 3722-3742.

[48] Stevens, E.S. 2002. How green are green plastics? *BioCycle*, *43*(12): 42.

[49] Phillips, A.L. 2008. Bioplastics boom. *American Scientist*, *96*(2): 109-110.

[50] Stevens, E.S. 2002. *Green Plastics: An introduction to the new science of biodegradable plastics.* Princeton, NY: Princeton University Press.

[51] Schut, J.H. 2008. What's ahead for "green" plastics. *Plastics Technology54*(2): 64- 89.

[52] Queiroz, A.U.B., & Collares-Queiroz, F.P. (2009). Innovation and industrial trends in bioplastics. *Polymer Reviews*, *49*(2): 65-78.

[53] Schut, J.H. 2007. Extruding biopolymers. *Plastics Technology*, *53*(2): 60-75.

[54] Auras, R.A., Harte, B., Selke, S., & Hernandez, R. (2003). Mechanical, physical, and barrier properties of poly(lactide) films. *Journal of Plastic Film & Sheeting*, *19*(2): 123-135.

[55] Siracusa, V., Rocculi, P., Romani, S., & Rosa, M.D. 2008. Biodegradable polymers for food packaging: a review. *Trends in Food Science & Technology*, *19*(12): 634-643.

[56] Sherman, L. M. (2008). Additives are needed for toughness, heat resistance & processability. *Plastics Technology*, 64(7): 58-63.

[15] Dartee, M. 2010. It's time to get to know your way around bioplastics. *Plastics Technology, 56*(3): 18-22.

[16] Teschler, L. May 24, 2007,. How "green" are green plastics? Retrieved from http://machinedesign.com/article/how-green-are-green-plastics-0524.

[17] Knights, M. 2009. Injection molding biopolymers. *Plastics Technology*, *55*(4): 39-48.

[18] Pitzi, T. J. 2010. Injection molding PHA bioplastics: validating moldability for paper mate pens. *Plastics Technology, 56(8):* 27-28.

[19] Schut, J. H. 2007. Foamed PLA Shows Promise In Biodegradable Meat Trays. *Plastics Technology*, (53)12: 39-43.

[20] Rustin, D. 2009. Being green can turn into green. *PD&F* , 30(1): 8-11.

[21] Bregar, Bill October 18, 2010. Greenwashing leads to consumer skepticism. *Plastics News*:12.

[22] Greer, D. 2006. Plastic from plants, not petroleum. *BioCycle*, *47*(6): 33-35.

[23] Khare, A., & Deshmukh, S. 2006. Studies toward producing eco-friendly plastics. *Journal of Plastic Film & Sheeting*, *22*(3): 193-211.

[24] Inomata, I. 2009. The current status of bioplastics development in Japan. *Bioplastics, 4(1):* 42-44.

[25] Morale, R., Pulido, D., Ticas, S., Trigo, M. 2009. The Brazilian bioplastics revolution. *Knowledge@Wharton*, Retrieved from http://knowledge.wharton.upenn.edu/articlepdf/2219.pdf?CFID=26443395&CFTOKEN=77195739&jsessionid=a830dfb3afb369eaa99c3243144d47681638.

[26] Blackburn, R. S. 2005. *Biodegradable and sustainable fibers (Ed.).* Cambridge, UK: Woodhead Publishing Limited.

[27] Hockensmith, D. October 4, 2010. P&G outlines broad sustainability plans. *Plastics News*: 1, 20.

[28] Patey, W. 2010. Thermoforming pla: how to do it right. *Plastics Technology*, *56*(3): 30-31.

Biography

ZAKI KURUPPALIL, Ph.D. is currently an Assistant Professor in the Department of Engineering Technology and Management at Ohio University. His areas of interest include plastics, machining, and lean and agile manufacturing. Dr. Kuruppalil can be reached at kuruppal@ohio.edu.

LEARNING EFFECTS OF DESKTOP VIRTUAL REALITY (VR) ENVIRONMENTS IN COLLEGE AND CAREER TECHNICAL TRAINING

Debra Steele, University of Arkansas Fort Smith; Argie Nichols, University of Arkansas Fort Smith

Abstract

The Occupational Education Virtual Reality Research Team at Oklahoma State University conducted a research project with a regional college in Arkansas with the purpose of determining the learning effects of desktop virtual reality (VR) in college and technical training. Participants were students from a two-year surgical technicians program and students from a career tech center. In this paper, the authors describe what the research team discovered to be important factors in its successful implementation.

Introduction

The research team was a group of students in the Ph.D. Occupational Education Studies program at Oklahoma State (OSU), who investigated the design and performance effects of desktop virtual reality and virtual environments (VR/VEs) through small-scale mixed-method studies. The studies combined theory-based quasi-experiments consisting of qualitative interviews with learners exposed to desktop VEs for surgical operating rooms [1].

Specifically, the research conducted by the team compared the learning effects of two different types of desktop virtual reality (VR) in presenting scenes and equipment in surgical operating rooms. This technology was used in a way that supports instruction, where adult learners can use technology to obtain information and meet their learning needs.

The use of technology for adult literacy and education has grown from computer-assisted instruction to the information highway to the use of personal computers in management and information systems [2]. Virtual Reality technologies allow users to occupy, navigate, manipulate, and control realistic computer-generated environments. These VEs can immerse users/learners in a bounded graphical space and give them a strong feeling that they have actually been in a particular environment. Desktop Virtual Reality creates and delivers VEs in the form of on-screen "movies" that users can "enter" and explore interactively by moving a mouse or other navigation device. The user determines what movements to make and when to make them; the user explores the imagery on the computer screen in real time as if actually moving within a place in the physical world. Movement can include panning and rotating the scene to simulate physical movements of the head and body, zooming in and out to simulate movements toward and away from objects or parts of the scene, and clicking on "hot spots" to navigate to additional embedded scenes and objects [3].

Administering the Research Test

The VR group from OSU went to a hospital's operating room to create the images for the VR scenes. The desktop operating room VR "movies" were created by taking a series of digital still photographic images and then using special VR software (VR WORKS, PANO WEAVER, TOUR WEAVER) to stitch and blend the images into a single panoramic scene that the user can "enter" and explore individually and interactively. The user would employ a mouse to move and explore within an on-screen virtual environment as if he or she were actually moving within a space in the real world. Movements could include rotating the panoramic image to simulate physical movements of the body and head, and zooming in and out to simulate movements toward and away from objects or parts of the scene. Embedded individual virtual objects can be picked up, rotated, and examined as the user chooses, and clickable "hot spots" can also be used to navigate at will [4]. An example is shown in Figure 1.

Figure 1. Desktop Operating Room VR

Each subject was given a demographic survey to complete and a copy of the *Successive Perception Test 1* (SPT1) answer sheet, which is a level of visualizing skill assessment

using the SPT1, which is a video-based test that requires subjects to recall and select the screen picture [5].

The Successive Perception Test1 (SPT1) instrument was used to measure Lowenfeld's visual/haptic typology. Lowenfeld discovered that individuals with visual learning abilities had a higher chance of discriminating details that were visual. Furthermore, their reaction was also noted to be more impersonal. On the other hand, haptic learners (those with learning abilities based in the sense of touch) were not in a position to discriminate details that were visual and had a higher chance of reacting to situations with more emotions. Lowenfeld revealed that a number of individuals that were partially blind had the ability to make use of the little sight that they possessed to either view an object or apply their other senses as a way of expressing themselves. However, other individuals that were also partially blind were not in a position to utilize their eyes. These individuals found it more useful to apply touch senses [6].

The participant was then trained on how to operate the type of VR treatment he/she would be using during the activity. Each subject was assigned to either navigated or non-navigated VR treatments, so the VR group only needed to train each subject on how to operate one kind of presentation. It was explained to the subject that the researcher would show him/her a computer presentation that would demonstrate how to work the VR program.

Conducting the Qualitative Interviews with Selected Subjects

The researcher asked the subject numerous questions, such as, "I would like to find out more about your experiences with the Virtual Reality (VR) program. Have you had any previous experiences with virtual reality? Have you ever experienced virtual reality before?"

Using the completed data forms, the researchers coded all data and created an SPSS data file. Quantitative analysis was done with SPSS. Qualitative data was analyzed through thematic analysis and coded for statistical analysis. Learning performance variables included: tests of spatial orientation within a visual environment (measured by multiple-choice responses to questions requiring location of items in the environment relative to specified locations of the user), perceived performance confidence (measured on defined Likert-type scales), and perceived task difficulty (measured on defined Likert-type scales).

Theoretical and Empirical Foundations for the Studies

The experimental VR studies developed by the VR research team have been guided by predictive research hypotheses situated in a collection of theoretical bases and supporting empirical research literature. These have included the following:

LOWENFELD'S VISUAL/HAPTIC TYPOLOGY: Lowenfeld and Brittain describe haptic and visual styles of learning as being on opposite ends of the continuum. It has been noted that a majority of people usually fall between the two extremes. Persons that are visually oriented are not able to adapt to a given situation via means of kinesthetic and touch functions with ease. Lowenfeld has noted that as individuals advance in age, their haptic and visual perception also tends to diminish in importance [7].

This may be regarded as more of a developmental effect as an increasing number of individuals turn more visual as they advance in age. Compared with other forms of perceptual styles, haptic perceptual style has a lot more significance among adults. Lowenfeld and Brittan state "that for some children, not only those who might be termed extreme haptics, school may be frustrating because of the emphasis on visual learning". Lowenfeld and Brittain go on to say, "the person with haptic tendencies, on the other hand, is concerned primarily with body sensations and subjective experiences, which are felt emotionally" [7].

AGE AND TECHNOLOGY: Well-known research on age and generational differences in technology experience and self-efficacy has presented evidence that these differences may relate to perceptions and performance with technology-based learning. A recent study of older adult computer users suggests there is a gender difference in anxiety levels in older adult computer users, with women displaying more anxiety and reporting less computer knowledge, despite the fact that males and females reported similar levels of computer usage [8].

AGE, COMPUTER SKILLS, AND PRIOR GAMING EXPERIENCE*:* While these variables were included, the VR studies at the university found that one of the limitations of the study may be the small sample size and limited range of these variables. These findings indicated that in the study between the college and OSU there were no differences in age and technology, and what was found were deficiencies in learner preparation and training for VR.

Conclusions

The main question was whether age affects the levels of technophobia. However, the Arkansas regional college and OSU study showed there were no differences in the use of technology between the different age levels observed at the two schools during the five years of research. It was observed that in the study between the college and OSU there were no differences in age and technology; what was found were deficiencies in learner preparation and training for VR.

References

[1] Ausburn, L., Ausburn, F.B., Steele, D., Krouter, P., Dotterer, G., "et al". "Critical Elements for Successful Performance in Desktop Virtual Reality Environments". The Hawaii International Conference on Education 1-7 January 2010.

[2] Hopey, C. (1999) Technology and Adult Education: rising expectations. *Journal of Adult Learning*, 10(2).

[3] Hogan, M. , (2006). Technophobia Amongst Older Adults in Ireland, *Irish Journal of Management*. 27(1), 21.

[4] Ausburn, L.J. Martens, J., Washington, A., Steele, D., & Washburn, E. Spring 2010 "A Cross-Case Analysis of Gender Issues In Desktop Virtual Reality Learning Environments". *Journal of Industrial Teacher Education*, Vol. 46, pp. 1-34.

[5] Lowenfeld, V. (1954). *Your child and his art: A guide for parents*. New York: Macmillan.

[6] Lowenfeld, V. (1970). *Creative and mental growth*. New York: Macmillan.

[7] Lowenfeld, V., and Brittain, W. L. (1987). *Creative and mental growth*. New York: Macmillan Publishing Company.

[8] Karavidas M., Lim N.K. & Katsikas S. (2005). *The Effects of Computers on Older Adult Users*. Computers in Human Behavior, 21(5), 697-711.

Acknowledgments

The authors are thankful to University of Arkansas Fort Smith Faculty Development Fund and IJERI Journal for the support to develop this document.

Biographies

DEBRA STEELE, Ph.D., is an instructor for the College of Applied Science and Technology at the University of Arkansas Fort Smith, an Oklahoma State University graduate student of Occupational Education Studies at Oklahoma State University, and a member of the Oklahoma State University Virtual Reality team. Debra Steele may be reached at dsteele@uafortsmith.edu

ARGIE NICHOLS, Ed.D, is a Professor at the College of Applied Science and Technology at the University of Arkansas Fort Smith and also a graduate of Oklahoma State University. She has designed, developed and administered a four year Bachelor of Science degree in Animation. Argie Nichols may be reached at anichols@uafortsmith.edu.

CHALLENGES OF EVS AND HVS TO THE U.S. ELECTRICAL POWER GRID

Faruk Yildiz, Sam Houston State University; Kenan Baltaci, University of Northern Iowa

Abstract

Environmental concerns, depletion of fossil-fuel resources, and the increase in gas prices boost the demand for Electric Vehicles (EV) and plug-in Hybrid Vehicles (HV) because of their high efficiency and low or no gas emissions. But, despite their advantages, the rapid increase in EVs and HVs has brought challenges including a lack of sufficient electric power, lack of electrical transmission line capacity, dependence on foreign batteries, and other obstacles. Envisaging electrical power need with consideration for the time when everyone may have EVs and HVs and planning the country's energy policy are critical. The high demand for HVs and EVs will bring a high load to the transmission lines. Because of this increased demand for HVs and EVs, there will be a significant shift in use of energy from gasoline to electricity, which brings an important question to mind. Can the U.S. electric energy generation capacity meet the energy demands from HVs and EVs during the next 20 years? This extensive study was conducted regarding potential problems and challenges EV/HV technology will face in the near future.

Introduction

For more than a century, people have attempted to harness electricity, the clean and versatile fuel, for personal transportation. Ideas for an electric vehicle were first introduced in 1835 by Professor Stratingh, and thus cannot be considered a new idea in our century [1]. The earliest electric cars emerged in the mid 19th century and in the early years of the 20th century, when they competed effectively with gasoline-powered cars. Early in the 19th century, there were more EVs than internal-combustion-engine (ICE) vehicles, but ICE vehicles had advantages such as available gasoline resources and less technology in terms of control of the vehicle and energy storage. EV production dwindled in comparison with ICE vehicles until the mid 1990s. In 1997, The Toyota Prius was introduced to the Japanese market. First-year sales were nearly 18,000 [2]. Today, major automobile companies have their own hybrid car models commercially available [3-11]. Demands for HVs are promising. Considering the depletion of fossil-fuel resources, the higher efficiency of EVs, and environmental concerns, it can be said that demand for HVs and EVs will increase significantly. Increase in demand for HVs and EVs implies a significant shift in usage of energy from gasoline to electricity, which brings an important question to mind. Can the U.S. electric energy generation capacity meet energy requirements in case of a high demand for HVs and EVs in next 20 years? The following sections explain the current condition of power generation capacity, future expectations, and battery technology for EVs and HVs.

Over the years, improvements in internal combustion engine technology, such as reduction in noise, vibration, and other advances, led to the supremacy of cars powered by gasoline, since they have better range and decreased fueling time compared to electric vehicles. Electric vehicle technology continued in the form of electric powered trains and fork lift trucks. There have been various attempts over the years to reintroduce the concept of electric vehicles, with updated improvements. However, issues with battery charging times, slow battery technology improvements, and range concerns (the fear of running out of energy with no locally available charging stations), have contributed to the inability of EVs to penetrate the market. Recently, because of increased gas prices, concerns about the link between carbon-based fuels and climate change (global warming issues), the environmental impact of oil and gas exploration as evidenced by the current oil spill in the Gulf of Mexico [12], improvements in battery technology and charging infrastructure, interest in EV vehicle technology has returned to the market place and is being considering for consumer production by many vehicle companies [13].

After a long term of research and development processes, EV and HV technology is reaching the highways. Environmental concerns, depletion of fossil-fuel resources, and increase in gas prices boost the demand for EVs and plug-in HVs because of their high efficiency and low or no gas emission. But despite their advantages, the rapid increase in EVs and HVs have brought several challenges such as the lack of sufficient electric power, lack of electrical transmission line capacity and dependence on foreign batteries. EV and HV technologies can be a good alternative to conventional combustion-engine car technology as long as the required infrastructure is established. This infrastructure includes sustainable electric power, reliable transmission capacity, a safe and high-capacity battery, domestic production of EVs/HVs and their parts, and waste management. Envisaging the electrical power needed if the majority of automobile owners have EVs and HVs and planning the country's energy policy is critical. A high demand for HVs and EVs will bring a high

load to the transmission lines. One of the most important motivations for developed countries to provide large funding for research on HVs and EVs technologies is to avoid dependence on foreign energy resources. This can be accomplished if and only if some critical parts of HVs and EVs, such as batteries, are manufactured domestically. Waste management is also a very important issue in HV/EV technologies. Batteries in HVs and EVs contain huge amount of hazardous materials. Eliminating or lowering the toxic material in batteries and lessening their impact to the environment is imperative. A study by Electrical Engineering Technology and Industrial Technology students and faculty was conducted regarding potential problems and the challenges EV/HV technology will face in the future so that solutions for those challenges might be discovered.

Manufacturers of electric and hybrid vehicles have produced exciting developments and it is obvious that EVs and HVs may be here to stay if appropriate infrastructure is created. These vehicles currently offer such advantages as lower cost to operate, reduced dependence on oil, ecological advantages to reduce global warming concerns and issues. However, it may become an issue for the electric industry due to required power for battery charging purposes. A major concern for the electric utilities is the impact of the additional current drain that will be required to charge these vehicles. It is assumed that most of the owners of these new technologies will use 240V chargers to provide an assured overnight charge. These battery chargers will draw an amount of electric current from the grid that is equal to or greater than an average home use during the night time. For example, the Nissan Leaf draws 40A at 240V, representing a 9.6KW demand on the electric grid. The grid is usually established with local sub-stations consisting of several transformers for every 6-10 homes on average. One vehicle connected to the grid putting more load on a transformer may not create problems, but the concern is that the number of vehicles will increase in the near future, which will put more of a load on these transformers. If the number of electric vehicles increases in specific locations, there is a very real concern that the additional load will cause transformers to fail, especially if the vehicles are allowed to charge during peak hours. Taking these issues into consideration, precautions should be taken before adapting electric vehicle technologies to our daily lives. For example, a demand response [14] is a key Smart Grid solution that needs to be in place to enable the expected growth in EVs, but there are unique aspects of demand response that come into play [13].

Transmission Lines

According to the U.S. Department of Energy, the U.S. electric transmission system is under stress. Growth in electricity demand, lack of investment in new transmission facilities, and the incomplete transition to fully efficient and competitive wholesale markets have allowed transmission bottlenecks to emerge. These bottlenecks increase electricity costs to consumers and increase the risks of blackouts [15], [16]. Over the past decade, the cost trends for transmission plants have increased 23% and those for distribution plants have increased 21% [17]. As is shown in Figure 1, the cost of electric utilities increased about 20-30% around the U.S. [18], [19]. Investments in transmission infrastructure dropped by $117 million between 1975 and 2000 [19]. Increases in costs of transmission plants and distribution plants are about the same. Low investments with an increase in cost worsen the situation.

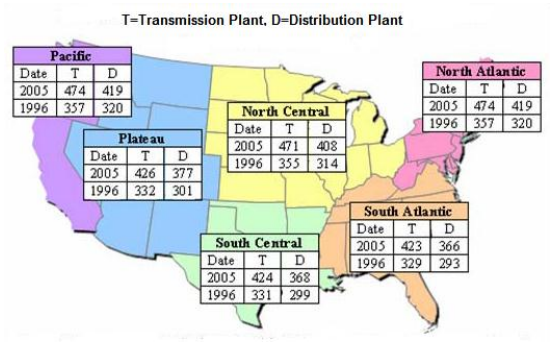

Figure 1. Cost Trend of Electric Utility Construction by Geographic Division and Type of Plant, 1996-2005 [14]

Unless substantial amounts of capital are invested over the next several decades in new generation, transmission, and distribution facilities, service quality will degrade and costs will go up [19]. As is shown in Figure 2, investment in new transmission facilities has declined steadily for the last 25 years [20], [21].

Transition from combustion engine vehicle to HVs and EVs will bring a heavy load to U.S. transmission lines in the near future. The current status is not sustainable in terms of electric transmission and distribution. In case of a high demand for EVs and HVs in the next 20 years, the U.S. Electric Transmission and Distribution system will face serious problems such as low efficiency, blackouts, congestion, transmission bottlenecks, and increase in the cost of electric energy [17-21].

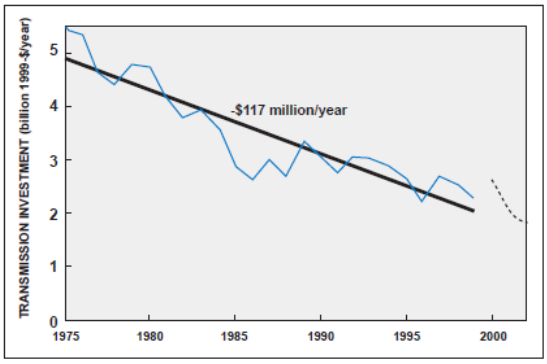

Figure 2. Transmission System Investment Over Time [21]

Smart-grid systems are currently available and under research for improvements. Smart grid may be a viable solution to link the charging of electric vehicles with available renewable energy systems such as solar and wind technologies. For instance, as wind capacity increases, EVs would be allowed to charge faster but when the renewable power on the grid drops, the EVs charge would decrease. This concept can be used to integrate charging stations with residential or commercial generation capacity from wind, solar or other alternative energy sources [13]. Utility companies are building infrastructure and involving research for charging stations to address all of the aforementioned issues and concerns. Companies such as Batter Place, AeroVironment, and Coulomb Technologies are offering vehicle charging services to their customers using advanced networking technologies.

Energy Consumption by the Transportation Sector

Transportation sectors strictly depend on energy and are one of the major consumers of energy. Figure 3 shows the energy consumption of sectors in the U.S., according to 2005 year data. Energy is primarily consumed by the industrial and transportation sectors, followed by the residential and commercial sectors [22]. According to the Energy Information Administration revisions, total energy use was 99.6 quadrillion BTUs in 2008 with transportation using 28.2% [23]. The transportation sector consumes 28% of the total energy consumption in the U.S., which includes all types of vehicle whether commercial or noncommercial. Light-duty vehicles (LDV), such as cars, pickup trucks, sport utility vehicles, and vans, consume 48% of the total energy (Table 1). As shown in Figures 3 and 4, 84% of the energy consumed today for transportation in the U.S. comes from fossil fuels [24].

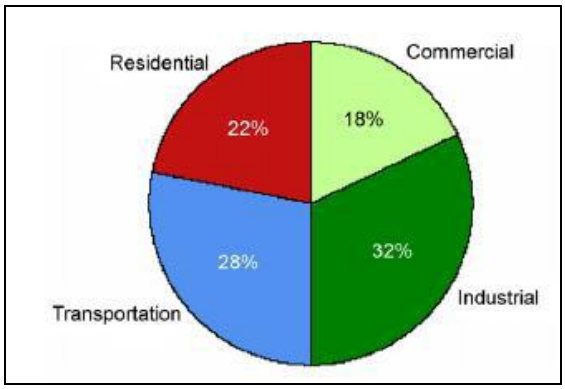

Figure 3. End-use Sector Shares of Total Energy Use in the U.S., 2005 [25]

Table 1. Energy Use by Type of Vehicle [22]

Type of Vehicle	Energy Use
Automobiles	32%
Light Trucks	16%
Aircraft	9%
Water	5%
Construction & Agriculture	4%
Pipelines	3%
Trains & Buses	2%

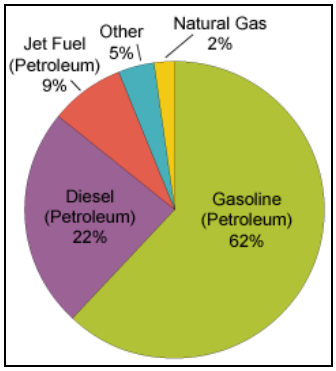

Figure 4. Fuel Used for Transportation [24]

An increase in demand for HVs and EVs implies a significant shift in usage of energy from gasoline to electricity, which brings an important question to mind. Is the U.S. electric energy generation capacity able to meet the energy requirements in case of high demand for HVs and EVs in next 20 years? We need to look at emerging technologies and different prospects about the future of HVs and EVs to answer these questions.

Future Prospect of Hybrid Vehicle Sales

HV sales are increasing rapidly. Figure 5 shows actual HVs sales from 2000 to 2006 and projected sales from 2007 to 2013. According to the U.S. Energy Information Administration's (EIA) Annual Energy Outlook 2009 report, unconventional vehicles (vehicles that can use alternative fuels, electric motors and advanced electricity storage, advanced engine controls, or other new technologies) account for 63% of total new LDV (cars, pickup trucks, sport utility vehicles, and vans) sales in 2030 in the AEO2009 case study [26].

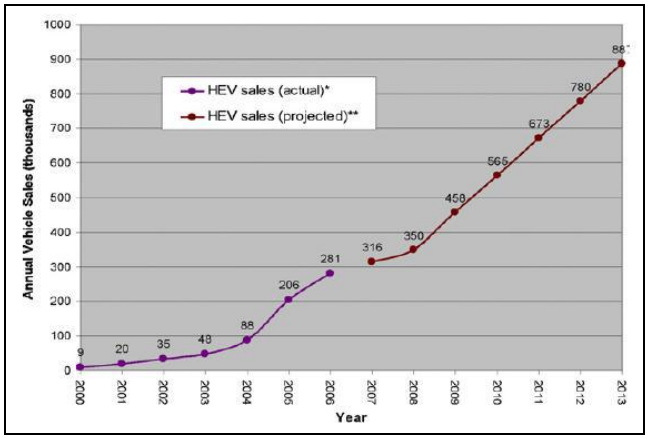

Figure 5. Annual Hybrid Vehicle Sales [22]

Hybrid vehicles, including both standard hybrids and plug-in hybrid electric vehicles (PHEV), will represent the largest share of the unconventional LDV market in 2030, with 63% of all new unconventional LDV sales and 40% of all new LDV sales. As shown in Table 2, EIA projects that total hybrid sales will increase from 2.3% of new LDV sales in 2007, to 20.6% in 2015 and 39.6% (7.9 million vehicles) by 2030. Hybrid vehicles include micro hybrid, plug-in hybrid (PHEV), series hybrid, parallel hybrid, etc.

Table 2. Sales of Unconventional Light-Duty Vehicles by Fuel Type, 2007, 2015, and 2030 (thousand vehicles sold) [27]

Year	Total	Electric Hybrid	Micros	Flex Fuel	Diesel	Other
2007	1515	346	13	873	271	283
2015	6801	1247	2114	2895	529	543
2030	12631	4763	3169	2664	2014	2035

Battery Technology

There are major concerns about the battery systems used in EV technology. If the EV is going to take more than 10 minutes to charge, there is the challenge of who will purchase it unless it is used for local commuting and charged overnight. For instance, if EV technology is applied to utility trucks and school buses, it may be viable due to their short-distance ranges. While these vehicles are waiting afternoon pickups, this will be a time for the batteries to be charged for the next trip. Batteries also have disadvantages such as creating harmonics due to charging and discharging the electric grid. Most batteries have limited life cycles, different charging conditions, and the total number of times they can be charged and discharged. A quicker charging solution may be three phase, 480V charging technology, which may significantly cut charging time by using a three-phase power supply. Even this technology will not be able to cut charging time significantly due to battery charging requirements specified by battery manufacturers. In some of the battery types, factors such as heat generated while charging the batteries and the outdoor temperature will affect battery life. These two important issues should be addressed to increase battery charging and storage efficiencies. An intelligent charging station may be a good solution to avoid overcharges that create heat in the batteries. In cold weather, battery storage capability and charging station efficiency should be addressed as well [13]. Moreover, a sound strategy needs to focus on what can be done today to bring battery costs down and make electric vehicles attractive to consumers other than wealthy environmental advocates. A central part of that strategy must be to promote secondary commercial markets for advanced automotive batteries [28].

Although we agree with EIA's 2030 prospect about percentage of HVs, we differ with EIA in several respects. Development in super-capacitor and battery technology is quite promising. Battery technology was a barrier for HVs for decades because of their low range, long charging time, and safety. With new developments in the last several years, battery technologies can overcome almost all of these imperfections. Today, battery range is up to 69 miles depending on type and brand of HV [29]. For electric vehicles, the battery range is up to 240 miles [30].

Battery charging time is lower. MIT announced that their engineers have created a kind of beltway that allows for rapid transit of electrical energy using a well-known battery material, an advance that could usher in smaller, lighter batteries [31]. They are considerably smaller and lighter. Although there remain concerns about safety, much progress has been made during the last decade.

The battery is one of the most important parts of the HV or EV. There are many types of batteries that can be used by HVs such as Nickel Metal Hydride (NiMH), Nickel Cadmium (NiCd), Lithium Ion (Li-ion), etc. All contain very toxic materials for the environment and raise health

concerns. Currently, 98% of batteries are recycled in the U.S. [33]. With an increase in the use of hybrid cars, battery use will also increase, as indicated in Figure 6. This will bring challenges with it such as recycling costs, transportation of used batteries, etc.

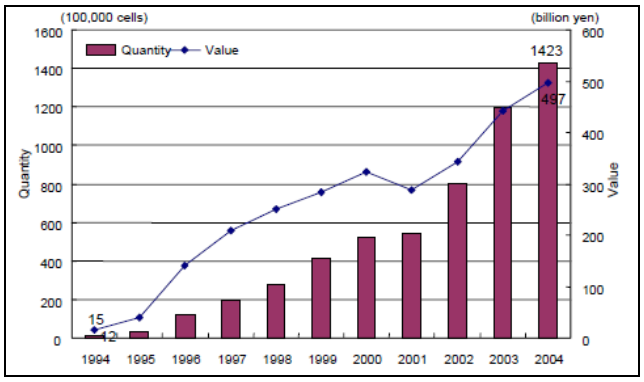

Figure 6. Growth of Lithium-Ion Battery Industry in the Past 10 Years [32]

The flat cost to recycle batteries is about $1,000 to $2,000 per ton [34]. The estimated number of HVs and EVs in 2030 is conservatively 30 million. Today, the lifetime of the battery is around 70,000 miles. Each car needs 2-3 battery packs in its lifetime. Depending on type and brand of the car, battery packs weigh 70 to 150 pounds. Taking all of these numbers into consideration, and with the scenario of having 30 million HVs and EVs on our highways, the total cost of recycling batteries will be $4 billion per year.

Electric Vehicles

Emerging battery technologies and a rapid decrease in the cost of HV components can increase the percentage of hybrid vehicles in the total LDV market and percentage of PHEVs in the hybrid car market beyond the predictions of the Energy Information Administration. Also, there will be pure electric vehicles available on the market. Tesla offers a pure electric vehicle, the Tesla Roadster, which has a 244-mile range. Its battery life is seven years or 100,000 miles. Tesla offers the Roadster starting at $49,900 [30]. It takes about 3.5 hours to charge a battery. Nissan will soon unveil its pure electric car, the Nissan Leaf. The Leaf will have a range of 100 miles per charge under average, everyday driving conditions. Nissan claims to target a price in the range of other typical family sedans [35]. Toyota announced its launch of an urban-commuter battery electric vehicle (BEV) called FT-EV coming to market in 2012 [36].

EIA's case study does not include pure electric vehicles in its projection. Considering all emerging developments, it can be said that there will be a significant increase in sales of hybrid and pure electric vehicles in next twenty years. In this current study, the authors estimate the gross electric energy consumption with respect to 1-15% electric energy share in transportation based on EIA's electric energy consumption data. The total electric energy consumption in 2007 was 4.6 billion kWh per year. Figure 7 shows how the increase in share of electric energy in transportation affects gross electric energy consumption in the U.S. According to the table [25-27], a percent increase in share of electric energy in transportation elevates gross electric energy consumption 2.7% on average. That means that if 15% of energy consumption in transportation is provided by electric energy, gross electric energy consumption will increase about 40%.

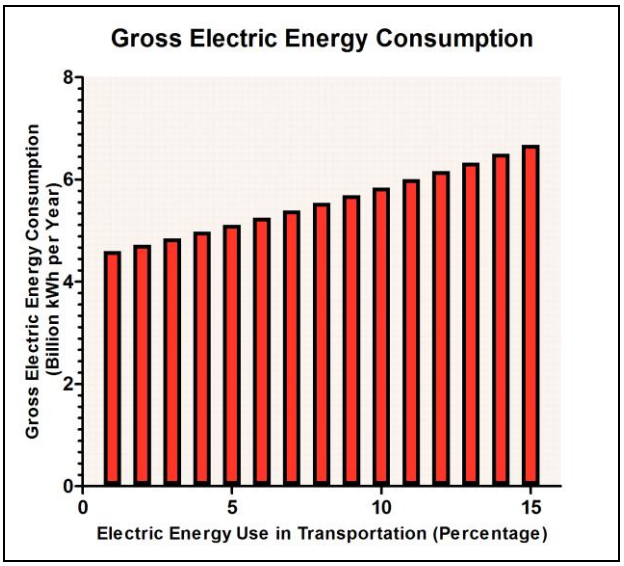

Figure 7. Projected Electric Energy Needs Depending on the Percentage of Electric Vehicles on the Road

Manufacturing of HVs, EVs and Batteries

As shown in Figure 8, major producers of batteries for HVs are Japan, South Korea and China. The U.S. does not have any significant battery production.

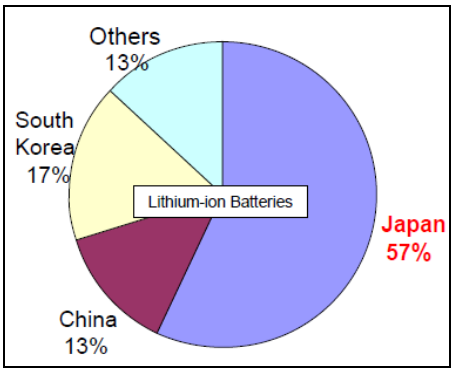

Figure 8. Global Market Share of Batteries, 2005 [29]

Today, the U.S. has the biggest ICE vehicle industry in the world, which constitutes both American companies and foreign companies, such as Japan and Germany. The automotive industry plays a major role in the American economy. It provides hundreds of thousands of jobs to American citizens. The growth of the HV and EV markets implies a decline in the ICE vehicle market. The U.S. is the biggest market for hybrid car sales. Japanese automotive companies produce about 80% of the total HVs (Figure 9). Although there are many American companies producing hybrid cars, they constitute less than 10% of total production. This current picture is not sustainable for the U.S. automotive industry. Without proper precautions, the American automotive industry can lose its market share, which implies a higher unemployment rate and economical downturn.

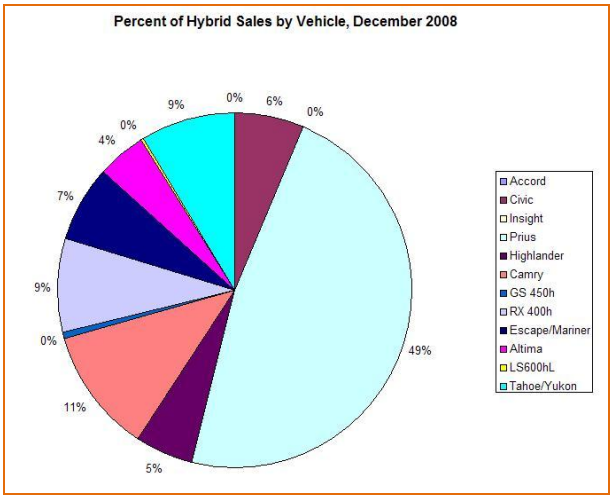

Figure 9. Original Data Supplied by the Battery Association of Japan [29]

Discussion and Conclusions

Although HVs and EVs offer alternatives to traditional energy resources with many advantages, they also bring challenges. The U.S. demand for HVs and EVs is increasing dramatically, which means electric energy consumption will increase in the future. Estimates show that 15% of our transportation needs will be filled by HVs and EVs in 2030. Data in this study show that planned energy production is less than required for such a scenario. Battery recycling costs will increase about $4 billion per year over the next twenty years. Transmissions lines are not capable of transmitting the electric energy needed in the future and require comprehensive inspection, maintenance and updating. Production of HVs and EVs domestically is strategic if we are to avoid dependence on foreign countries. The U.S. is far behind in the production of HVs and EVs compared to other developed countries such as Japan and Germany.

References

[1] The History of Electric Vehicles. Retrieved January 11, 2011, from, http://inventors.about.com/library/weekly/aacarselectrica.htm

[2] The History of Hybrid Vehicles. Retrieved January 18, 2011, from, http://www.hybridcars.com/history/history-of-hybrid-vehicles.html

[3] Luxury Hotel Green Energy. Retrieved February 28, 2011, from, http://www.microturbine.com/

[4] Honda, Hybrid and Alternative Fuels. Retrieved January 18, 2011, from, http://automobiles.honda.com/alternative-fuel-vehicles/

[5] Toyota, Prius Projects. Retrieved January 18, 2011, from, http://www.toyota.com/prius-hybrid/

[6] Tribix, Zero Emission Hybrid Bicycle-Car. Retrieved January 18, 2011, from, http://www.tribix.net/

[7] Electric Power and Hybrid Green Transportation. Retrieved March 1, 2011, from, http://www.wxabat.com/

[8] UQM Technologies, Power Technology. Retrieved October 28, 2010, from, http://www.uqm.com/

[9] Nissan Electric Vehicle. Retrieved December 28, 2010, from, http://www.nissanusa.com/leaf-electric-car/?intcmp=Electric_Car.Promo.Homepage.Home.P2#/car/index

[10] Chevrolet Hybrids. Retrieved December 28, 2010, from, http://www.chevrolet.com/pages/open/default/fuel/hybrid.doc

[11] The Hyundai Concept Cars. Retrieved January 28, 2011, from, http://www.hyundaiusa.com/vehicles/concept-cars.aspx

[12] Gulf of Mexico Response. Retrieved March 18, 2011, from, http://www.bp.com/extendedsectiongenericarticle.do?categoryId=40&contentId=7061813

[13] Electric Vehicles: Challenges and Opportunities for the Grid. Retrieved October 18, 2010, from, http://nialljmcshane.wordpress.com/2010/05/30/electric-vehicles-challenges-and-opportunities-for-the-grid/

[14] Demand Response. Retrieved December 1, 2010, from,http://nialljmcshane.wordpress.com/2010/05/09/so-what-is-smart-grid-anyway-smart-meters-and-demand-response/

[15] U.S. Department of Energy, 2006. Retrieved October 11, 2010, from, http://certs.lbl.gov/ntgs/main-1.pdf

[16] National Transmission Grid Study, 2002. Retrieved December 18, 2010, from, http://www.ferc.gov/industries/electric/indus-act/transmission-grid.pdf

[17] Office of Electricty Delivery & Energy Reliability, 2006. Retrieved October 18, 2010, from,http://sites.energetics.com/gridworks/pdfs/factsheet.pdf

[18] Sources: Edison Electric Institute. *EEI Statistical Yearbook Based on 2004 Data.* Aug. 2005. Retrieved March 18, 2010, from, http://sites.energetics.com/gridworks/pdfs/factsheet.pdf

[19] U.S. Department of Energy, Grid 2006. Retrieved January 18, 2011, from, http://sites.energetics.com/gridworks/grid.html

[20] National Transmission Grid Study, 2002. Retrieved January 18, 2011, from, http://www.ferc.gov/industries/electric/indus-act/transmission-grid.pdf

[21] E. Hirst and B. Kirby. 2001. *Transmission Planning for a Restructured U.S. Electricity Industry*. Edison Electric Institute.

[22] Milliken, J., Joseck, F., Wang., Yuzugullu, E. The Advanced Energy Initiative, *Journal of Power Sources*, Science Direct, Elsevier, 2007.

[23] Transportation Energy Data Book, Chapter 2 - Energyhttp://www-cta.ornl.gov/data/tedb28/Edition28_Chapter02.pdf

[24] Using & Saving Energy For Transportation. Retrieved October 18, 2010, from, http://tonto.eia.doe.gov/kids/energy.cfm?page=us_energy_transportation-basics

[25] U.S. Energy Information Administration Independent Statistics and Analysis. Retrieved October 25, 2010, from, http://www.eia.doe.gov/oiaf/forecasting.html

[26] U.S. Energy Demand. Retrieved October 1, 2010, from, http://www.eia.doe.gov/oiaf/aeo/pdf/trend_2.pdf

[27] Source: Annual Energy Outlook 2009. Retrieved January 8, 2011, from, http://www.eia.doe.gov/conf_pdfs/Monday/Schaal-eia.pdf

[28] Greenberger, J. National Strategy For Electric Vehicles Should Focus on Secondary Battery Use. Retrieved October 18, 2010, from, http://www.theenergycollective.com/jim-g/46003/national-strategy-electric-vehicles-should-focus-secondary-battery-use

[29] Recommendations for the Future of Next-Generation Vehicle Batteries. Retrieved January 8, 2011, from, http://www.meti.go.jp/english/information/downloadfiles/PressRelease/060828VehicleBatteries.pdf

[30] Go Electric. Retrieved October 21, 2010, from, http://www.teslamotors.com/goelectric

[31] Thomson, E.A. Re-engineered battery material could lead to rapid recharging of many devices, MIT News. Retrieved October 23, 2010, from, http://web.mit.edu/newsoffice/2009/battery-material-0311.html

[32] Vehicle Electrification. Retrieved November 6, 2010, from, http://ev.sae.org/news

[33] Recycling batteries. Retrieved February 16, 2011, from, http://www.batteryuniversity.com/partone-20.htm

[34] Buchmann, I. Recycling your Battery. Batteries in a portable world. http://www.buchmann.ca/Article16-Page1.asp

[35] Nissan LEAF. Retrieved October 1, 2010, from, http://www.nissanusa.com/leaf-electric-car/?intcmp=Electric_Car.Promo.Homepage.Home.P2#/battery

[36] FT_EV Concept Vehicles. Retrieved October 8, 2010, from, http://www.toyota.com/concept-vehicles/ftev.html

Biographies

FARUK YILDIZ holds BS in Computer Science degree from Taraz State University, KZ, MS in Computer Science degree from City University of New York, and Doctoral in Industrial Technology degree from University of Northern Iowa. He is an Assistant Professor in Industrial Technology Program at Sam Houston State University. His research is in renewable energy harvesting, conversion, and charging system and ambient energy sources. Dr. Faruk Yildiz may be reached at fxy001@shsu.edu

KENAN BALTACI is a doctoral student of Industrial Technology at University of Northern Iowa. He received B.S. Electrical Engineering degree from Istanbul Technical University in Turkey. Following master degree in Industrial Technology was granted from University of Northern Iowa. Mr. Baltaci is currently working on hybrid vehicle systems as a research.

INTEGRATED REMOTE MANAGEMENT FOR BIO-PROCESSING EXPERIMENTS

Ali Givmanesh, University of Houston; Rupa Iyer, University of Houston; Driss Benhaddou, University of Houston

Abstract

Biochemical engineering researchers have used bioreactors as the primary fermentation device to grow and analyze various cells and tissues in the context of cell culture experiments. The University of Houston's biotechnology program currently uses the New Brunswick Scientific BioFlo 110 to grow transformed bacterial cells in two of its laboratory courses: BTEC 4301: Principles of Bio-processing Laboratory and BTEC 4350: Capstone Experience in Biotechnology. This paper details a theoretical study of the BioFlo 110 primary control unit and proposes a technique to enhance the functionality of the bioreactors as an educational tool by integrating remote monitoring capabilities. The software features presented in this research allow lab instructors and students to remotely view their experimental parameters and settings, thereby reducing the overall time spent in the laboratory and providing an additional layer of flexibility to the overall system.

Introduction

The BioFlo 110 is a modular fermentation structure for microbial and cell culture applications [1], which provides its users with a highly controlled environment in which to perform specific experiments. Modern techniques have inspired the development of genetically altered cells that create both new products and large quantities of scarce products including antibiotics, antigens, and enzymes [2]. In order to provide such an environment, the bioreactor's primary unit monitors and controls the following parameters in each of the bioreactor vessels: temperature, agitation, pH value, dO2, O2 and gas value, in addition to supporting three separate pumping units. Although the equipment within the University of Houston laboratory is fairly new, the technology available to improve their capabilities already supersedes them.

Currently, students and instructors rely on live-feed information presented by the bioreactor unit. Unfortunately, the unit does not provide a method for archiving data related to the experiment and is limited to a one-time viewing of information. In situations where experiments are running overnight, any unexpected changes will remain undetected and unrecorded. The main idea of this study is to develop a system that uses web services and networking techniques to design a monitoring tool, which can be used to view the bioreactor's parameters remotely over the Internet.

The initial research focused on understanding and deciphering the standard of communication used between a desktop computer and the primary control unit of the bioreactor. Once complete, the next phase of the project was to introduce and implement a method of remote monitoring that would allow students and instructors to view their respective experimental information on a dedicated website. This paper is organized first by an overview and explanation of the overall bioreactor system, followed by both the hardware and system requirements. Afterward is a review of the newly developed application design. The research concludes with an overview of the remote management web interface and its related functionalities.

System Overview

Producing new cell products requires lab instructors to perform small-scale experiments to test their procedures and chemical reagents. These initial tests have to be accurate, well-documented, and validated in order to reproduce successful results in larger quantities. The validation process uses the experimental results as proof that a particular process can consistently produce a product of the required quality, purity, and character, and that the bioreactors performance is acceptable during the production operation [2]. The system presented in this research aids in providing supplementary documents to help streamline the validation process and reduce the amount of time spent recording the necessary data.

A typical configuration of the BioFlo 110 module currently in use is depicted in Figure 1. The Primary Control Unit (PCU) acts as the operator interface that controls various parameters in each bioreactor growth chamber, and its functionality is similar to thermostats used to control air conditioning units found in many homes. Its main function is to set the operating point for each available parameter and manage the functions necessary to maintain the current value close to the operating point.

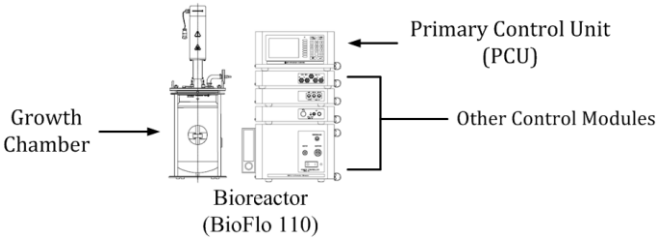

Figure 1. Bioreactor Setup [1]

The other control modules perform the assigned tasks by the PCU to achieve this goal. Lab instructors and students use the PCU's display screen and touch pad to view and control various parameters in each bioreactor vessel. An example of the display screen and parameters are shown in Figure 2. The first and second columns on the PCU screen displays the name of each parameter, along with the current values being read in the bioreactor. The third and fourth columns depict the set points and control options defined by the user. These values are chosen based on the experimental description and requirements. Set points are environmental values chosen by the user that are controlled and maintained in the bioreactor vessel based on their control option.

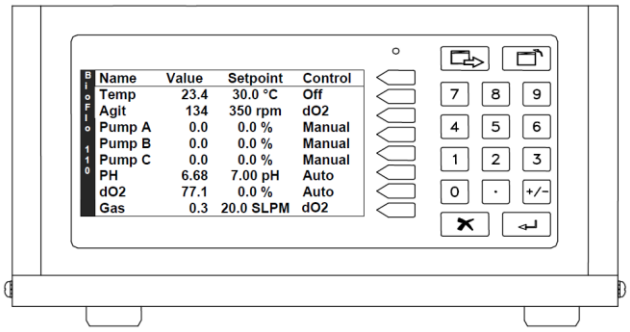

Figure 2. PCU and Bioreactor's Parameters [1]

Figure 3 represents the architecture of the overall bioreactor system and communication method used between each component. An alternative solution to access the PCU parameters is through a serial connection between the desktop and the bioreactor, which is setup and maintained by the newly proposed application in this paper. The desktop utilizes a pre-defined set of commands to capture and store the bioreactor information into text files on its hard drive.

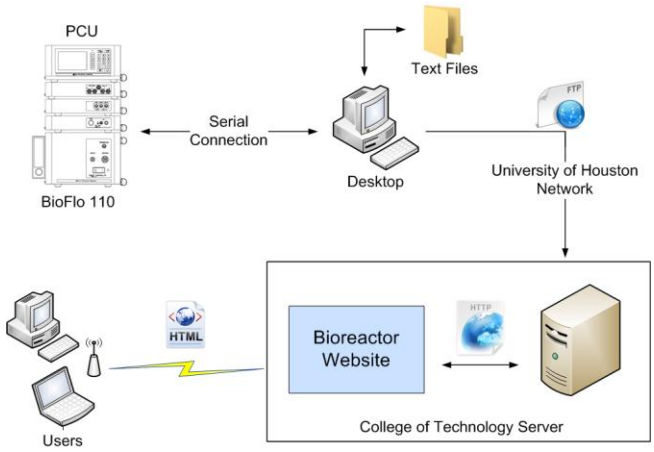

Figure 3. System Network Architecture

The application converts the stored data into a unique format and transfers the new files through the University of Houston network to a web server housed in the College of Technology. Every time users connect to the bioreactor website, the server dynamically updates the webpage contents, and presents the users with a live view of the experimental data.

Hardware and Software Components

The hardware added to the pre-existing bioreactor technology includes a desktop computer and a web server provided by the College of Technology. The desktop computer runs the main communication program and stores the bioreactor data locally on its hard drive. It connects to the PCU via an RS-232 serial cable through conversion of the manufacturer's proprietary AFS/ModBus 25-pin connector. There are several serial ports monitoring software platforms available to fully examine the data across the serial interface. The port monitoring program, 'Hercules 3.2.3', was chosen for this research because it is open source and provides an easy to use environment for testing multiple PCU request commands separately. This program was used to ensure the command messages sent to the bioreactor are in the right format and the messages received by the desktop are complete.

Table 1 lists the commands that are used on the serial port in order to communicate with bioreactors. The request format consists of four hexadecimal values. The first value represents the unique ID number pre-assigned to each bioreactor. The following two values define the request commands. The last value contains a carriage return indicating the end of each request. The ID numbers for the three bioreactors are 00, 04, and 88, respectively, preset by the manufacturer. The responses from the six commands

represent the bioreactor information displayed on the PCU screen.

Table 1. BioFlo Serial Commands

Request Command	Request Format
Get Loop Names	(ID#) (R) (A) (CR)
Get Current Value	(ID#) (R) (C) (CR)
Get Set Point	(ID#) (R) (D) (CR)
Get Output %	(ID#) (R) (E) (CR)
Get Control Mode	(ID#) (R) (J) (CR)
Get Unit	(ID#) (R) (L) (CR)

One of the main objectives of this study was to implement a web-based access system that adds remote monitoring capability to the parameters associated with the bioreactors. In order to employ this functionality, the desktop located within the laboratory updates and transfers the locally stored files to the remote web server. During the bioreactor experiments, every time the data is captured onsite, it is stored, formatted, and sent to the server. The Secure Shell File Transfer Protocol (SFTP) is employed to ensure communication between the desktop and web server is protected. SFTP is the main protocol used to transfer files via encrypted messages between two external devices. The free and open-source software Windows Secure Copy, or WinSCP, is used due to the operating system and financial constraints of the project. WinSCP includes SFTP capabilities to provide a flexible environment whereby a remote file on a corresponding device can be accessed on a local machine [3]. Each data transfer session requires a host name, port number, username, password, and a secure private key file. The software communicates over port 22, the default port for SFTP. The additional input settings were provided by the University of Houston IT department and are assigned to the remote web server. WinSCP offers programmers the option of using a command-line interface, in addition to providing a simple graphical interface. Input commands prompt the main program on the desktop to automate the file transfer process.

A web server is typically a physical computer or virtual machine that provides clients with the content of a web page. The primary protocol used in this process, HTTP (Hypertext Transfer Protocol), is used to bridge communications between the browser and the server. When a client sends a request via HTTP, it will invoke the web server, which processes and then returns the requested HTML content to the client. Early servers were only able to provide information by implementing static HTML pages. The current state of web applications centers on delivering users dynamic content through database queries and executable scripts.

Students and instructors can view the bioreactor's parameters by accessing the bioreactor website. Drupal, a free and open-source content management system, is used to develop the web-based GUI and deliver the website content to the client in a user-friendly manner [4]. For security purposes, the website will be built and tested on a local host at the University of Houston. Because of Drupal's modularity, the system can be easily ported from the local host to a remote domain provided by the IT department.

New Bioreactor Application

The BioFlo program follows a simple and reliable algorithm in order to provide the necessary functions to communicate with the PCU and send or receive data on the serial port. Developing a well-planned algorithm in the design phase of the program is critical for guaranteeing reliability of the application's logic. The new bioreactor program is written in C# and is responsible for storing and converting the acquired data from the bioreactor experiments. After the bioreactor experiment has begun, the main program is started and runs simultaneously alongside the bioreactor experiments, archiving the appropriate parameters every 15 minutes. This time interval is chosen because it reduces the transmission load while keeping the data accurate for further analysis. The flowchart for this program is shown in Figure 4, whilst the algorithm and steps required to capture the data in C# are listed below.

1. Check the serial port
2. If not in use, open the port and initialize the communication settings
3. Write the appropriate commands to the serial port (using commands from Table 1)
4. Read the serial buffer
5. Store the data in a text file
6. Repeat step 3 and 5 for every command
7. Time stamp the text file and save it
8. Convert the text file into a file transfer format
9. Use WinSCP commands to transfer the bioreactor files to the web server
10. Wait for 15 minutes
11. Repeat steps 3-11

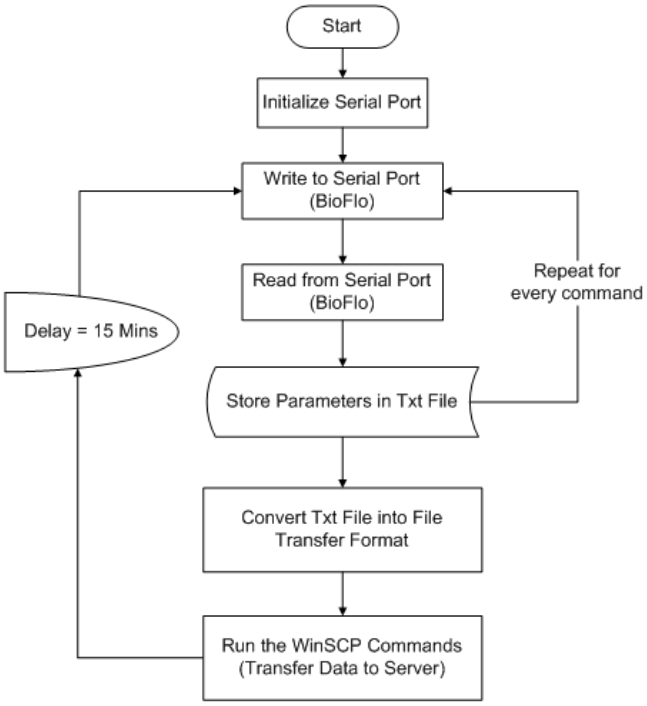

Figure 4. Bioreactor Application Flowchart

There are several ways to achieve code-level communication between the desktop and the PCU. This program uses a controller module called SerialPort, which was originally launched as Microsoft Visual Studio 2005, and is a controller based on the method of P/Invoke call [5]. In order to communicate with the serial port, the program uses the code in Figure 5 to open the port and set the communication parameters.

```
serialPort1.PortName = "COM1";
serialPort1.BaudRate = 9600;
serialPort1.Parity = Parity.None;
serialPort1.StopBits = StopBits.One;
serialPort1.Open();
```

Figure 5. Serial Port Initilazation Code (C#)

These standard RS-232 settings are defined in the BioFlo 110 manual. After initializing the serial port settings, main request commands are formatted for the bioreactors. The example shown in Figure 6 sends the RC command to ID# 88 and returns all the current values of parameters from the third bioreactor to the serial port buffer. Similarly, other messages in Table 1 are communicated through the serial port.

```
byte[ ] command = new byte[ ] { 0x88, 0x52, 0x45, 0x0D };
serialPort1.Write(c, 0, command.Length);
```

Figure 6. Example of the Bioreactor Command Code

Another function shown in Figure 7 included in the serial port library named, "Data Received Event Handler", will read all the existing bytes arriving at the serial port. Upon reading the response from each bioreactor, the information is saved using a string variable called "data". The following piece of code shows how this function is setup within the program.

```
mySerialPort.DataReceived += new
SerialDataReceivedEventHandler(DataReceviedHandler);
string data = mySerialPort.ReadExisting();
```

Figure 7. Data Receive Handler Function

Each time the data is received, it is appended to a simple text file and converted to a unique format, shown in Figure 8. Each set of messages is converted to this new format using "|" as the uniform character separating each field in the response messages. Upon completion of message formatting, the full sets of messages are transferred to the web server to update the bioreactor website. The same text arrangement is implemented on the server side to provide both end devices with a unique and pre-defined format.

```
Loop|Temp|Agit|PumpA|PumpB|PumpC|pH|dO2|Gas|O2
Main Unit|DegC|rpm|%|%|%|pH|%|SLPM|%
Control|Auto|dO2|Off|Off|Off|Auto|Auto|dO2|Auto|
Cur:Value|29.977|200.03|0.0000|0.0000|0.0000|7.0093|114.61|3.0138|0.0000|
OP Points|30.000|200.00|100.00|20.000|50.000|7.0000|100.00|3.0000|0.0000|
Output%|9.0256|25.872|0.0000|0.0000|0.0000|0.0000|0.0000|13.151|0.0000|
```

Figure 8. File Transfer Format

The script shown in Figure 9 runs simultaneously with each data-capture loop on the main program to transmit the formatted files across the University of Houston network. The WinSCP library should be included within the code to enable SFTP functions. WinSCP.com is the program executed to write the communication commands on the terminal. After setting the initial settings for WinSCP program, the C# application connects to the server named btech@tech.uh.edu, which is set up and dedicated in the College of Technology for this project. Each file is sent to the server using the "put" command and, for security purposes, each session is terminated to finish the process. This process will be repeated every time the main program captures new sets of data. The implementation of the transferred data on the server side is explained in the next section.

```
// Run hidden WinSCP process and set the parmeters
Process winscp = new Process();
winscp.StartInfo.FileName = @"C:\Program Files\WinSCP\WinSCP.com";
winscp.StartInfo.UseShellExecute = false;
winscp.StartInfo.RedirectStandardInput = true;
winscp.StartInfo.RedirectStandardOutput = true;
winscp.StartInfo.CreateNoWindow = true;
winscp.Start();

// Feed in the scripting commands
winscp.StandardInput.WriteLine("option batch abort");
winscp.StandardInput.WriteLine("option confirm off");

// Connect to the server and specify the remote directory
winscp.StandardInput.WriteLine("open bteclab@tech.uh.edu");
winscp.StandardInput.WriteLine("cd /home/cot_sites/bteclab/htdocs");

// Send each bioflo file seperatly using put command
winscp.StandardInput.WriteLine("put BioFlo.A.txt");
winscp.StandardInput.WriteLine("put BioFlo.B.txt");
winscp.StandardInput.WriteLine("put BioFlo.C.txt");
winscp.StandardInput.Close();

// Exit the program
winscp.WaitForExit();
```

Figure 9. WinSCP Transfer Script Code

Bioreactor Website

The bioreactor website is updated by a web server while the program is still running. The bioreactor experiments may take up to three days to complete, so it is important to access and monitor the data outside of the laboratory. The dedicated bioreactor website can be accessed using the following URL: http://tech.uh.edu/bteclab/. The initial webpage developed for bioreactors is shown in Figure 10.

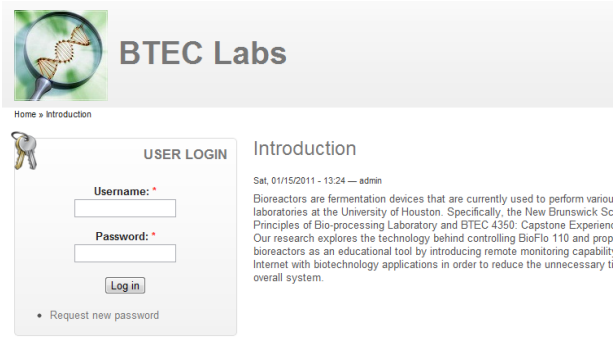

Figure 10. Login Web Page

The website is hosted on a College of Technology web server and is maintained using Drupal as the content management framework. Drupal provides the website administrator with a powerful and flexible environment to perform different tasks through available modules. The design and layout also allows users to easily navigate and search through the website. Users are created by the administrator and must authenticate at a login page before gaining access to the web pages. After providing a username and password at login, the user can access the three bioreactors' web pages via links within the "Live View" menu shown in Figure 11. Two roles are defined in the Drupal system: Lab Instructor and Student. Each role can be modified and customized in order to give various permissions to each account. Student and lab instructors can freely access and view the information about their experiments. Additionally, the lab instructor may add comments or post new web contents.

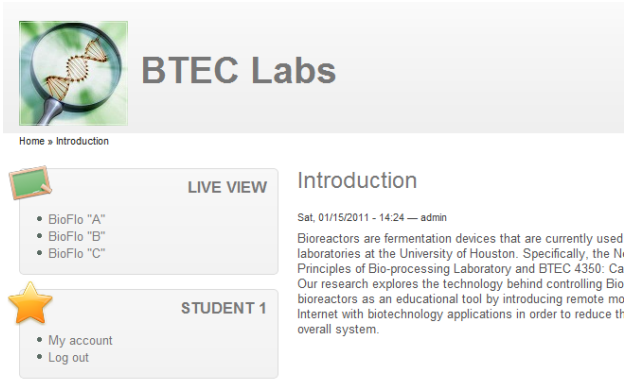

Figure 11. Initial Introduction Web Page

The dedicated bioreactor pages are designed to produce dynamic web content and provide the users with live experimental data. The example in Figure 12 shows the experiment parameters corresponding to the first bioreactor, BioFlo A. The time on the top of the page indicates actual time of the system, and the refresh button at the bottom can be used to retrieve the new table if the program in the laboratory has updated the web page.

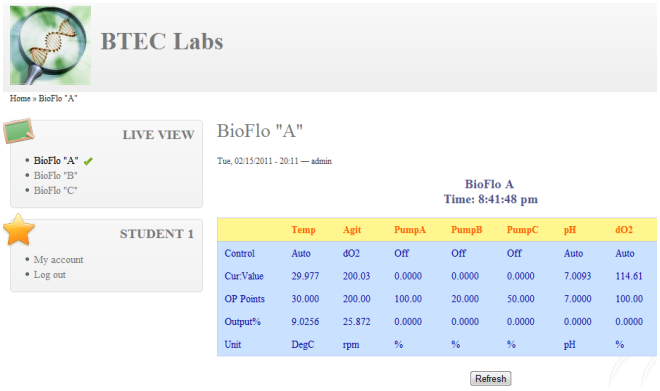

	Temp	Agit	PumpA	PumpB	PumpC	pH	dO2
Control	Auto	dO2	Off	Off	Off	Auto	Auto
Cur:Value	29.977	200.03	0.0000	0.0000	0.0000	7.0093	114.61
OP Points	30.000	200.00	100.00	20.000	50.000	7.0000	100.00
Output%	9.0256	25.872	0.0000	0.0000	0.0000	0.0000	0.0000
Unit	DegC	rpm	%	%	%	pH	%

Figure 12. Bioreactor Live View Example

The web pages are created using standard HTML coding schemes combined with PHP scripts [6]. The PHP script is employed within the HTML code to provide the user with a live view of each bioreactor's parameters in the dedicated table. The PHP code presented in Figure 13 accesses the files originating from the desktop in the laboratory to update each page. After retrieving the information from the text

files, basic table tags and commands are used to produce the table shown in Figure 12.

Providing students and instructors with remote monitoring through the bioreactor website reduces the unnecessary time spent in the laboratory and assures the experiment is running properly without onsite supervision. In case of any error, the logged data on the desktop can be used to identify and resolve any issues with the bioreactor run.

```
<?php   // Start PHP script
$fp = fopen('sites/default/files/Bioflo.A.txt','r');// open the file for A
if (!$fp) {echo 'ERROR: Unable to open file.</table></body></html>'; exit;}
$loop = 0; //initialize the loop

while (!feof($fp)) {
        $loop++;
        $line = fgets($fp,1024); //Read one line
        $field[$loop] = explode ('|', $line); // use "|" as the seperator
        echo '
<tr> // create the rows for the table using the text file
<td>'.$field[$loop][0].'</td>
<td>'.$field[$loop][1].'</td>
<td>'.$field[$loop][2].'</td>
<td>'.$field[$loop][3].'</td>
<td>'.$field[$loop][4].'</td>
<td>'.$field[$loop][5].'</td>
<td>'.$field[$loop][6].'</td>
<td>'.$field[$loop][7].'</td>
<td>'.$field[$loop][8].'</td>
<td>'.$field[$loop][9].'</td>
</tr>';
        $fp++;
}
fclose($fp); ?> // End of PHP code
```

Figure 13. PHP Update Script Code

Conclusion

Bio-processing and growing cell cultures require both sensitive and accurate instruments, as well as a tightly controlled environment. An essential component for achieving both viable and reproducible results requires the tracking and archiving of all the parameters and procedures necessary to duplicate the results accurately and increase the yield of the cell product. The program introduced in this paper allows students and instructors to view and monitor the necessary data from the BioFlo 110 lab remotely, offering a better understanding of the fermentation process, increasing productivity and efficacy, and allowing for more efficient troubleshooting. This program also enables lab personnel to perform experiments overnight while maintaining access over the Internet to monitor the bioreactors' performance. The flexibility introduced by the system will increase productivity of lab managers. The remote monitoring system invokes readily available communication technologies, which greatly improves the data analysis and study of bioreactor experiments.

References

[1] "BioFlo 110 Modular Benchtop Fermentor: Guide to Operations." New Jersey: New Brunswick Scientific Co., Inc., 2007, pp. 1,139-141.

[2] W. L. Hochfeld. (2006). *Producing Biomolecular Substances with Fermenters, Bioreactors and Biomolecular Synthesizers*. Available: http://EV7SU4GN4P.search.serialssolutions.com/?V=1.0&L=EV7SU4GN4P&S=JCs&C=TC0000228257&T=marc

[3] X. Liu, *et al.*, "Design of secure FTP system," in *Communications, Circuits and Systems (ICCCAS), 2010 International Conference on*, 2010, pp. 270-273.

[4] J. Fu, *et al.*, "A Multi-sites Scheme Based on Open Source CMS, Drupal," in *Multimedia and Information Technology (MMIT), 2010 Second International Conference on*, 2010, pp. 239-241.

[5] Z. Yue-Qin and G. Wen, "- Design and Implementation for Communicating between Computer Serial Port and Mobile Phone," vol. -, pp. - 186, 2009.

[6] T. Suzumura, *et al.*, "Performance Comparison of Web Service Engines in PHP, Java and C," in *Web Services, 2008. ICWS '08. IEEE International Conference on*, 2008, pp. 385-392.

Biographies

ALI GIVMANESH received the B.S. degree in Electrical Engineering from the University of Houston in 2008, the M.S. degree in Engineering Technology from the University of Houston, Texas, in 2011. He was involved in the IEEE student organization in his undergraduate program. His objective for his graduate thesis has been to integrate academic study and network communication solutions to enhance bio-processing equipments. His teaching and research areas include biotechnology, smart grids and solar energy, and programming. Ali Givmanesh may be reached at agivmanesh@uh.edu

RUPA IYER, Ph.D., is an Associate Professor in the department of Engineering Technology, in the College of Technology at the University of Houston. She is the founding director of Biotechnology programs, and also directs the Center for Life Sciences Technology. In this capacity she has been responsible for developing the Biotechnology degree program and the core initiatives of the center that include, education, research workforce development and outreach. Her research interests are in environmental biotechnology and interdisciplinary research-based education. riyer@central.uh.edu

DRISS BENHADDOU, Ph.D., is an Associate Professor with the University of Houston, Texas, where he is actively involved in optical networking and sensor networks research activities. He developed state of the art wireless and optical networking research lab at the engineering technology department (www.tech.uh.edu/won). Dr. Benhaddou was a senior technical staff member at Lambda Optical Systems Inc, where he played a key role in protocol development and systems integration activities. During his earlier tenure at Sprint, he implemented an extensive broadband test-bed for vendor equipment certification and research/development activities. He holds two doctoral degrees in optoelectronics and telecommunication engineering from the University of Montpellier II, France, in 1995, and the University of Missouri in 2002. dbenhadd@central.uh.edu

INSTRUCTIONS FOR AUTHORS
MANUSCRIPT REQUIREMENTS

THE INTERNATIONAL JOURNAL OF ENGINEERING RESEARCH AND INNOVATION is an online and print publication, specifically for the Engineering, Engineering Technology, and Industrial Technology professionals. Submissions to this journal, such as an article submission, peer-review of submitted documents, requested editing changes, notification of acceptance or rejection, and final publication of the accepted manuscript will be handled electronically.

All manuscripts must be submitted electronically. Manuscripts submitted to the International Journal of Engineering Research and Innovation must be prepared in Microsoft Word 98 or higher (.doc) with all pictures, jpg's, gif's. pdf's included in the body of the paper. All communications must be conducted via e-mail as described on journal web site: www.ijeri.org.

The editorial stuff of the International Journal of Engineering Research and Innovation reserves the right to format any submitted word document in order to present submissions in an acceptance PDF format for the print journal. All submitted work content will not be changed without express written consent from the author(s).

1. Word Document Page Setup: Top = 1", Bottom = 1", Left=1.25", and Right = 1.25". This is the default setting for Microsoft Word. Do Not Use Headers or Footers

2. Text Justification: Submit all text as "LEFT JUSTIFIED" with No Paragraph Indentation.

3. Page Breaks: No page breaks are to be inserted in your document.

4. Font Style: Use 11-point Times New Roman throughout the paper except where indicated otherwise.

5. Image Resolution: Images should 96 dpi, and not larger than 460 X 345 Pixels.

6. Images: All images should be included in the body of the paper. (.jpg or .gif format preferred)

7. Paper Title: Center at the top with 18-point Times New Roman (Bold).

8. Author and Affiliation: Use 12-point Times New Roman. Leave one blank line between the Title and the "Author and Affiliation" section. List on consecutive lines: the Author's name and the Author's Affiliation. If there are two authors follow the above guidelines by adding one space below the first listed author and repeat the process. If there are more than two authors, add on line below the last listed author and repeat the same procedure. Do not create a table or text box and place the "Author and Affiliation" information horizontally.

9. Body of the Paper: Use 11-point Times New Roman. Leave one blank line between the "Author's Affiliation" section and the body of the paper. Use a one-column format with left justification. Please do not use space between paragraphs and use 0.5 indentation as break between paragraphs.

10. Abstracts: Abstracts are required. Use 11-point Times New Roman Italic. Limit abstracts to 250 words or less.

11. Headings: Headings are not required but can be included. Use 11-point Times New Roman (ALL CAPS AND BOLD). Leave one blank line between the heading and body of the paper.

12. Page Numbering: The pages should not be numbered.

13. Bibliographical Information: Leave one blank line between the body of the paper and the bibliographical information. The referencing preference is to list and number each reference when referring to them in the text (e.g. [2]), type the corresponding reference number inside of bracket [1]. Consider each citation as a separate paragraph, using a standard paragraph break between each citation. Do not use the End-Page Reference utility in Microsoft Word. You must manually place references in the body of the text. Use font size 11 Times New Roman.

14. Tables and Figures: Center all tables with the caption placed one space above the table and centered. Center all figures with the caption placed one space below the figure and centered.

15 Page limit: Submitted article should not be more than 15 pages.

College of Engineering, Technology, and Architecture

University *of* Hartford

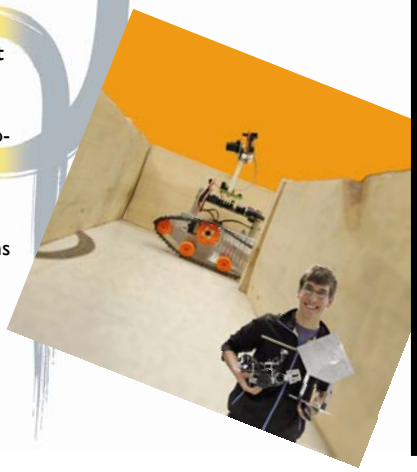

For more information please visit us at www.hartford.edu/ceta

For more information on undergraduate programs please contact Kelly Cofiell at cetainfo@hartford.edu.

For more information on Graduate programs please contact Laurie Grandstrand at grandstran@hartford.edu.

Toll Free: 1-800-766-4024
Fax: 1-800-768-5073

DEGREES OFFERED :

ENGINEERING UNDERGRADUATE

Acoustical Engineering and Music (B.S.E)
Biomedical Engineering (B.S.E)
Civil Engineering (B.S.C.E)
-Environmental Engineering Concentration
Environment Engineering (B.S.E)
Computer Engineering (B.S.Comp.E.)
Electrical Engineering (B.S.E.E.)
Mechanical Engineering (B.S.M.E.)
- Concentrations in Acoustics and
- Concentrations in Manufacturing

TECHNOLOGY UNDERGRADUATE

Architectural Engineering Technology (B.S.)
Audio Engineering Technology (B.S.)
Computer Engineering Technology (B.S.)
Electronic Engineering Technology (B.S.)
-Concentrations in Networking/ Communications and Mechatronics
Mechanical Engineering Technology (B.S.)

GRADUATE

Master of Architecture (M.Arch)
Master of Engineering (M.Eng)
- Civil Engineering
- Electrical Engineering
- Environmental Engineering
- Mechanical Engineering
  - Manufacturing Engineering
  - Turbomachinery

3+2 Program (Bachelor of Science and Master of Engineering Degrees)
E^2M Program (Master of Engineering and Master of Business Administration)

College of Engineering, Technology, and Architecture
UNIVERSITY OF HARTFORD

The International Journal of Engineering Research & Innovation (IJERI) is the second official journal of the International Association of Journals and Conferences (IAJC). IJERI is a highly-selective, peer-reviewed print journal which publishes top-level work from all areas of engineering research, innovation and entrepreneurship.

IJERI Contact Information

General questions or inquiry about sponsorship of the journal should be directed to:

Mark Rajai, Ph.D.

Editor-In-Chief

Office: (818) 677-5003

Email: editor@ijeri.org

Department of Manufacturing Systems Engineering & Management

California State University-Northridge

18111 Nordhoff St.

Room: JD3317

Northridge, CA 91330